Tip leakage reduction in small turbines for rocket applications

R.J. Theussing

Technische Universiteit Delft

TU Delft Delft University of Technology

Challenge the future

TIP LEAKAGE REDUCTION IN SMALL TURBINES FOR ROCKET APPLICATIONS

by

R.J. Theussing

in partial fulfillment of the requirements for the degree of

Master of Science
in Aerospace Engineering

at the Delft University of Technology,
to be defended publicly on Thursday April 1, 2021 at 10:00 AM.

Supervisor:	Dr. Ir. M. Pini	
Thesis committee:	Prof. dr. Ir. Colonna,	TU Delft
	Dr. Ir. M Pini,	TU Delft
	Dr. Ir. A. Cervone,	TU Delft
	Ir. F. Lindemann	Dawn Aerospace

This thesis is confidential and cannot be made public until April 1, 2023.

TU Delft Delft University of Technology

PREFACE

This thesis marks the fulfilment of the master in aerospace engineering at the track propulsion&power at the university of Delft. I would like to thank the people that helped me during my thesis and made my student time a time I like to think about.

First I would like to thank Dr. Matteo Pini, both for his guidance during this thesis and his valuable feedback and for his clear courses on internal flows and turbomachinery which sparked my interest in the world of turbines.

I would like to thank Dawn Aerospace for giving me the opportunity to do my master thesis at them and see my work being directly applicable to the industry. I also want to thank them for the good times at the office, the online Frimibo's and last but certainly not least the Christmas parties.

From Dawn Aerospace I would especially like to thank Felix, who supervised me. His feedback was essential to this thesis.

Last but certainly not least I want to thank my parents, my friends and my girlfriend who kept me sane during the many hours I put into this thesis.

R.J. Theussing
Delft, April 2021

ABSTRACT

Dawn Aerospace is developing a small launch vehicle in the form of a spaceplane, which is powered by a turbopump driven rocket. To reach higher engine efficiency and save weight, there is a need for a small highly-power dense turbine. The efficiency of small turbines strongly depends on the tip gap sizes compared to the blade height. Existing turbine loss models predict large efficiency penalties due to excessive clearance losses, caused by the relatively large tip gap over blade height ratio. To build a competitive small launch vehicle, it is necessary to develop a highly efficient turbine.

The objective of the work presented here is to first analyse and then minimize the clearance losses occurring in a representative small turbine for the spaceplane by applying seals on top of the shroud. Turbine loss models presented in the literature are limited to predicting losses for labyrinth seals only. As more advanced seals, like the brush seal, are being used more regularly there is a need for more accurate modelling of clearance losses in shrouded rotors.

In order to calculate the leakage through seals, first bulk flow models (BFM) were developed for the labyrinth, annular and brush seal. BFMs use the zeroth-order of a perturbation equation to calculate leakage. Two- and three-dimensional numerical models were developed to simulate the mass flow rate through the seals with the help of commercially available software. Next, the BFMs and numerical models were validated against experimental data obtained from literature. BFMs could predict leakage rates through seals with an accuracy up to 15%, when suitable empirically determined constants/equations were used. The numerical models performed slightly worse for the annular seals with a minimum accuracy of 25%, while good predictions were obtained for labyrinth seals and brush seals. Little difference could be seen between 2D and 3D CFD when assessing leakage through shaft seals.

The turbine design of Dawn Aerospace was evaluated in CFD and compared to the loss model of Dunham&Came. First, an unshrouded case was designed to assess the profile and secondary losses arising in the turbine. In the unshrouded case the loss model agreed with CFD. In the case of the shrouded turbine a large discrepancy existed between CFD and the loss model. The difference in loss was attributed to the fact that the loss model massively over predicted the clearance loss of the turbine, by over predicting the leakage over the shroud.

A new loss model has been developed which can be used to more accurately predict the clearance loss of a turbine. This improvement is achieved by using Denton's equation for clearance loss and Dunham&Came's equations for profile and secondary loss. Denton requires the determination of the leakage mass flow rate through the shroud. The leakage mass flow rate is dependent on the inlet, the seal and the outlet. The leakage through the shroud can be calculated with the usage of BFMs. The inlet and outlets of the shrouds are modelled as labyrinth seals while placing the actual sealing system in between. This means that now not only simple labyrinth seals can be predicted, but brush seals as well and possible other seals for which leakage equations are available. It has been shown that the model can accurately predict losses for a range of turbines. The efficiency predictions of the loss model for a range of designed turbines were within 5.6% when compared to CFD

During the sensitivity analysis on the model it was found that the influence of the inlet and outlet cavity width on the mass flow rate is significant in small turbines. Especially if the sealing mechanism on top of the shroud is simple, which is the case for an annular seal or a single finned labyrinth seal. Whenever multiple fins were adopted or the brush seal is used the inlet and outlet width become less important in the sealing system for reducing leakage rate over shrouds in small axial turbines.

CONTENTS

List of Figures

List of Tables

NOMENCLATURE

(Sorted by alphabetical order and lower and upper case)

PARAMETERS

Symbol	Description	Unit
a	viscous resistance coefficient?	-
A	Clearance area under the fin	m^2
b	inertial resistance coefficient	-
b_b^{min}	Minimum brush thickness	m
B	Turbine tip type multiplier	-
c	Blade chord	-
c_p	Specific heat capacity at constant pressure	J/(kgK)
$\bar{C}$	Mean clearance size of the annular seal	m
C_{in}	Inlet clearance size for the annular seal	m
C_L	Blade lift coefficient	-
C_{out}	Outlet clearance size for the annular seal	m
Cr	Clearance between the fin and the rotor	m
d	bristle diameter	m
D_{abr}	Diameter of the aft backing-ring	m
D_{fbr}	Diameter of the front backing-ring	m
D_r	Diamter of the rotor	m
f_{error}	Error function for the labyrinth seal	-
f_{r0}	Zeroth order friction coefficient for the rotor	-
f_{s0}	Zeroth order friction coefficient for the stator	-
g	Gravitational acceleration	m/s^2
g_R	Rotor gap clearance	m
h	Blade height	-
h_0	Dimensionless clearance in the annular seal	-
h_1	Enthalpy in front of the blade	J
h_{2r}	Real enthalpy after the blade	J
h_{2s}	Isentropic enthalpy after the blade	J
I_{sp}	Specific impulse	s
k	Turbine tip clearance	m
k'	Effective tip clearance	m
k_l	Annular seal entrance loss coefficient	-
l	non-dimensional annular seal length	
l	bristle pack thickness	m
L	Spacing between labyrinth seal fins	m
L	Bristle pack thickness	m
m_0	Initial vehicle mass	kg
m_f	Final vehicle mass	kg
m_r	Hir's lubrication coefficient rotor	-
m_s	Hir's lubrication coefficient stator	-
$\dot{m}$	Mass flow rate	kg/s
$\dot{m}_{i+1}$	Mass flow rate in the next cavity	kg/s
$\dot{m}_i$	Mass flow rate in the current cavity	kg/s
$\dot{m}_0$	Mass flow rate in the first cavity	kg/s
$\dot{m}_L$	Shroud leakage mass flow rate	kg/s
$\dot{m}_m$	Turbine main flow mass flow rate	kg/s

M_0	Zeroth order mach number	-
n_r	Hir's lubrication coefficient rotor	-
n_s	Hir's lubricantion coefficient stator	-
NT	Number of fins	-
N	Bristle density	bristles/m
p	pressure	Pa
P_a	Pressure at ambient conditions	-
p_{in}	Turbine inlet pressure	Pa
p_{out}	Turbine outlet pressure	Pa
p_0	Zeroth order pressure	Pa
p_{01}	Total pressure in front of a blade	Pa
p_{02}	Total pressure after a blade	Pa
p_1	First order pressure	Pa
p_2	Static pressure in after a blade	Pa
P_i	Pressure at the current labyrinth seal cavity	Pa
P_{i+1}	Pressure at the current labyrinth seal cavity	Pa
P_{in}	Inlet pressure	Pa
P_{NC}	Pressure at the last labyrinth cavity	Pa
P_{out}	Power output	W
P_{out}	Outlet pressure	Pa
r	radius at inner position	m
r_m	Turbine meanline radius	m
r_r	Turbine root radius	m
r_t	Turbine tip radius	m
r_{t2}	Radius of the tip at station 2	m
r_{t3}	Radius of the tip at station 3	m
r_2	radius at outer position	m
R	Specific gas constant	J/(kgK)
Re_{a0}	Reynolds number annular seal	-
s	Blade spacing (solidity)	-
s_i	Pressure ratio parameter Chaplygin	-
t	Blade thickness	m
T	Temperature of the fluid	-
T_{in}	Turbine inlet temperature	K
u_{z0}	Non-dimensional zeroth order velocity in the axial direction	-
$u_{\theta 0}$	Non-dimensional zeroth order circumferential velocity for in the annular seal	-
U	Velocity through the brush seal	-
V	Volume of the brush cavity	m^3
V_{solid}	Volume of the bristles	m^3
y^+	dimensionless wall distance	-
$Y_{clearance}$	Clearance pressure loss coefficient	-
$Y_{profile}$	Profile pressure loss coefficient	-
Y_{total}	Total pressure loss coefficient	-
$Y_{P(\beta_2=0)}$	Profile pressure loss coefficient for reaction blades	-
$Y_{P(\beta_2=\beta_3)}$	Profile pressure loss coefficient for impulse blades	-
Y_N	Nozzle pressure loss coefficient	-
Y_R	Rotor pressure loss coefficient	-
z	Dimensionless axial position for the annular seal	-
Δv	Change in vehicle velocity	m/s
ΔP	Pressure drop over the brush seal	Pa

Parameters (Greek)

Symbol	Description	Unit
α	Blade flow angle	°
α_2	blade angle at position 2	°
α_l		
α_m	mean blade angle?	°
α_i	Blade flow angle at a certain position	°
β	Flow angle	°
β_1	Flow angle at position 1	°
β_2	Flow angle at position 2	°
β_3	Flow angle at position 3	°
β_k	Empirical coefficient for brush seal?	-
γ	Heat capacity ratio	-
ϵ	Perturbation parameter	-
ϵ	Porosity	-
ζ	Entropy loss coefficient	-
η_t	Total efficiency	-/%
θ	Labyrinth seal flow exit angle	°
λ	Degree of reaction of the turbine	-
μ	Dynamic viscosity	Pa s
μ_{1i}	Flow coefficient?	-
μ_2	Kinetic energy coefficient?	-
ρ	Density	kg/m^3
ρ_0	Zeroth order density	kg/m^3
ρ_a	Ambient density	kg/m^3
ϕ	Flow coefficient	-
ϕ	bristle angle with the shaft	°
ψ	Stage loading coefficient	-
ω	Rotational speed	rpm

1

INTRODUCTION

The space industry has seen an increasing number of satellite launches over the past decades. To satisfy the increasing demand for launch services, small satellites (smallsats) have become the focus. Smallsats often take rideshares on government-funded satellite launches to reduce launch costs, which means they are the secondary payload. Being the secondary payload has consequences, as to not getting the ideal orbit for the satellite and other restrictions in place to protect the main payload. To launch smallsats on the appropriate orbit there thus is a demand for dedicated smallsat launch vehicles [15, 16].

Dawn Aerospace is developing a revolutionary launcher in the form of a spaceplane. The Mk-II is a scaled-down proof of concept, which can be seen in figure 1.1, to comply with the demand for small satellite launch vehicles. Contrary to conventional rockets the space plane can be launched from an airport without the need of closing the airspace, as for the first part of its flight it is operated as an aircraft. In addition, the spaceplane will land at the same airport and can be refuelled and fly again on the same day. This space plane will be powered by a rocket engine and to deliver high pressure propellants to the rocket engine pumps are used. To keep the spaceplane as light as possible the pumps will be powered by a turbine, instead of using electric motors with batteries. Turbopumps are extremely complex machinery and crucial for every liquid rocket engine with high performance. The rocket engine will be of the closed engine cycle type, this means that the propellants from the tank will go through the pumps, cooling channels, turbine and that all fluids will exit through the engine's nozzle. The oxidiser of the engine is hydrogen peroxide and the fuel will be kerosene. The hydrogen peroxide will be decomposed in a catalyst pack after which it will drive the turbine, before going to the combustion chamber.

Figure 1.1: The Mk-II Aurora spaceplane at the airport

The performance of a space vehicle is typically described by the Tsiolkovsky equation given in equation 1.1. Δv describes the capability of a space vehicle to either reach space or how much payload space vehicle can take with it and still reach space. The equation thus shows that the performance of a space vehicle is dependent on the specific impulse (I_{sp}) and the wet to dry mass ratio (m_0/m_f). The specific impulse is mainly influenced by the chamber pressure that can be reached in the rocket engine, while the mass ratio is dependent on the component weight and the fuel weight. Employing a turbine to power the pumps reduces the component weight when compared to an electrical pump system as there is no need to bring large batteries. To achieve high combustion pressure the turbine should extract as much energy from the fluid as possible, with a limited pressure drop, as the rocket engine is a closed-loop system. The combustion chamber pressure is crucial in order to get a high I_{sp}, which is a measure of how efficiently an engine uses its fuel. Consequently a higher I_{sp} results in a higher Δv. Without altering the mass flow rate ($\dot{m}$) this can only be achieved if the turbine operates at high efficiency (η_t), as is described in equation 1.2.

$$\Delta v = I_{sp} g \ln\left(\frac{m_0}{m_f}\right) \tag{1.1}$$

$$P_{out} = \dot{m}\eta_t c_p T_{in}\left(1 - \frac{p_{out}}{p_{in}}^{\frac{\gamma-1}{\gamma}}\right) \tag{1.2}$$

Figure 1.2 shows the change in Δv for the increase in turbine efficiency, η_t. It only takes into account the higher pressure in the combustion chamber due to a higher power output of the turbine, the mass ratio used is 3.5. The higher turbine power output will result in higher pump outlet pressures. It can be seen that in this range of pressure increase and at this fuel and oxygen ratio of the propellants the rocket engines performance, Δv, increases by 0.2% for every 1% in turbine efficiency increase. the 0.2 % for each 1% in turbine efficiency is generally not significant. However, seeing that the initial turbine efficiency was very low, that gave room for a substantial improvement of about 3 - 4 % in Δv if a turbine efficiency could be achieved in the range of 90 - 95 %.

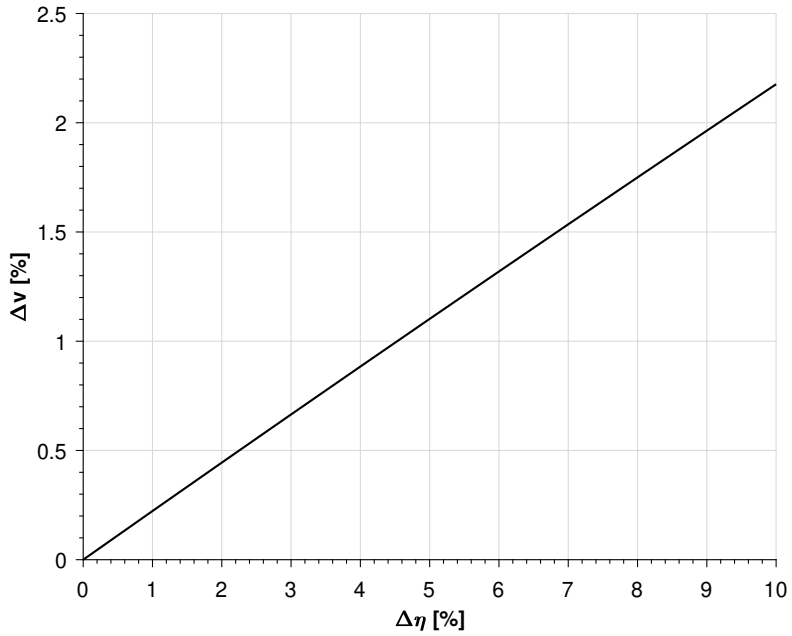

Figure 1.2: Change in Δv as a function of turbine efficiency.

The turbine of small rocket engines (< 15 kN) is often very small and rotate at high rotational speeds in order to be as lightweight and efficient as possible. The small size brings consequences such as manufacturing constraints due to limits in manufacturing precision. This means that gaps needed between rotating and stationary components become relatively large. The typical gap to blade height ratio is around 1-2% [17] while the turbine of Dawn Aerospace has a gap to blade ratio of around 10%. For unshrouded turbines clearance

losses due to the clearance at the tip can already become as large as one-third of all the losses in the turbine [18]. This loss is mainly dependant on the leakage flow in this gap, which in turn is proportional to the relative size of the gap compared to the blade. This thesis aims to reduce the losses caused by clearance gaps in small turbine and make the usage of small turbines more rewarding.

The scientific background and theoretical basis of this thesis can be found in chapter 2. Chapter 2 also presents the research objective and research questions. The methodology of this thesis is presented in chapter 3, it includes the development of analytical and numerical models used throughout the thesis. Chapter 4 focuses on the validation of the developed shroud model, the design of new turbines with the model and presents a sensitivity analysis of the model. The thesis closes with chapter 5 where the conclusions and recommendations of this work are discussed.

2

SCIENTIFIC CONTEXT AND THEORETICAL BASIS

In the previous chapter, the spaceplane of Dawn Aerospace was introduced. It was shown that increasing the turbine performance would increase overall vehicle performance. The chapter also discussed that due to the small engine size, the relative clearance sizes in the turbine are larger than in conventional turbines and would severely impact turbine efficiency.

This chapter aims to give more context for why this research is conducted. The mitigation methods for reducing clearance losses and the process of turbine design are discussed. It describes the need for a more modular approach to turbine shroud sealing, to assess the turbine performance with different types of seals in the preliminary design stage. A general overview of turbine design and its losses is presented in section 2.1. In section 2.2 an overview is given on the possibilities for reducing tip clearances found in the literature. Section 2.3 continues to discuss rotary seals which can be used on top of shrouds. The state of the art and motivation for this thesis are discussed in section 2.4. Section 2.5 specifies the research goals and research questions of this thesis.

2.1. AXIAL GAS TURBINES: DESIGN AND LOSSES

Turbines are commonly used in power generation and aerospace. In the case of rocket engines, it is part of the turbopump and drives the pump(s) in a direct way or through a gearbox. The more efficient the turbine the more power can be provided to the pump for the same mass flow rate through the turbine. This means that the pump can achieve higher pressure and this will increase the pressure in the combustion chamber. A higher combustion pressure means that the I_{sp} of the propellants will be higher, which is a measure of the propellants efficiency. There exists a finite gap between rotational parts and stationary parts, to ensure that the rotor can rotate freely. Figure 2.1 shows the gap width denoted with g_R and is often as small as possible, while still taking into account the rotor growth due to thermal expansion of materials and due to centrifugal forces.

To design an axial turbine the mean line design approach is used. It calculates the velocity triangles, which dictate the angle of the blades at the mean radius of the turbine, indicated by r_m in figure 2.1. The calculated blade angles can be used to construct the turbine blades and to calculate the performance of the turbine with the help of empirically determined loss models. These loss models are available from literature and are mostly developed within the 1970-1980s. The loss model discussed below is developed by Dunham&Came (DC) [19], who updated the method of Ainley&Mathieson (AM) [20] to also be applicable to turbines with aspect ratio's (height of the blade over the chord length) smaller than two and with a larger range of Reynolds numbers. They achieved this by including the aspect ratio in the prediction for the losses, such that it also became valid for smaller turbines.

The 2D blade profile of the turbine is further defined with the 11 parameter method developed by Pritchard [1], from which the thickness/blade chord ratio of the blade is obtained. The thickness over chord ratio plays a role in the profile losses as can be seen later on in this section. The 11 parameters come from either the meanline design code, i.e. blade angles or from user inputs. An example of a generated blade design is given in figure 2.2. The method allows the calculation of every point of the blade by first calculating 5 key points,

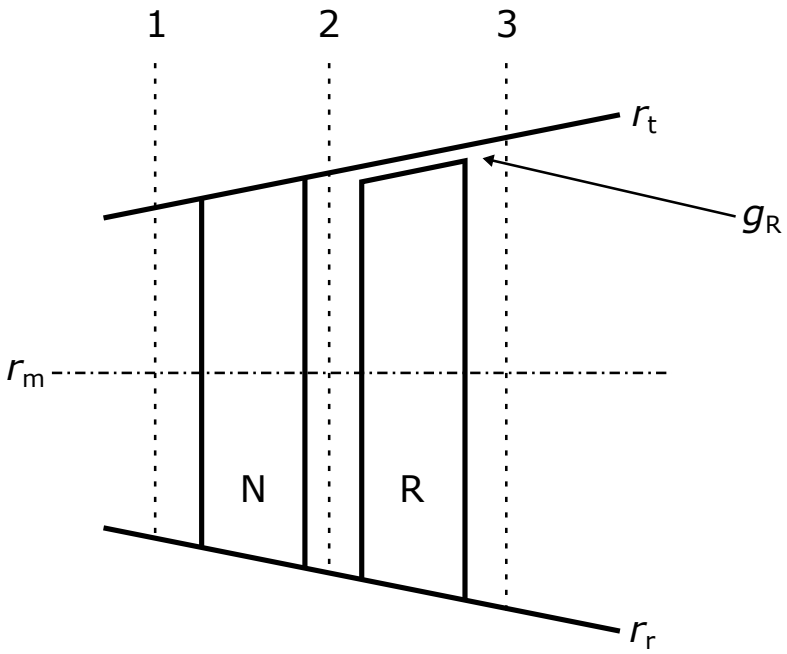

Figure 2.1: Schematic of the meridional view of the turbine with indication of positions used by the meanline design program.

the 4 points where the leading edge and trailing edge join up with the pressure and suction side, number 1, 3, 4 and 5 in the figure and the last point is positioned at the throat, number 2 in the figure. The points are connected with 5 equations, 3 circular and 2 third-order polynomials as indicated in figure 2.2. This method gives rise to a wide variety of different blade designs, without the need for user interaction.

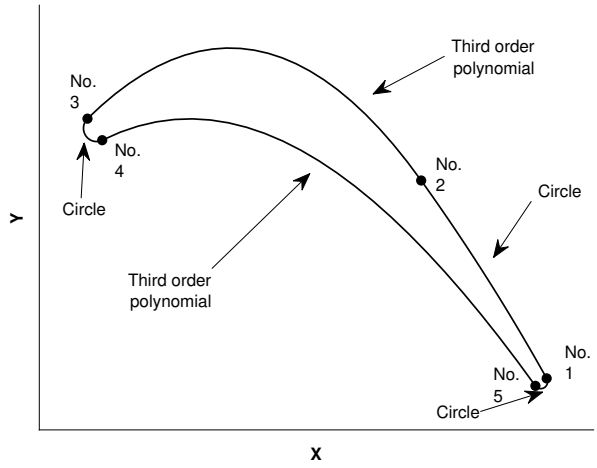

Figure 2.2: Eleven parameter blade design example of Pritchard [1] where the 5 key points and the surface equations are indicated.

The losses of a turbine are often characterized by the loss models into three categories: 1) profile losses, 2) secondary losses and 3) clearance losses. This thesis uses the pressure loss coefficient notation. This allows for the calculation of pressure loss for each individual loss component and easy summation to obtain the total pressure loss coefficient of the blade row as can be seen in equation 2.1.

$$Y_{\text{total}} = Y_{\text{profile}} + Y_{\text{secondary}} + Y_{\text{clearance}} \tag{2.1}$$

The losses will be explained in some detail below together with how the existing loss model of Dunham&Came calculates them. The loss computation for clearance losses is especially important during this thesis.

2.1.1. PROFILE LOSSES

Profile losses are related to the loss generation caused by the boundary layer of the blade profile, see figure 2.3. The blade influences the velocity profile downstream of the blade. This zone where the velocity distribution changes is called the wake as indicated in the picture. It is assumed that the profile loss is a two-dimensional loss. In the loss model of Dunham&Came, the loss from the trailing edge is included in this loss [4, 19, 21]. The profile losses are determined by cascade tests performed by Ainley&Matiehson [20]. The loss is also determined to be dependent on pitch/chord ratio and is investigated for impulse and reaction blades [22]. Equation 2.2 shows how to calculate the profile loss, where $Y_{P()}$ is read from a graph published by Ainley&Mathieson [20]. The graphs of Ainley&Mathieson are valid for a range of thickness/blade chord ratios (t/c in equation 2.2) of 0.15 to 0.25. In equation 2.2 β_2 and β_3 respectively correspond to the incoming flow angle and outgoing flow angle. Whenever $\beta_2 = \beta_3$ the graph is used for impulse blading and when $\beta_2 = 0$ the graph is used for reaction blading.

$$Y_{\text{profile}} = \left(Y_{P(\beta_2=0)} + \left(\frac{\beta_2}{\beta_3}\right)^2 \left[Y_{P(\beta_2=\beta_3)} - Y_{P(\beta_2=0)} \right] \right) \left(\frac{t/c}{0.2}\right)^{\beta_2/\beta_3} \tag{2.2}$$

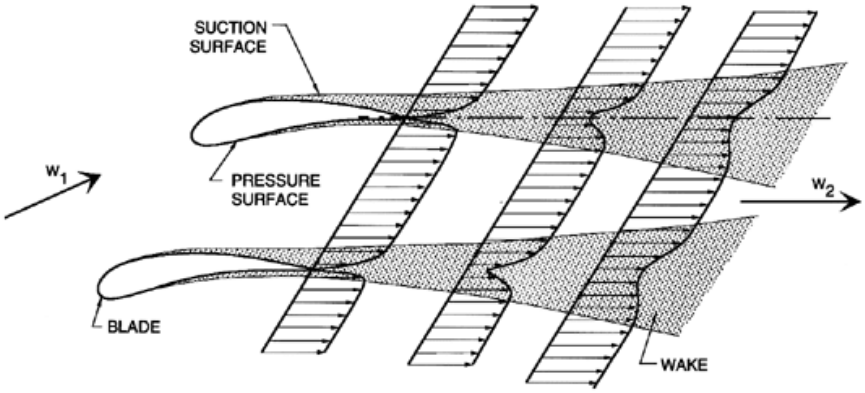

Figure 2.3: Schematic illustration of boundary layers forming on the blade surface and the wake forming afterwards, which is captured in the profile losses in loss models. Figure obtained from [2]

2.1.2. SECONDARY LOSSES

Secondary losses are generated by the interaction between the boundary layer and blade, which forms three-dimensional vortices, so-called horseshoe vortices as shown in figure 2.4. For short turbine blades, the horseshoe vortex can take up a major part of the blade surface, resulting in large losses. The secondary losses can account for almost 30%-50% of the total pressure loss according to Sharma and Butler [3]. The pressure loss generated by the secondary loss is calculated with an empirically determined equation given equation 2.3. In the equation, c/h denotes the chord length of the blade over the blade height, α and β are the metal angle and flow angle respectively. C_L is the lift coefficient of the blade and s/c is the pitch to chord ratio.

$$Y_{\text{secondary}} = 0.0334 \left(\frac{c}{h}\right) \left(\frac{\cos(\alpha_2)}{\cos(\beta_1)}\right) \left[\left(\frac{C_L}{s/c}\right)^2 \frac{\cos^2(\alpha_2)}{\cos^3(\alpha_m)} \right] \tag{2.3}$$

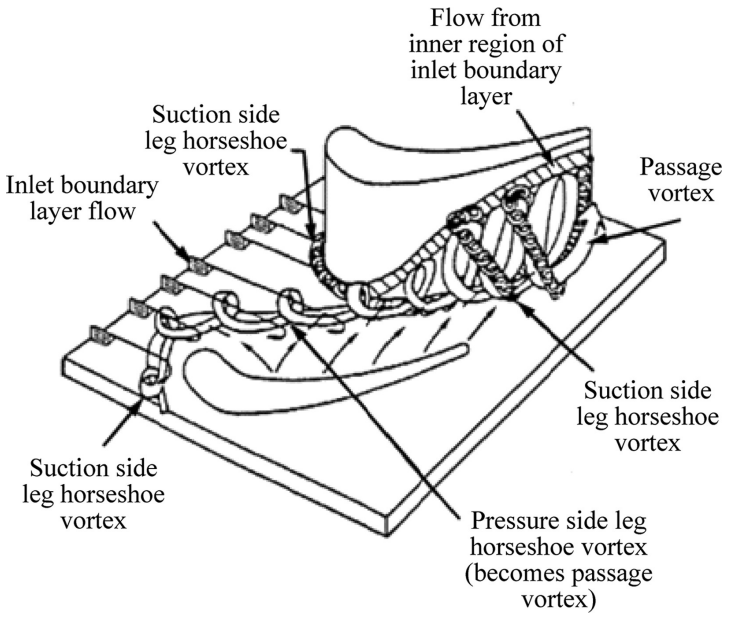

Figure 2.4: Schematic of the secondary flow vortex structure in an axial turbine, reproduced from [3].

2.1.3. CLEARANCE LOSSES

Clearance losses in axial turbines happen for both unshrouded and shrouded turbines, albeit with different leakage paths. In the case of an unshrouded turbine, there exists a gap between the suction and pressure side of the blade. Instead of following the blade contour, a small portion of the flow will leak from the pressure to suction side of the blade, where it mixes with the main flow and causes a disturbance. In the case of the shrouded turbines, a leakage flow exists from the front of the rotor blade over the shroud to the aft of the rotor blade, where it gets injected into the main flow as can be seen in figure 2.5. This injection into the main flow contributes most to the leakage loss [23], due to the viscous mixing between the flows. Dunham&Came developed a model in the form of equation 2.4 for the calculation of losses in axial turbines, where B is a constant and represents the difference between the shrouded (0.37) and unshrouded (0.47) case and k the actual clearance. k' Is the effective sealing clearance and is a function of the number of fins that are present for the labyrinth seal on the shroud, represented in equation 2.5.

$$Y_{\text{clearance}} = B\frac{c}{h}\left(\frac{k'}{c}\right)^{0.78}\left[\left(\frac{C_L}{s/c}\right)^2\frac{\cos^2(\alpha_2)}{\cos^3(\alpha_m)}\right] \tag{2.4}$$

$$k' = \frac{k}{(\text{number of fins})^{0.42}} \tag{2.5}$$

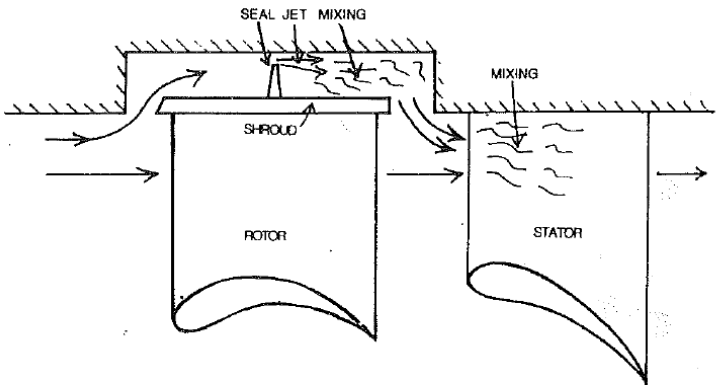

Figure 2.5: A schematic of the leakage path for shrouded axial turbines, reproduced from [4].

Denton [4] proposed a more physical based approach to calculating losses in turbines which is shown in equation 2.6. He achieves this by considering the generation of entropy (ζ) as a characteristic for lost work. His loss model for shrouded turbines laid the base of the focus for loss reduction associated with a shroud. Denton based his model on the mixing of a jet with the main flow, since he identifies the mixing of the flows as the main mechanism that causes the loss. Denton's model suggests that there are two sources responsible for the generation of entropy due to mixing. First, the mass flow rate ratio m_L/m_m, where m_L is the leakage rate over the shroud and m_m is the main flow through the turbine. Secondly the difference in flow angle between the incoming flow angle α_1 and the outgoing flow angle α_2, which serve as an approximation between the actual difference in the flow angle at the shroud outlet and the flow angle of the main flow after the rotor blade. Two methods to reduce clearance losses according to Denton his equation are thus: reducing the leakage flow and/or to reduce the difference in circumferential velocity through the application of turning vanes at the exit of the shroud. This means that the losses calculated by Denton's equation depend on accurately calculating the mass flow through the seal, for which he does not propose a satisfying relation that can include multiple sealing configurations.

$$\zeta_{\text{clearance}} = 2\frac{m_{\text{L}}}{m_{\text{m}}}\left(1 - \frac{tan(\alpha_1)}{tan(\alpha_2)} sin^2(\alpha_2)\right) \tag{2.6}$$

2.2. THEORETICAL BACKGROUND ON CLEARANCE LOSS MITIGATION

In the literature, several clearance loss mitigation techniques can be found. There are three different types of rotor tips: unshrouded, partially shrouded and fully shrouded, different techniques are applied to each tip. To clarify the division of different tips with their techniques a diagram has been constructed and can be seen in figure 2.6. All techniques have their own benefits and specific uses. In the sections below the techniques will be shortly discussed and at the end an explanation will be given why the focus of this thesis lies on shrouded turbines with seals.

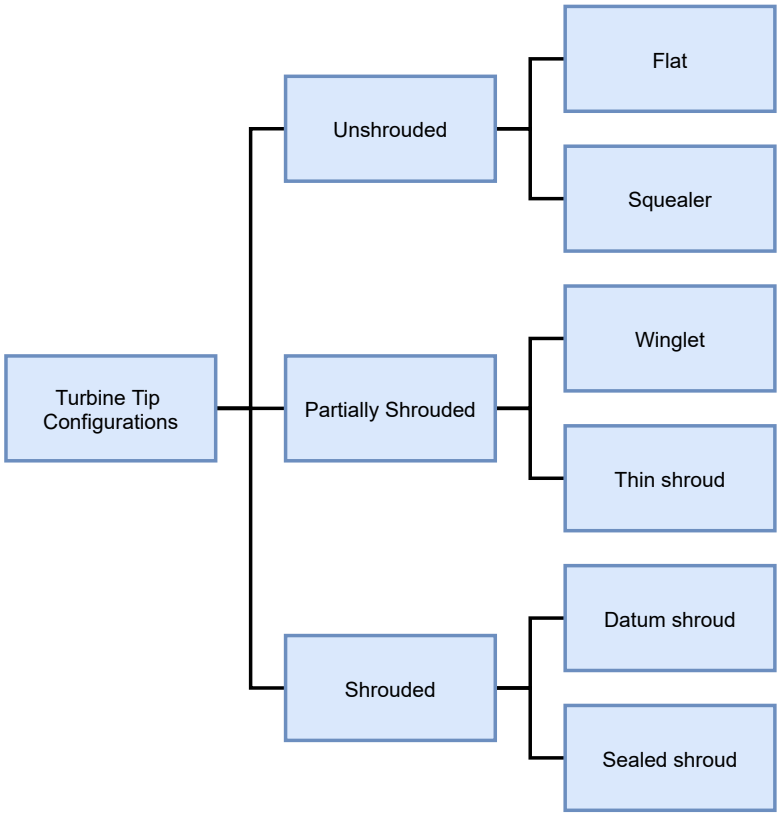

Figure 2.6: Diagram of the separate clearance mitigation techniques.

2.2.1. UNSHROUDED

Unshrouded turbines are a widely covered and well-understood class of turbines. The unshrouded turbines have no extension into the circumferential direction, they stay true to the original blade form of a turbine blade. This class can be further divided into the flat tip and squealer tip configuration.

FLAT TIP

The case of a flat tip is often covered in literature as it is the most basic turbine design, a side view of a blade cut-through is given in figure 2.7. As can be seen, no explicit leakage mitigation method is used to reduce leakage from pressure to the suction side of the blade. It is however, the easiest method to manufacture and therefore also the cheapest. Whenever leakage only plays a marginal role this method is used.

SQUEALER TIP

Squealer tips are extensions to the flat tip in the radial direction, as can be seen in figure 2.8. They exist on the pressure side, suction side or on the complete perimeter of the blade. Whether a squealer on the pressure side only works better than one on the suction side only is debated in the literature, although there is consensus that the complete squealer does have the best performance and that the performance is better compared to a flat tip [24]. The squealer tip acts as a labyrinth seal on top of the blade, where the flow first sees a contraction, expansion in the gap and then a contraction again. The benefits of the reduced mass flow rate outweigh the additional entropy generation due to mixing losses.

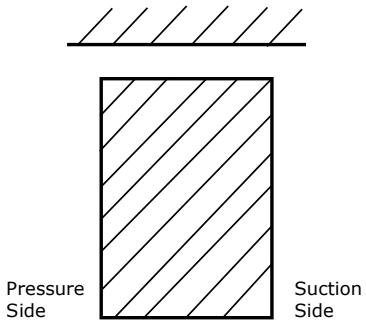

Figure 2.7: Schematic of a flat tip as viewed from a side cut.

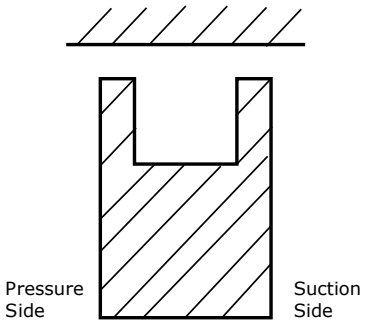

Figure 2.8: Schematic of a squealer tip as viewed from a side cut.

2.2.2. PARTIALLY SHROUDED

Partially shrouded turbines are turbines that incorporate an extension in the circumferential direction on top of the blade but do not fully cover the blade chord length or connect to the other blades to make a continuous ring. In this category, two types of configurations are found: winglets and thin shrouds.

WINGLETS

Figure 2.9 shows a schematic of a winglet tip configuration with extensions of the tip into the tangential direction. They have been investigated on the pressure, suction and on both sides. They act as a physical barrier for the flow to go from the pressure to the suction side. Coull et al. [25] mentions that efficiency gains can be achieved when comparing winglets to flat tips.

THIN SHROUD

Thin shrouds are placed on top of the rotor blades all along the circumference, an example of such a configuration is given in figure 2.10. However, in contrast to full shrouds they are only placed on the part where the highest amount of leakage normally would occur, physically prohibiting a flow in this region. Their main advantage is that they are lighter than the full shroud, which helps to reduce blade stresses, especially for longer blades [5].

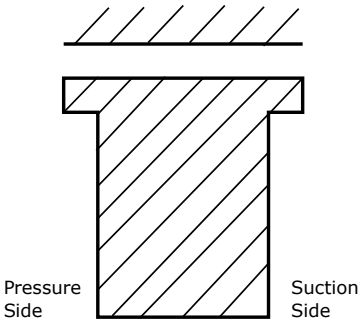

Figure 2.9: Schematic of a winglet as viewed from a side cut.

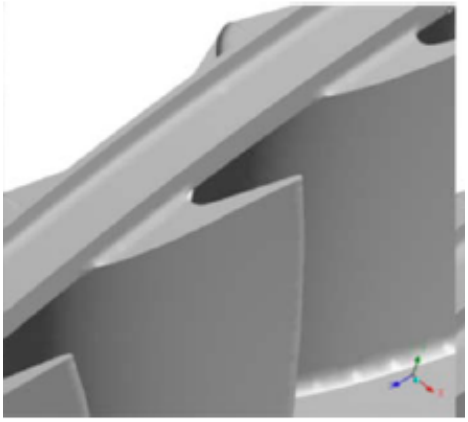

Figure 2.10: An example of a thin shroud on top of a turbine, obtained from Porreca et al. [5].

2.2.3. SHROUDED

Shrouded turbines are turbines that have a ring on top of the blades. This means that the blades are connected in the circumferential direction and cover the whole blade chord. There exist two types of configurations: datum shrouds and sealed shrouds.

DATUM SHROUD

The datum shrouded turbine is a turbine that has a ring on top of its blades. The ring physically prevents the fluid to flow from the pressure to the suction side, by creating a new flow path. The fluid now leaks from the front of the blade over the ring to the aft of the blade. Figure 2.11 shows a schematic of how such a datum shrouded turbine looks.

SEALED SHROUD

Apart from the datum shrouded turbine, which is just a ring placed on top of the rotor blades, seals have been placed on top of the shroud. The most widely applied seal is a labyrinth seal however, honeycomb/holepattern and more recently brush seals have also been applied. The ring prevents the flow physically from flowing from the pressure side to the suction side, but a new leakage path is formed from the front of the rotor to the aft. An example of a shrouded turbine sealed by several labyrinth seal configurations can be seen in figure 2.12.

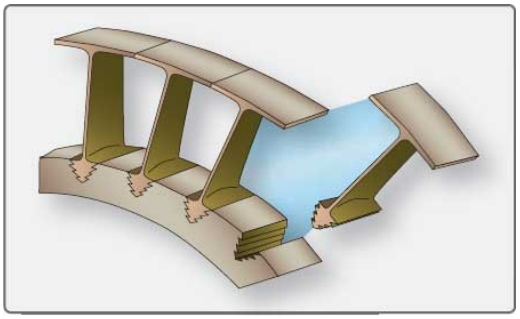

Figure 2.11: Schematic of shrouded turbine sealed by labyrinth seals

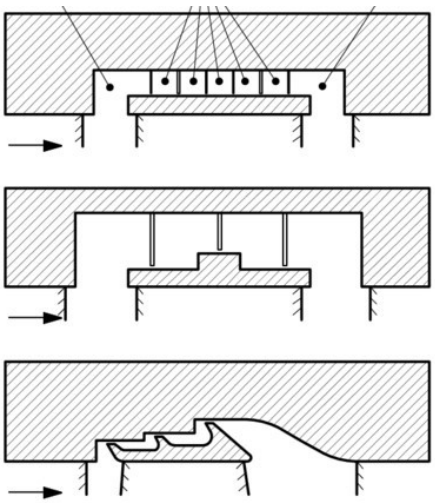

Figure 2.12: Schematic of shrouded turbine sealed by labyrinth seals

2.2.4. CHOSEN MITIGATION TECHNIQUE

Due to the small size of the turbine, most of the mitigation techniques become infeasible. For squealer tips and winglets, it is believed that they would be so small that they would either break or they just simply cannot be manufactured. The thin shroud solution poses a problem for to 3D printing of the turbine, as it would require support material to support the shroud printed in the middle of the blade.

The options of the flat tip, datum shroud and sealed shroud thus remain. From these three options, it is determined that the sealed shroud would have the most potential to reduce the clearance losses. It is easily implemented on an already datum shrouded turbine and would most likely give the lowest leakage rate, resulting in lower clearance losses.

2.3. ROTARY GAS SEALS

In the previous section, it is noted that the most promising method of reducing tip clearance in the small turbine of Dawn Aerospace is applying seals on top of the shroud. The seals that can be used on top of a turbine shroud are rotary gas seals. Rotary gas seals often compromise of non-contacting type of seals due to the high friction resistance that would occur when two materials rub against each other at high velocity. There exists a wide variety of seals that can be used in such applications. Seals are used to reduce/control secondary leakages, the reduction of those leakages can result in efficiency gains for the overall machine. The seals described above fall into the category of clearance seals, which have the problem that due to the clearance there will always exist a certain amount of leakage. Flitney [26] mentions clearance seals can be used for several reasons:

- Very low friction (none)
- High speed
- Absence of wear (maybe occasional rub contact during transients)

There exists a large variety of clearance seals. Since not all seals could be investigated in the limited amount of time of this thesis, three different seals are chosen. These seals are chosen because they are widely used, applicable to the turbine of Dawn Aerospace and are in line with current design trends. The seals to be investigated are an annular seal, labyrinth seal and brush seal. A short description of the seals and how the seal works is given for each seal in the sections below.

2.3.1. ANNULAR SEAL

An annular seal reduces leakage by ensuring a small clearance gap between the rotor and the stator. The gap has to be large enough for the rotor to vibrate without touching the stationary outer casing. This often means that the gap is larger than desired. The gas flows from the high pressure to the low pressure side through this gap. A schematic of an annular seal can be seen in figure 2.13. "The leakage is a function of the seal geometry, such as clearance, length, roughness and machine operating conditions such as the pressure differential and rotor speed."[27].

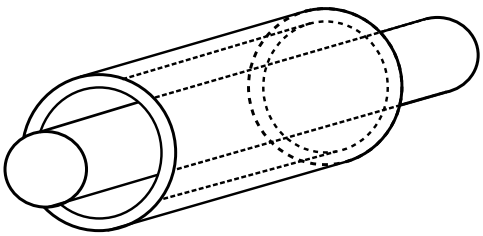

Figure 2.13: Schematic drawing of an annular seal

2.3.2. LABYRINTH SEAL

A labyrinth seal uses fins to disturb the fluid to flow through the leakage path. The fins have a small clearance with the shaft to minimize leakage flow, while still large enough to make sure no contact happens similarly to the annular seal. It is used to limit the mass flow rate between two areas with different pressures [10]. Due to the teeth, the flow is contracted and expanded at each fin reducing the pressure at each cavity. As the pressure

drop is the driving mechanism behind the mass flow rate, this means that the leakage reduces [26]. Figure 2.14 shows a schematic of a labyrinth seal. There are multiple configurations possible for the labyrinth teeth, such as interlocking, step and see-through. In this thesis, only a see-through configuration is considered, due to its simplicity and coverage in literature.

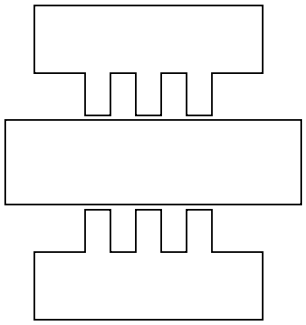

Figure 2.14: Schematic drawing of a labyrinth seal

2.3.3. BRUSH SEAL

Brush seals are made of 2 rings, one in the front and one in the back, with bristles in the middle joint by a weld. The bristles often touch the shaft in design condition, to minimize leakage. The backplate has a close clearance with the shaft to support the bristles. Brush seals have been used in turbomachinery for quite a while however, due to increasing research the applicability has been increased for both shaft and turbine shroud sealing. The bristles are arranged to have an angle with the shaft in the circumferential direction, which also means that the shaft can only rotate in one direction. The brush seals reduce leakage compared to the labyrinth seals and also take up less space in the axial direction. The other benefit is that the brush seal can deal with some shaft run-out better than other seals, as the bristles will not break, but rather buckle with the shaft and deform back into position [26]. The flow has to find a path through the bristles, causing a pressure drop and reduces leakage. There are several methods for the fluid to flow through the brush seal like rivering [28]. Rivering is the phenomenon where most of the flow pushes through a certain gap in the brush closing off the other near gaps by pushing the bristles together

Helm et al. [29] investigated the effect of brush seals on the upstream and downstream swirl flow. As when reducing the swirl the leakage flow becomes more aligned with the rotor blade outlet flow angle, which improves turbine performance due to reduced mixing losses. The preswirl tested ranges over 100 to 300 m/s, common velocities in turbines. They found out that brush seals can reduce the incoming swirl up to 10% as well as the ability from numerical codes which use porous medium models to match the experimental data presented.

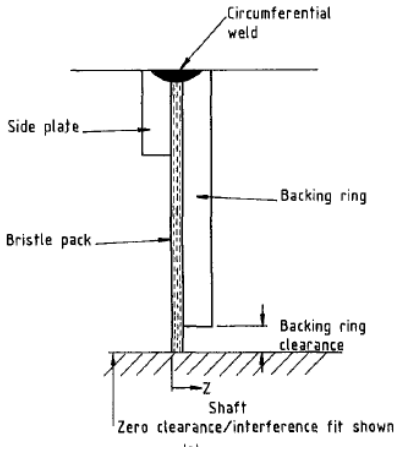

Figure 2.15: Schematic drawing of a brush seal taken from [6]

2.4. STATE OF THE ART & THESIS MOTIVATION

There exists a vast amount of research on turbine design and performance calculations. The performance calculations mainly date from the 1970-1980s, which uses empirical equations to predict efficiencies of turbines in a preliminary design stage. Together with the meanline design method for turbines, Dawn Aerospace developed a tool that can design a turbine stage. This design tool is based on the loss model of Dunham&Came and predicted that a major part of the turbine loss originates from clearances losses. A reduction of the clearance loss was limited due to the way the tool was set up, providing little design freedom and clearance loss mitigation.

While the loss methods did incorporate the use of a shrouded turbine and the application of fins on the turbine, it does not incorporate any other seal. Honeycomb, hole pattern and brush seals are just some of the seals that are being used more frequently in turbine shroud applications. In order to come to an optimum design, it is important to know the effect of each of these seals on the overall performance of the turbine. Several authors researched the effect of placing seals on top of the shroud. For example, Ma et al. [30] noted that brush seal research in the past has focused on being applied to the shaft, but it was not investigated if it also could reduce shroud leakage. They investigated the application of a brush seal on top of the shroud numerically and confirmed that it can improve the efficiency of the turbine. Another noteworthy investigation has been done by Yan et al. [31, 32] who investigated the honeycomb and hole pattern seal and the effects on turbine performance compared to a labyrinth seal. Yan showed that honeycomb only had better sealing performance than labyrinth seals when small clearances could be ensured and that honeycomb performed better than hole pattern seals. However, little information is available in the literature on the preliminary designs of seals for shrouded turbines.

In any engineering application, the designer strives to produce the optimal design for a given set of requirements. As could be seen in chapter 1 a gain in vehicle performance can be made if the turbine efficiency is improved. To reduce the cost of testing different designs, there is a need to generate a model that can assess performance in an early stage of the design process. This way numerous possibilities can be explored without all the costs of testing. Advanced numerical simulations, such as Computational Fluid Dynamics (CFD), are already a huge advantage and are starting to replace a number of early tests in a development program. The downside of such advanced models is that it takes an extensive amount of pre-knowledge to set-up the simulations and they still take too much computational time to be used in the preliminary design of complex systems. Therefore, a simpler model would be the preferred tool for the preliminary design.

2.5. RESEARCH GOALS AND RESEARCH QUESTIONS

In chapter 1 it was shown that the spaceplane of Dawn Aerospace would see an increase in performance when the efficiency of the turbine is increased. It also mentioned that clearance losses of the turbine would likely be large as the gap clearance is relatively large compared to the blade height. Section 2.2 showed that the most promising technique to reduce clearance losses is to apply sealing methods to a shrouded turbine. Thereafter, three candidate clearance seals for further investigation are covered in section 2.3. In section 2.4 it could be seen that seals used on top of the shroud are moving away from labyrinth seals to more elaborate seals such as brush seals. In literature, no existing turbine loss model can be found that includes these new seals or offers the modularity to include them into the existing clearance loss.

Seals are well investigated in literature and almost for every used seal there exist equations to calculate the leakage through them. The loss model of Dunham&Came, used by Dawn Aerospace, does not accept the leakage rate calculated with seal leakage equations as an input to predict turbine losses. That is why the clearance loss of Denton is introduced in section 2.1.3. Based on these observations the following research objective is formulated:

1. **Research objective:** *To reduce clearance losses arising in small axial turbines by developing a model that uses seal leakage calculations in combination with existing turbine loss models to predict clearance losses for shrouded turbines whom incorporate seals.*

To achieve the research objective a research question is formulated. The research question is subdivided into multiple sub-questions. The research question is as follows:

Primary research question: *To what extend can existing seal leakage calculation methods be used with existing loss models to improve the prediction of turbine efficiency at a preliminary design stage?*

To help to formulate an answer to this research questions the following sub-questions (**SQ**):

- **SQ1:** How can the seal leakage equation be combined with existing loss models?

- **SQ2:** How accurate can seal leakage equations predict the amount of leakage flow through a shroud seal configuration?
- **SQ3:** How accurate are the efficiency predictions of the combined seal leakage equation and existing leakage models?
- **SQ4:** What is the best configuration for the small turbine of Dawn Aerospace in order to reduce leakage rate through the shroud?

3

METHODOLOGY

Chapter 2 discussed the scientific context and theoretical bases of this thesis. It identified the gap in the literature on the preliminary loss calculation for a shrouded turbine that uses new sealing systems. While showing that the usage of seals on top of shrouds is a promising solution to reduce clearance losses. The previous chapter also presented the objective of this thesis to investigate how seal leakage equations can be combined with existing loss models to more accurately predict losses of shrouded turbines that make use of a seal.

In this chapter, the steps taken to achieve the research objective are outlined. In the end, a model is developed utilizing seal leakage equations combined with the clearance loss model of Denton. It also discusses how the new clearance model can be used by the meanline design program in order to generate new turbine designs.

At first, a reference turbine similar to the turbine of Dawn Aerospace is discussed in section 3.1. In section 3.2 the seal leakage equations are discussed for the annular, labyrinth and brush seal respectively. This is followed by the setup of numerical models in the commercial software ANSYS 19.2R for the seals in section 3.3. The analytical and numerical models are both validated in section 3.4 while only the analytical models are verified in section 3.4, because the commercial software is assumed to be verified already. Section 3.5 goes into details of the development of the new shroud model. The chapter continues to explain the integration of the model into the meanline design method in section 3.6. In section 3.7 the setup of the numerical model for the turbine CFD is discussed for unshrouded and shrouded turbines. Section 3.8 presents the comparison between the loss model of Dunham&Came and the numerical model for an unshrouded and shrouded turbine as a validation case.

3.1. REFERENCE TURBINE

The actual turbine of Dawn Aerospace is proprietary, therefore the development of the shroud leakage model has been done on a reference turbine. The reference turbine is similar but uses slightly different design parameters compared to the actual turbine. The design parameters used for this turbine are given in table 3.1. Throughout, this chapter whenever blade or turbine geometries are given it is of the reference turbine. It will be used to indicate trends and to conceptually explain phenomena that are observed during this study. In the table λ, ψ and ϕ are the duty coefficients and are the degree of reaction, stage loading coefficient and flow coefficient, respectively.

3.2. SEAL ANALYTICAL LEAKAGE MODELS

To calculate leakage through seals several options are available. The first simple analytical equation was developed already in 1908 for a labyrinth seal [33]. This equation needs geometrical inputs and pressures at the inlet and the outlet of the seal to calculate the leakage. Later the development of the more sophisticated bulk flow model (BFM) started to calculate rotordynamic behaviour of the seals. For this, the mass flow rate was required and more detailed analytical equations, often iterative, were developed. In the recent decade, with the rise of powerful computers, computational fluid dynamics (CFD) are more frequently used to analyse leakage through seals. Even though CFD can be accurate, depending on the simplifications made, the time it takes to set-up and run the simulation still limits the usefulness as a preliminary design tool. In this thesis

Table 3.1: Reference turbine design parameters

Parameter	Value [unit]
λ	0.39 [-]
ψ	3.4 [-]
ϕ	0.8 [-]
Design speed	76000 [rpm]
Aspect ratio	1 [-]
Zweifel number	0.8 [-]
mean radius	0.021 [m]
Inlet pressure	110 [bar]
Pressure ratio	1.16 [-]
Mass flow rate	2.0 [kg/s]

it is opted to utilise the BFM to predict the leakage rate through different seals, primarily because the BFM uses more geometrical inputs making it more adjustable for a wider range of seals. In addition, it provides intermittent pressures and the BFM can be extended to solve rotordynamic problems. It provides the user with all these benefits while still being easy to use and not computationally demanding thus making them a suitable tool for the preliminary design phase. In this chapter the development of the bulk flow models for annular, labyrinth and brush seals will be discussed. Once the models are developed and verified they will be validated against experimental data from the literature in 3.4.

The first bulk flow model was developed to solve a rotordynamic problem with the main engine turbopumps of the space shuttle [34]. Rotordynamics is the study concerned with vibrations of rotating shafts, these vibrations can become excessive when the rotor passes a certain critical speed. To calculate the rotor dynamic coefficients introduced by seals, used to analyse rotor stability, a perturbation analysis was developed. This included a zeroth-order term, which calculates pressures and leakage at eccentric positions, and a first-order term, which calculates the rotor dynamic coefficients when the shaft moves in an elliptical orbit [7, 35].

The perturbation analysis is used to linearise the governing equations for a small motion around the centered position. Equation 3.1 shows an example of the perturbation variables on the non-dimensionalised pressure, where p is the non-dimensional pressure and ϵ the perturbation parameter defined as the eccentricity ratio e/Cr or distance of shaft from eccentric position over the nominal seal clearance [35, 36]. Because this work is only concerned with leakage through the seals, the coded bulk flow models only incorporate the zeroth-order solution.

$$p = p_0 + \epsilon p_1 \tag{3.1}$$

The bulk flow model for the annular seal is discussed in 3.2.1. Section 3.2.2 goes into detail on an iterative method for calculating leakage rates through labyrinth seals. The solution procedure for the brush seal is discussed in 3.2.3.

3.2.1. ANNULAR SEAL

The bulk flow model chosen for an annular gas seal from the literature is the bulk flow model developed by C.C. Nelson [7, 36]. The bulk flow model described by Nelson can be used for both straight and tapered annular seals, with either smooth stators and rotors or rough ones (for example honeycomb stators and a smooth rotor). Nelson makes use of Hir's lubrication equations [37] to simulate the wall roughness. The following paragraphs will elaborate on the solution procedure.

In order to solve the zeroth order the initial conditions denoted with the subscript 0 the variables p_0, ρ_0, u_{z0} and $u_{\theta 0}$ need to be determined, which are located at the seal inlet. Where p_0 is the pressure, ρ_0 is the density of the gas, u_{z0} the axial velocity and $u_{\theta 0}$ is the circumferential velocity. Nelson uses an iterative procedure which begins by guessing an initial value for the Mach number, M_0. Equation 3.2 and 3.3 can be used to calculate the pressure and density respectively.

$$p_0 = \frac{1}{\left[1 + (\gamma - 1)(1 + k_l) M_0^2\right]^{\frac{\gamma}{\gamma - 1}}} \tag{3.2}$$

$$\rho_0 = \frac{\left[1 + \frac{(\gamma-1)M_0^2}{2}\right]}{\left[1 + \frac{(\gamma-1)(1+k_l)M_0^2}{2}\right]^{\frac{\gamma}{\gamma-1}}} \tag{3.3}$$

In equations 3.2 and 3.3 γ is the specific heat ratio of the gas and k_l is the entrance loss coefficient with an initial guessed value of 0.1 as suggested by Nelson. With the initial density and pressure known the axial velocity can be calculated (equation 3.5) as soon as the pressure coefficient P_c is calculated according to equation 3.4. The subscript a is used as an indication for the user specified boundary conditions.

$$P_c = \frac{P_a}{(R\omega)^2 \rho_a} \tag{3.4}$$

$$u_{z0} = \sqrt{\frac{M_0^2 \gamma p_0 P_c}{\rho_0}} \tag{3.5}$$

Where in equation 3.4 P_a is the reservoir pressure, ρ_a the density of the gas at the reservoir, R the radius and ω is the rotational speed of the rotor. With p_0, ρ_0, u_{z0} and $\overline{C}$ the axial Reynolds number can be calculated (equation 3.6). $\overline{C}$ is the nominal clearance of the annular seal with respect to the inlet and exit clearance, $(C_{in} - C_{out})/2$. The μ in the denominator is the viscosity of the working fluid.

$$Re_{a0} = \frac{2\rho_0 u_{z0}(R\omega)\overline{C}}{\mu} \tag{3.6}$$

With the Reynolds number a new approximation is made for the entrance loss coefficient, which can be seen in equation 3.7.

$$k_l = \sqrt{\frac{5.3}{log_{10}(Re_{a0})}} - 1 \tag{3.7}$$

For a single guess Mach number, the entrance loss coefficient is repeatedly calculated until the difference between k_l for consecutive runs is lower than a convergence limit, set by the designer. When the Reynolds number reaches 200000 k_l is set to 0. Together with the user-specified preswirl ratio ($u_{\theta 0}$) all initial conditions are known and the solution procedure for the zeroth-order governing equations can be started.

The zeroth-order governing equations for a tapered annular seal as derived by Nelson are given in equation 3.8 to equation 3.11 and consist of the continuity, momentum and energy equations. In the equations z is the dimensionless seal coordinate in the axial direction and l is the dimensionless seal length defined as the seal length over the shaft radius.

$$\rho_0 u_{z0} \frac{\partial h_0}{\partial z} + \rho_0 h_0 \frac{\partial u_{z0}}{\partial z} + u_{z0} h_0 \frac{\partial \rho_0}{\partial z} = 0 \tag{3.8}$$

$$-\frac{P_c}{\rho_0 l}\frac{\partial p_0}{\partial z} = \frac{u_{z0}}{c h_0}[f_{s0} + f_{r0}] + \frac{u_{z0}}{l}\frac{\partial u_{z0}}{\partial z} \tag{3.9}$$

$$0 = \frac{1}{c h_0}[u_{\theta 0} f_{s0} + (u_{\theta 0} - 1) f_{r0}] + \frac{u_{z0}}{l}\frac{\partial u_{\theta 0}}{\partial z} \tag{3.10}$$

$$0 = u_{\theta 0}\frac{\partial u_{\theta 0}}{\partial z} + u_{z0}\frac{\partial u_{z0}}{\partial z} + \frac{P_c \gamma}{\rho_0(\gamma-1)}\left(\frac{\partial p_0}{\partial z} - \frac{p_0}{\rho_0}\frac{\partial \rho_0}{\partial z}\right) + \frac{l(u_{\theta 0} - 1) f_{r0}}{c h_0 u_{z0}} \tag{3.11}$$

Equation 3.10 makes use of the friction coefficient for the rotor, f_{r0} and for the stator f_{s0}, which can be calculated using equation 3.13 and eqution 3.12 respectively. The coefficients n_s, m_s and n_r, m_r are coefficients for Hirs' turbulent lubrication equations on the stator and rotor respectively. They are a measure for the roughness of the surface.

$$f_{s0} = \frac{n_s}{2}\left(u_{\theta 0}^2 + u_{z0}^2\right)^{\frac{m_s+1}{2}} (2Re_{co})^{m_s} \tag{3.12}$$

$$f_{r0} = \frac{n_r}{2}[(u_{\theta 0} - 1)^2 + u_{z0}^2]^{\frac{m_r+1}{2}}(2Re_{co})^{m_r} \tag{3.13}$$

In literature several authors give deviating values for Hir's lubricant coefficients for a smooth surface. The table 3.2 below gives the exact values found for smooth surfaces in the literature, this results in $-0.25 \leq m \leq -0.1691$ and $0.0396 \leq n \leq 0.066$.

Table 3.2: Lubrication coefficient for smooth surface

source	n	m
Nelson [7]	0.03976	-0.1691
Childs [38]	0.066	-0.25
Dawson [9]	0.0586	-0.2170

The governing equations are numerically integrated in the axial direction with the Euler integration method. The Euler integration method solves partial differential equations by taking the previous value and adding the derivative of that equation divided by the number of steps specified by the designer, this is mathematically expressed in equation 3.14.

$$y_n = y_{n-1} + \frac{1}{N-1}y'_{n-1} \tag{3.14}$$

At the current state, there are 4 equations and 5 unknowns, but $\frac{\partial h_0}{\partial z}$ is a simple linear function when taper is applied and zero if the seal is straight. When taper is applied this equation can easily be calculated before the governing equations making it 4 equations and 4 unknowns. The four equations that are solved are: pressure, density, axial flow velocity and circumferential flow velocity. As the partial differential equations are dependent on each other they are solved in matrix form, the matrix can be seen in appendix A. After integrating the governing equations a check is done whether the pressure calculated at the outlet is within a convergence limit of the pressure specified by the designer as a boundary condition at the outlet. If the calculated pressure is higher than the boundary condition the Mach number is increased and if the calculated pressure is lower the Mach number is decreased. This is continued until the pressure boundary condition is reached. Or the exit Mach number reaches 1 and the pressure ratio of the calculated pressure at the outlet and specified pressure at the outlet is higher than the critical pressure ratio.

To calculate the mass flow through the seal the area of the seal outlet is used in combination with the density and calculated velocity as described in equation 3.15.

$$\dot{m} = \rho A u_{z0} \tag{3.15}$$

3.2.2. LABYRINTH SEAL

There are several methods to calculate leakage through a labyrinth seal. A widely used model is the bulk flow model described by Childs [35]. The model by Childs makes use of an iterative method to calculate the leakage, which is computationally expensive compared to analytical approaches which do not iterate.

The bulk flow model used for labyrinth seals in this thesis is described by Childs [35]. His methods is a one control volume approach that uses a leakage model. The zeroth-order leakage through a see-through labyrinth seal is described by equation 3.16, and the leakage equation Childs suggests from Neumann [39] is calculated with equation 3.17 and is iteratively solved for each cavity. In the equation $\dot{m}$ is the mass flow rate and i is the chamber of the seal.

$$\dot{m}_{i+1} = \dot{m}_i = \dot{m}_0 \tag{3.16}$$

$$\dot{m}_i = \mu_{1i}\mu_2 A\sqrt{\frac{P_i^2 - P_{i+1}^2}{RT}} \tag{3.17}$$

Where μ_1 is the kinetic energy carry-over coefficient (KE) and μ_2 is the flow coefficient. Childs suggest using the equation defined by Neumann [39] for flow through an orifice for μ_1 and the equation described by Chaplygin for μ_2. The equations can be found in table 3.3 and table 3.4 for μ_{1i} and μ_2 respectively. What combination of these coefficients can be best used in the leakage equation has to be proven during the validation in Chapter 3.4.

Table 3.3: Kinetic energy carry-over coefficient equations found in literate.

Source	equation	parameter
Hodkinson	$\mu_{1i} = \sqrt{\frac{1}{1-\left(\frac{NT-1}{NT}\right)\left(\frac{Cr/L}{(Cr/L)+0.02}\right)}}$	-
Vermes	$\mu_{1i} = \sqrt{\frac{1}{(1-\alpha_i)}}$	$\alpha_i = \frac{8.52}{\frac{L}{Cr}+7.23}$
Kurohashi	$\mu_{1i} = \sqrt{\frac{1}{1-2\alpha_i+\alpha_i^2}}$	$\alpha_i = \frac{(Cr/L)}{(Cr/L)\mu_2+tan(\theta)}$
Neumann	$\mu_{1i} = \sqrt{\frac{NT}{(1-\alpha_i)NT+\alpha_i}}$	$\alpha_i = 1-(1+16.6Cr/L)^{-2}$

Table 3.4: Flow coefficient equations or constants found in literature.

Source	Equation	Parameter
Chaplygin	$\mu_2 = \frac{\pi}{\pi+2-5s_i+2s_i^2}$	$s_i = \left(\frac{P_i}{P_{i+1}}\right)^{\frac{\gamma-1}{\gamma}} - 1$
Eser	$\mu_2 = 0.716$	-

To clarify all variables from table 3.3 and table 3.4, figure 3.1 and figure 3.2 are used. Figure 3.1 shows the control volume approach followed by Childs. It shows the location of m_i and that P_i in equation 3.17 is the pressure in the current gap while P_{i+1} is the pressure at the next gap. In figure 3.2 r is the rotor radius used in combination with Cr, the clearance, to calculate the ring area between the fin and the wall on the other component. L is the spacing between the consecutive fins in the labyrinth seal and θ, the angle at which the flow underneath the tooth expands into the next cavity. NT used in the equations represents the number of fins used in the labyrinth seal.

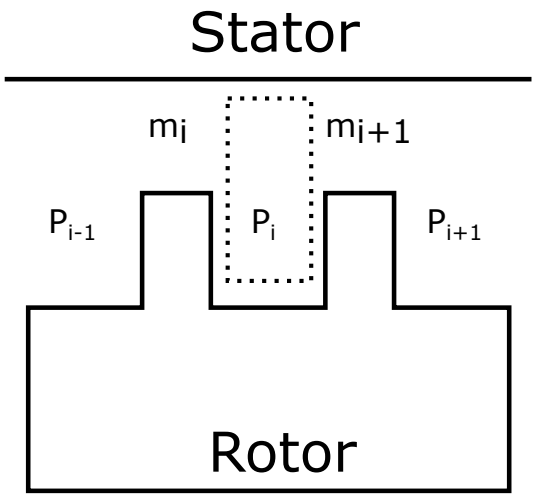

Figure 3.1: Control volume of the Childs BFM model.

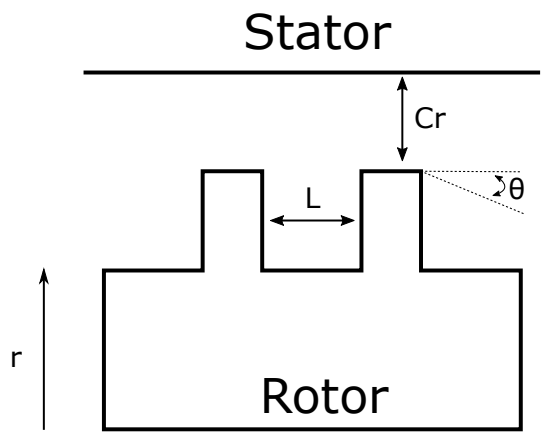

Figure 3.2: Labyrinth seal with BFM input parameters indicated.

In order to solve the bulk flow model the approach by Eldin [10] is followed, which iterates upon the leakage rate until the outlet pressure boundary condition is satisfied. The procedure starts with assuming a linear pressure drop for each cavity. Those pressures are used with equation 3.17 to calculate the mass flow rate for each cavity. From those values the minimum leakage is chosen as the initial guess to solve the bulk flow model.

With the guess mass flow rate and the user-specified inlet pressure (P_i) the pressure in the next cavity (P_{i+1}) can be calculated. However, it is near to impossible to manipulate equation 3.17 in such a way that the pressure at the next cavity is of explicit form. In order to solve this, an error function is made, such that the mass flow rate and known pressure can be filled in and a pressure guess for the next cavity can be iterated upon until the value is close to zero. This is continued until the pressure at the exit is calculated and compared to the boundary condition value. If the calculated pressure is higher than the boundary condition the mass

flow rate is increased and when it is lower the mass flow rate is decreased until convergence is reached.

$$f_{\text{error}} = \dot{m}^2 - \left(\mu_{1i} \mu_2 A \sqrt{\frac{P_i^2 - P_{i+1}^2}{RT}} \right) \tag{3.18}$$

However, when the flow through the seal is choked Fliegner's equation 3.19 is used to calculate the mass flow rate, which assumes the pressure in the last cavity (P_{NC}) to be equal to the critical pressure for choking.

$$\dot{m} = \frac{0.510 \mu_2}{\sqrt{RT}} P_{\text{NC}} A \tag{3.19}$$

$$\dot{m} = \frac{A P_{\text{in}}}{\sqrt{RT}} \sqrt{\frac{1 - \left(\frac{P_{\text{out}}}{P_{\text{in}}}\right)^2}{NT - ln\left(\frac{P_{\text{out}}}{P_{\text{in}}}\right)}} \tag{3.20}$$

3.2.3. BRUSH SEAL

Brush seals comprise of a series of bristles in a housing which rubs on the shaft. The housing of the bristles has a close clearance with the shaft to support the bristles. The flow needs to find a path through the bristles, which makes it harder for a gas to flow through it. The most popular method to calculate leakage through a brush seal is the porous medium method and is described below.

The porous medium model described here is discussed by Chew et al. [6]. The name derives from the fact that this paper assumes that the bristle pack can be modelled as a porous medium. A fluid flow through a porous medium can be simulated with resistance laws, see equation 3.21. Where a and b are the inertial and viscous resistance coefficients respectively. Furthermore, p is the pressure, z is the axial distance and U is the velocity of the fluid flow.

$$-\frac{dp}{dz} = a\mu U + b\rho U^2 \tag{3.21}$$

To calculate the resistance coefficients Chew first calculates the porosity of the seal, which according to Neef et al. [40] can be described as equation 3.22. V_{solid} is the volume taken up by the bristles and V is the total volume of the porous region. It can be written with the geometrical parameters according to equation 3.23. Where d is the bristle diameter, N is the bristle density in bristles per meter, l the axial length of the brush seal and ϕ the lay angle of the bristles with the shaft.

$$\epsilon = 1 - \frac{V_{\text{solid}}}{V} \tag{3.22}$$

$$\epsilon = 1 - \frac{\pi d^2 N}{4 l \sin(\phi)} \tag{3.23}$$

According to Chew a and b can be calculated as in equation 3.24 and equation 3.25. In the equation α and β are empirically determined constants, ϵ is the porosity as calculated in equation 3.23 and d is the bristle diameter.

$$a = \alpha \frac{80(1-\epsilon)^2}{d^2 \epsilon^3} \tag{3.24}$$

$$b = \frac{\beta}{2} \frac{1-\epsilon}{d\epsilon^3} \tag{3.25}$$

For α and β Chew suggests $\alpha = 1$ and $\beta = 2.32$, whom are empirically determined by Kay and Nedderman [41]. However, a range for those values exists in literature and are often adjusted to calibrate the model on the experimental data. For completeness additional values from literature are given in table 3.5.

After integration equation 3.21 can be written as equation 3.26, where L is the length of the brush seal and ΔP is the pressure drop over the seal. With inlet and outlet pressure know, there can be iterated over the velocity until the pressure drop is equal to that of the boundary conditions. The velocity can be used in combination with the mass flow rate equation 3.15 to obtain the mass flow rate through the seal.

$$\frac{\Delta P}{L} = a\mu U + b\rho U^2 \tag{3.26}$$

Table 3.5: Values for α and β found in literature

source	α	β
Chew [6] (Kay & Nedderman)	1	2.32
Axstream	0.7075	1.42
Pugachev (Proster) [14]	1	2.32
Neef [40]	0.83375	2.34
Ergun [42]	1.875	3.5

3.3. SEAL NUMERICAL LEAKAGE MODELS

In this section both the development of 2-dimensional and 3-dimensional numerical models will be described. The development of the 2D seal is used as a stepping stone to the 3D numerical model, it also provides insight if a reduced-order approach would work for seal design. The development of the numerical model of the seal as a standalone provides confidence about the development of a numerical model on top of the shroud at a later stage. The CFD program ANSYS R19 is used for all numerical simulations.

Numerical models need fewer assumptions than empirical correlations as they take into account all geometrical parameters and resolve the flow field in 2D or even 3D. If modelled correctly the numerical model is expected to give results close to experimental data. This means that a good and detailed numerical model can be used to validate the analytical models. Section 3.3.1 discusses the boundary conditions and other parameters for the CFD-setup. The sections 3.3.2, 3.3.3 and 3.3.4 describe the setup of the annular, labyrinth and brush seal respectively. The final section, section 3.3.5 highlights the mesh sensitivity study for each modeled seal.

3.3.1. MODEL PARAMETERS

Basic settings for the numerical simulation which are used throughout all seal designs, for instance boundary conditions, are presented here to avoid repetition. The working fluid in most of the seals is air and is modelled as an ideal gas. Surface roughness is not taken into account as it was often not specified in the validation data, thus walls are set to smooth with the no slip condition. At the inlet of the seal total pressure and total temperature boundary conditions are used while a static pressure boundary is used for the outlet. These boundary conditions are chosen as they are known to be robust. The simulations performed are of a steady-state nature, which means that they can be simulated with the Reynolds Average Navier Stokes (RANS) equation. The k-omega Stress transport (k-ω SST) model of Menter [43] is used as a turbulence model. This model can cope with adverse pressure gradients and is often used in turbine design as will be explained in chapter 3.7. An overview of the most important parameters can be found in table 3.6.

Table 3.6: Boundary conditions used in the seal numerical models

Boundary Condition	Setting
Inlet	Total Pressure, Total Temperature
Outlet	Static Pressure
Energy Equation	Total Energy
Walls	No slip, smooth walls
Turbulence model	k-ω SST
Calculation scheme	High resolution

3.3.2. ANNULAR SEAL

The annular seal is a relatively simple and low-cost seal, where a small clearance between a stator and a rotor allows a leakage flow through the seal. The construction of the 2D and 3D numerical model are very similar to each other as a 2D case can be rotated around the z-axis, which is also the rotational axis.

The 2D numerical model cannot deal with the rotational velocity of the wall in the actual annular seal, as this would make the simulation three dimensional. This does mean that the influence of the rotational speed, which is more significant for annular seals than for other seals, is not taken into account for the 2D case. Due to the simple geometry of the seal the mesh has been created directly in ICEM. To ensure that the y+ is lower

than one, exponential growth has been applied along the height of the seal. Figure 3.3 shows the mesh at the inlet of the seal, which is continued along the length of the seal.

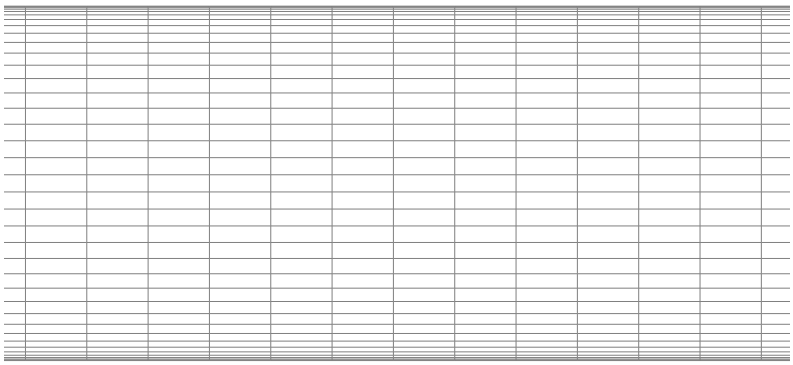

Figure 3.3: A zoomed in view of the mesh of the annular seal.

3.3.3. LABYRINTH SEAL

The labyrinth seal is a sealing method that makes use of several fins to hold a tight gap between the stationary and rotating wall. The subsequent larger gaps cause an expansion of the fluid, which dissipates mechanical energy causing a total pressure drop. The multiple smaller pressure drops result in less of a driving mechanism for the fluid to flow from the high pressure zone in front of the seal to the low pressure zone at the aft of the seal.

The 2D case takes into account all geometric parameters (except curvature), including fin thickness and cavity depth who are omitted in the BFM. For the case of the labyrinth seals the mesh will be a bit more complicated, as cavities and sharp corners are present. Again, the 2D case neglects the rotational velocity of the rotor.

To mesh the fluid domain ICEM is used, to properly mesh the labyrinth and each cavity the mesh is divided into several blocks. Figure 3.4 shows where the mesh is cut into separate blocks and 5 distinct positions are present. The first block in figure 3.4 is part of the inlet and outlet section at the radial height of the fin, it is cut with block 2 such that a fine mesh near the walls underneath the fins can be realised. Block 3 is created underneath the fin such that the mesh can be refined on either side of the fin in blocks 1, 2, 3 and 5. Block 5 is again copied, and thus also block 4, to ensure that the mesh near the walls underneath the fin can be refined. The mesher automatically connects the nodes at the borders of each block to align with each other.

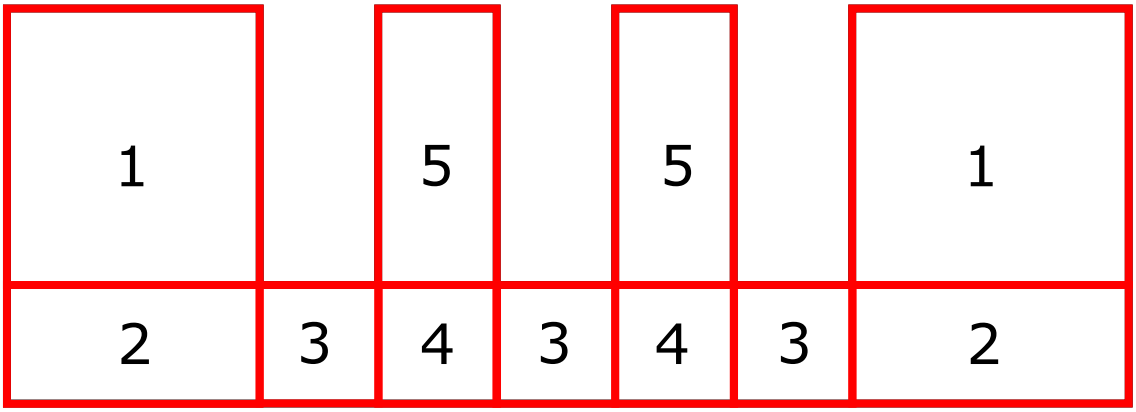

Figure 3.4: Schematic of the labyrinth seal on where the different blocks are located.

The total mesh looks like figure 3.5 and close attention is paid to the sharp corners for which figure 3.6 shows a zoomed-in version. The mesh near the walls is small enough to ensure that the y+ value is lower than 1.

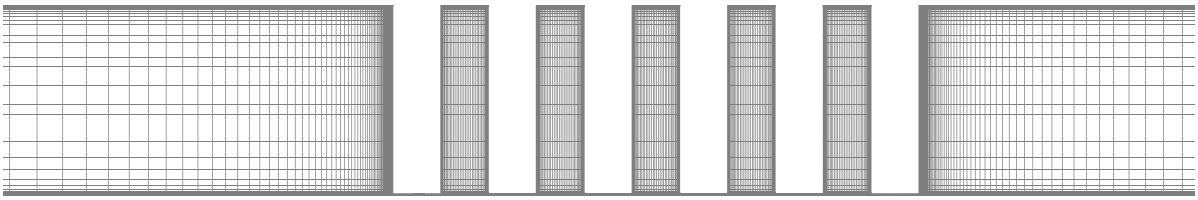

Figure 3.5: An example mesh used for the labyrinth seal cases.

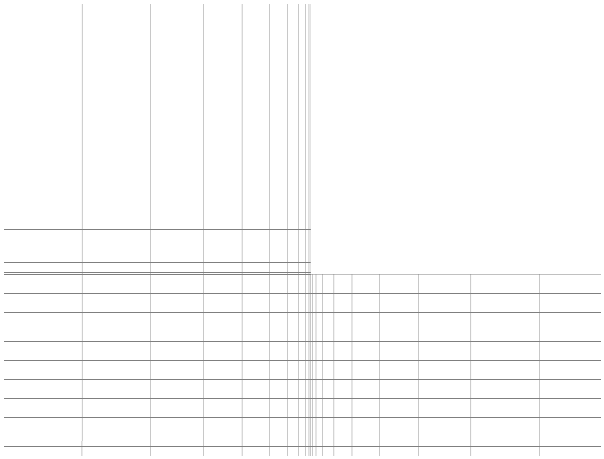

Figure 3.6: Zoomed in version of the example mesh around the fin corners.

3.3.4. BRUSH SEAL

Brush seals in CFD can be modelled in two ways: modeling the individual bristles or using the porous medium approach. The first approach includes all physical effects that can be seen in a brush seal, it would need to be coupled to a mechanical solver to calculate bristle deflections. This requires very large mesh sizes and computational power. The latter option uses a similar approach as the analytical leakage model does in section 3.2.3, where it replaces the bristle pack with a porous medium. This method is less universal as it relies to some extent on calibration with experimental data, although some empirical relations give good estimates on the viscous (a) and inertial (b) resistance coefficients as used in equation 3.21 [40]. Neef et al. [40] mention that when the porous medium approach is correctly set up and good estimates for a and b are used, the porous medium approach provides sound results for the leakage through a brush seal.

The geometry of the brush seal is dictated by the papers to which the CFD will be validated. Important geometrical parameters for the brush seal are the rotor diameter, size of the front and aft backing ring and bristle thickness. The parameters are indicated in figure 3.7 with D_r, D_{fbr}, D_{abr} and L respectively. The figure

also shows that the fluid domain is split into 3 different sections, 1) the volume underneath the front backing ring, 2) the porous medium domain replacing the bristle pack and 3) the volume underneath the aft backing ring. Gresham [44] found that when analysing leakage rate through a brush seal it is enough to only model the three parts of the brush seal described above, reducing the number of nodes necessary. Thus for the validation of the brush seal CFD only the area under the brush seal is modelled.

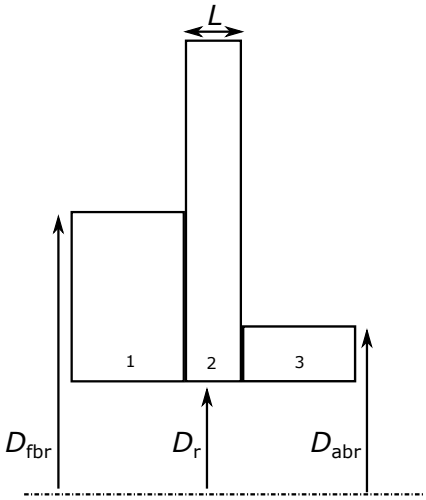

Figure 3.7: Schematic of the brush seal with important parameters. 2) denotes the porous medium region in the CFD model.

Figure 3.8 shows the numerical model for the brush seal tested by Carlile [12]. The mesh in figure 3.8 is fine near the walls and near sharp corners in order to deal with boundary layers and separation to keep the y+ lower than 1.

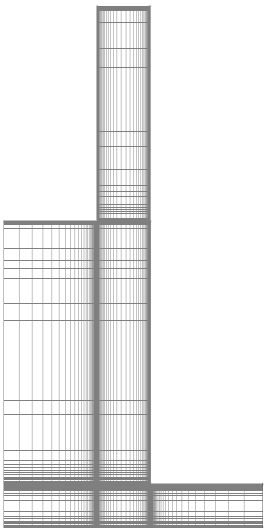

Figure 3.8: Mesh used for Carlile brush seal.

In this thesis the porous medium approach is used to model the bristle pack in brush seals, as it is shown to be suitable by earlier authors, it is simple to set up and computationally less demanding than the full bristle simulation. In CFX one can assign the bristle pack as a porous medium and input porosity and the resistance coefficients. These resistance coefficients work in a similar way the coefficients work in the one dimensional model of Chew, although CFD uses them in all directions. Pugachev [14, 45] gives a clear overview of how to model the brush seal in CFD and shows that when the right coefficients are used the results are in agreement with experimental data. Several authors, of which most noteworthy Pugachev and Ergun, have investigated

the usage of the porous medium model in CFD to calculate leakage rates. They concluded that the porous medium model can be used, but proper calibration is necessary. The calibration of the model can be done either by tweaking the brush seal thickness (Pugachev mainly focuses on this) or by finding the inertial and resistance coefficient which best fits the CFD data to the experimental data. The following paragraph takes a look at both methods.

To find the brush thickness Pugachev uses equation 3.27 to calculate the theoretical minimum thickness of the brush seal in combination with the actual thickness of the brush seal in an unused state. In the equation d is the bristle diameter, N is the brush density in the circumferential direction and ϕ the lay angle of the bristles with the shaft. The calibrated value of the brush thickness lies somewhere in between the two thickness values and gives good agreement with experimental data.

$$b_{\mathrm{b}}^{min} = d + \frac{\sqrt{3}d}{2}\left(\frac{dN}{cos\phi} - 1\right) \tag{3.27}$$

Another option is using the inertial and viscous resistance coefficient that best matched the experimental data from the literature. Tweaking the model at this stage to match literature exactly would prove of little to no use when a different brush seal would be placed on top of the actual turbine, which might have different resistance coefficients. Instead matching the trend line and giving reasonable agreement is much more important. To do this Pugachev and Ergun both provide empirically relations to calculate a and b. They propose different values for α and β, but also differ in their views of using anisotropic coefficients, that is different α and β being used in different directions. Pugachev uses different coefficients depending on the direction, while Ergun uses the same coefficients for all directions. To calculate the coefficients in all directions equations 3.28 and 3.29 can be used, where the subscript k denotes the direction in axial, radial and circumferential. Pugachev suggests the value of 1, 0.4ϵ (porosity) and 1 for α respectively and uses 2.32, 0, 2.32 for β [14], see table 3.7 for a clearer overview. Ergun [42] uses 1.875 for α and 3.5 for β.

$$a_k = 80\alpha_k \frac{(1-\epsilon)^2}{\epsilon^3 d^2} \tag{3.28}$$

$$b_k = \frac{\beta_k}{2}\frac{1-\epsilon}{\epsilon^3 d} \tag{3.29}$$

Table 3.7: α and β in the axial, radial and circumferential direction as specified by Pugachev [14].

	α (Pugachev)	β (Pugachev)	α (Ergun)	β (Ergun)
axial	1	2.32	1.875	3.5
radial	0.4ϵ	0	1.875	3.5
circumferential	2.32	2.32	1.875	3.5

However, to be able to compare the CFD cases with the analytical model it was opted to use the brush thickness specified in the validation data and not tweak the brush thickness here. This means that the inertial and viscous resistance coefficients of Pugachev and Ergun will be used as explained above. The validation in chapter 3.4 determines which of the two will be used.

3.3.5. MESH SENSITIVITY STUDY

In order to make sure that the solution of the CFD simulation are mesh independent and no unnecessarily large mesh is used, a mesh sensitivity study is performed. The mesh sensitivity study is done for all seal numerical models in the same manner. First, the mesh is made mesh independent for the 2D case, where special attention is paid to corners and the mesh near walls, making sure that $y+ < 1$. For the 3D case, the 2D mesh is chosen that was first mesh independent and the number of nodes in the circumferential direction is increased, until it again becomes mesh independent. In each respective section, a plot of the mesh sensitivity study is presented to show at what point the solution becomes mesh independent for both the 2D and 3D case.

ANNULAR SEAL

The 2D mesh sensitivity study for the annular seal can be seen in figure 3.9, as stated above it was ensured that the y+ of all cases was kept below 1. The figure shows the total number of nodes on the x-axis and

the mass flow rate calculated by CFD on the y-axis. This solution is deemed mesh independent when the total mesh size reached 12000 nodes, 60 in the y-direction (set to bi-exponential) and 200 in the x-direction (bi-geometric). This mesh will be used for the mesh sensitivity study on the 3D case, where the nodes are changed only in the circumferential direction. From figure 3.10 it can be seen that the mesh becomes mesh independent when 20 nodes in the circumferential direction are used, resulting in a total amount of nodes of 240000.

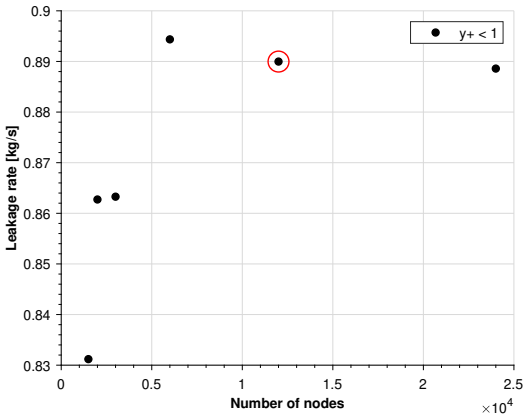

Figure 3.9: Results of the mesh sensitivity study of the 2D annular seal case, all y+ values are kept below 1.

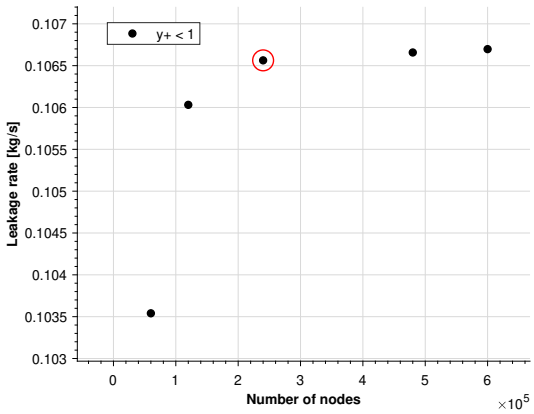

Figure 3.10: Results of the mesh sensitivity study of the 3D annular seal case, all y+ values are kept below 1.

LABYRINTH SEAL

The mesh sensitivity for the labyrinth seal is performed on Gamal A1, this labyrinth seal has 2 fins thus 1 cavity section. Whenever labyrinth seals with more fins are simulated their cavities are set with the same number of nodes. Figure 3.11 shows the mass flow rate calculated by the 2D CFD as a function of the number of nodes used. It can be seen that the mesh does not influence the leakage rate much after approximately 11000 nodes however, still some variation can be seen at a higher number of nodes. To be certain that the mesh would play no/minor role in the solution the mesh of 28698 nodes is chosen. This mesh used a 60x60 node block for the cavity section (block 5 in figure 3.4) and a 30x30 nodes for the mesh block under the fins (block 3).

Figure 3.12 shows the predicted CFD leakage rate for nodes of the 3D case with the labyrinth seal. Again, the 2D mesh that is determined to be mesh independent is chosen and the nodes in the circumferential direction are increased. Due to the already relatively large number of nodes needed for the 2D case the 3D case is only rotated to 1/8th of a circle. The total number of nodes needed for the 3D case to be mesh independent is 475156, which boils down to 15 nodes needed in the circumferential direction.

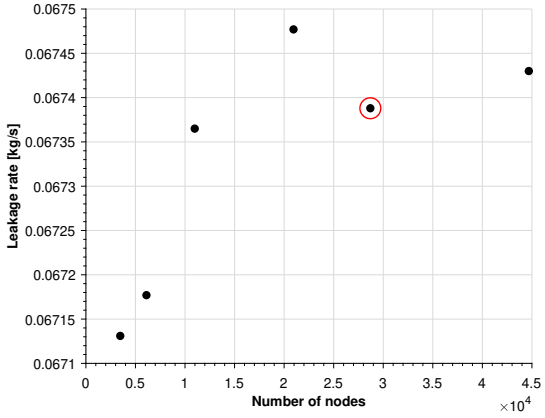

Figure 3.11: Results of the mesh sensitivity study of the 2D rush seal case, all y+ values are kept below 1.

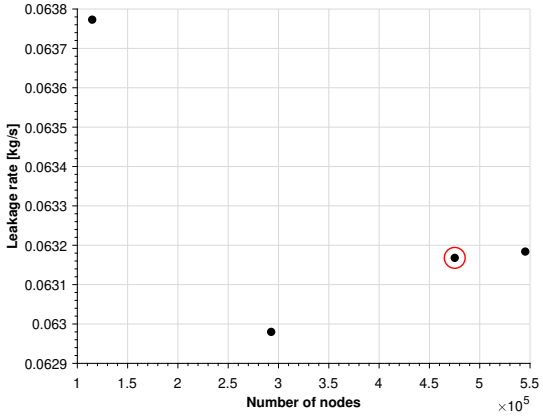

Figure 3.12: Results of the mesh sensitivity study of the 3D brush seal case, all y+ values are kept below 1.

BRUSH SEAL

The brush seal mesh sensitivity analysis is executed on the brush seal investigated by Bayley. Figure 3.13 shows the leakage rate calculated by CFD as a function of the number of nodes used in the simulation for the 2D case. It shows that 6801 nodes are needed for a mesh independent solution. Figure 3.14 shows the mesh sensitivity performed for the 3D case, which consisted of a quarter circle with periodic boundary conditions. It uses the chosen mesh from the 2D case and the number of nodes in the circumferential direction is increased. After 147126 the solution becomes mesh independent, which means that 20 nodes are needed in the circumferential direction.

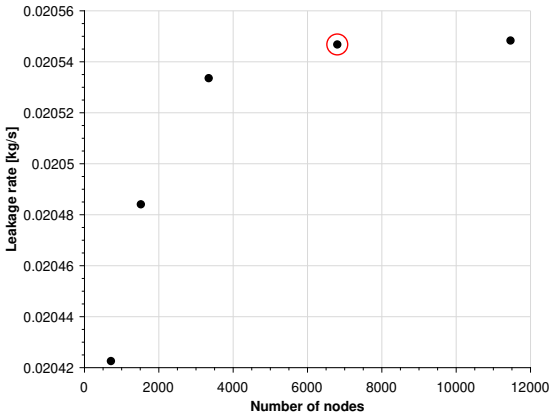

Figure 3.13: Results of the mesh sensitivity study of the 2D brush seal case, all y+ values are kept below 1.

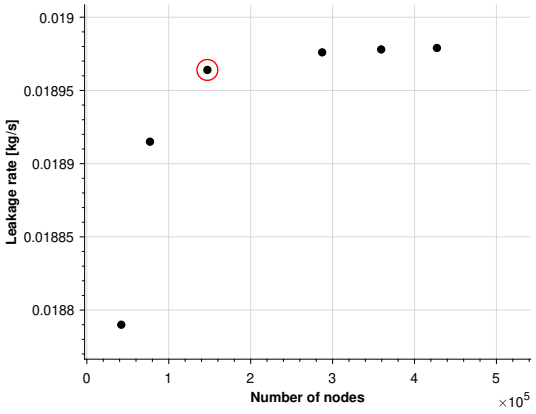

Figure 3.14: Results of the mesh sensitivity study of the 3D brush seal case, all y+ values are kept below 1.

3.4. LEAKAGE MODELS VERIFICATION AND VALIDATION

Before the previously presented numerical seal models and bulk flow models can be used, it is important to validate them with experimental data. The experimental data used here to validate the numerical models is taken from extensive test campaigns documented in the literature. The data contained all the necessary information needed to appropriately model the seals. It is also of importance to verify the coded bulk flow models. The state of computational fluid dynamics has been widely accepted to be sufficient to give detailed information on the flow behaviour of a multitude of fluid dynamic problems, including seal design, so no verification of the CFD program is presented.

Section 3.4.1 presents the verification and validation of the annular seal for both the smooth stator and rotor case and the roughened (honeycomb) stator and smooth rotor case for the BFM. The CFD of the annular seal is only done in the smooth stator and rotor case, as the rougehned stator and smooth rotor case is very time-consuming. In section 3.4.2 the BFM and CFD results are discussed for the labyrinth seal, where the validation is done on seals investigated by Eldin [10]. The brush seal model validation for both BFM and CFD is done in section 3.4.3, which also includes the verification of the coded BFM.

3.4.1. ANNULAR SEAL

As explained above, first the validation is done only for the BFM. Later the validation of both the BFM and numerical model is done.

VERIFICATION

The bulk flow model of the annular seal written during this thesis is verified against the model outputs presented by Nelson [7]. Nelson used his developed model to investigate the effect of the taper ratio on an annular seal. The clearance at the exit is kept constant at 0.2540, the inlet and outlet pressures used are 34 Mpa and 26.4 Mpa respectively. The rotor had a radius of 7.282 mm and the length of the seal was 2.527 mm. Figure 3.15 shows the leakage rate calculate by the model of the author and the values presented by Nelson against the taper ratio. It can be seen that some discrepancy between the two models exists. The discrepancies can be explained by various reasons, i.e. Nelson does not mention what integration method he uses to solve the equations nor does he mention what convergence criteria were used. Nevertheless, the close com-

parison and the exact same trend being followed give confidence that the model is implemented correctly by the author.

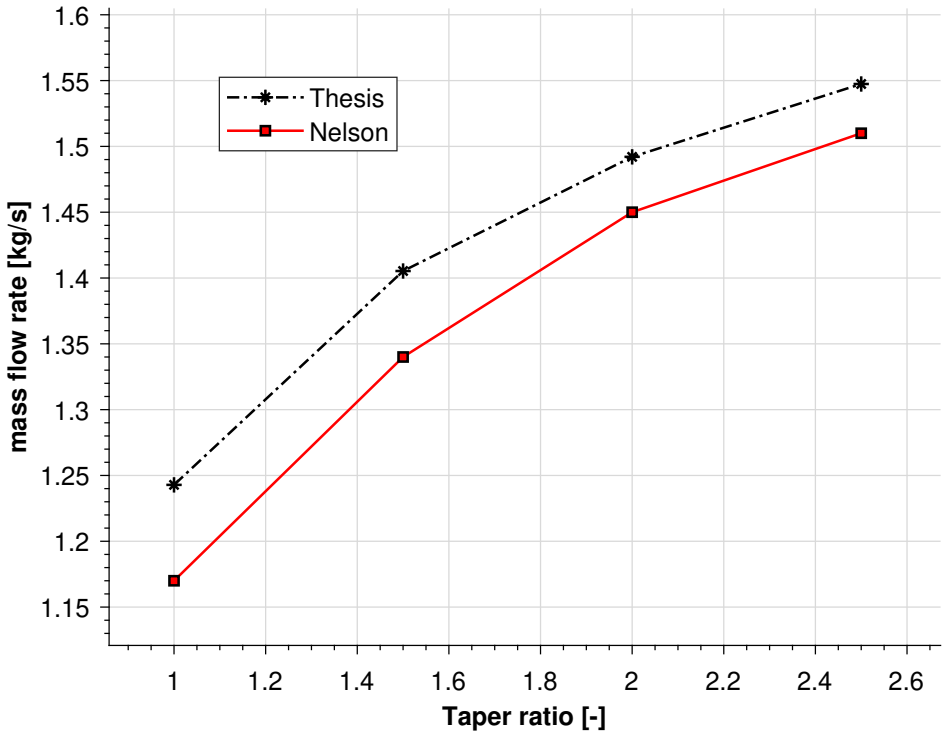

Figure 3.15: Verification of the model created by the author of this thesis, compared against the model outputs of Nelson [7]. The mass flow rate is plotted against the taper ratio

VALIDATION

In addition to the data Nelson [8] used to validate his bulk flow model, experimental leakage data of Dawson [9] is used. It has to be noted that Dawson only gives the leakage for a honeycomb stator, although he also investigates the smooth stator rotor combination. Fortunately, he provides the friction coefficients needed for the honeycomb stator, such that his data can be compared with Nelson's BFM. Honeycomb stators are much more elaborate to model in CFD and since they are outside of the scope of this thesis, no CFD model has been made for the experiments presented by Dawson.

Figure 3.16 shows the comparison between experimental data of an annular seal obtained by Nelson et al. [8] and predictions of the developed annular seal bulk flow model. The annular seal has an inner radius of 76.2 mm, a length of 50.8 mm and an inlet and outlet clearance of 0.7366 mm and is thus straight. The working fluid used in the test is air at 305 K, the inlet pressure is varied from 1.7 to 5.3 bar and the exit pressure is kept at 1 bar. The rotational speed of the shaft is 8000 rotations per minute. In figure 3.16 the leakage mass flow rate is plotted versus the pressure ratio of the seal, which is the ratio between inlet and outlet pressure. It can be seen that the bulk flow model follows a linear trend as the pressure ratio increases, this is in agreement with the experimental data. However, the bulk flow model under predicts the mass flow rate and the deviation increases with pressure ratio.

The 2D and 3D CFD results are also presented in figure 3.16, so a comparison between BFM, CFD and experimental data becomes possible. It can be seen that 2D and 3D CFD both follow a similar linear trend. The average deviation in mass flow rate between the 2D and 3D CFD case is 1.2%, where the 2D case predicts the higher mass flow rate. When comparing CFD to the experimental data a deviation from the upwards curve can be seen. Compared to the experimental data there is an agreement in linear trend for the pressure ratio up to 4. At the higher pressure ratios the experimental data trend curves upwards, as noted above. The CFD overpredicts the mass flow rate through the annular seal.

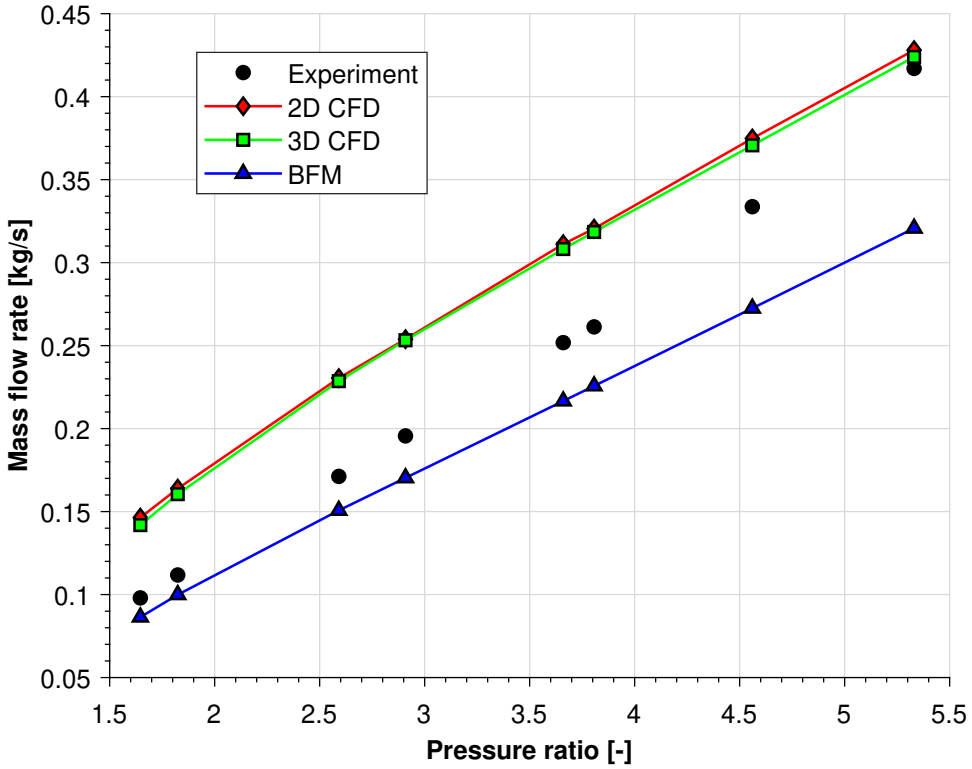

Figure 3.16: Comparison between experimental data,CFD and BFM for the annular seal presented by Nelson [8]

The average error between the BFM and experimental data is 14.5%, although some large differences exist at higher pressure ratios. At a pressure ratio of 1.7 the error is 11.8%, while at a pressure ratio of 5.3 the difference is 23.1%. For the development of a preliminary design tool an average error of 15% is deemed satisfactory. For CFD the average error compared to the experimental data is 26%, here again there exist large differences in the error varying with pressure ratio. At the lowest pressure ratio of 1.7 the deviation is 44.7%, while at a pressure ratio of 5.3 the error is 1.7%. A reason why the CFD cases have a larger error might be that the walls of the seals are set to smooth in the setup of the numerical model.

Comparing the leakage rate through the seal of the sophisticated numerical model and the bulk flow model, it is satisfactory to see that both predict a linear trend. The difference in the absolute values is substantial, where CFD predicts more than a 50% higher mass flow rate than the BFM at the lower pressure ratio, but is of less importance than the trend.

As mentioned in section 3.2.1 the bulk flow model for the annular seal uses empirically determined values to predict the effect of roughness on the leakage flow. The values used in the above comparison are given by the author who did the experiments and it might be for that reason that the BFM predicts the leakage rate of the annular seal to this extent. For the coefficients it holds that the higher the value, the rougher the surface is. With a rougher surface the leakage will reduce due to larger boundary layers. This is also a reason why annular seal surfaces get artificially roughened by using honeycomb and hole pattern seals for instance.

In figure 3.17, figure 3.18 and figure 3.19 experimental data obtained by Dawson [9] on an annular seal is compared to the predicted values from Nelson his bulk flow model for annular seals. In the figures the leakage mass flow rate through the seal is plotted against the pressure ratio, each plot represents a different rotational speed and the different coloured lines indicate different inlet pressures. The seal investigated by Dawson has an inner radius of 57.15 mm, a length of 85.7 mm and an inlet and outlet clearance of 0.19 mm. The working fluid through the seal is air at a temperature of 302 K, the inlet pressures used are 6.9 (red line), 12.1 (blue line) and 17.1 bar (black line) and the outlet pressures are 40% and 50% of the inlet pressures. The lubrication coefficients presented by Dawson are $n = 0.0586$ and $m = -0.2170$ for the smooth rotor and $n = 0.0785$ and $m = -0.1101$ for the honeycomb stator. It can be seen that the model overpredicts leakage in all cases, but the flow rate increase for increasing pressure ratio is covered by the BFM.

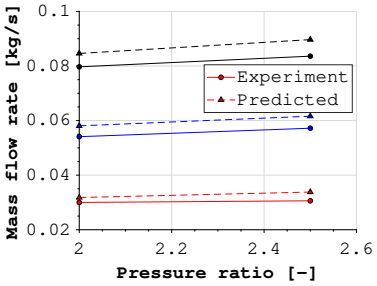

Figure 3.17: Comparison between annular bulk flow model and experimental test data performed by Dawson [9] on a honeycomb stator seal, at 10200 rpm

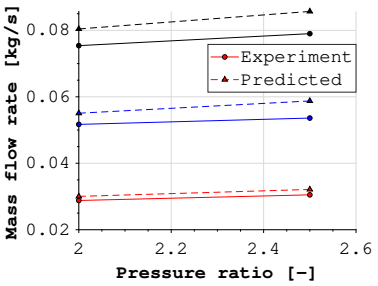

Figure 3.18: Comparison between annular bulk flow model and experimental test data performed by Dawson [9] on a honeycomb stator seal, at 15200 rpm

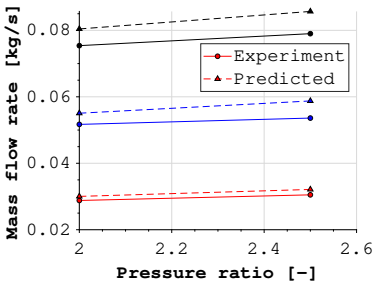

Figure 3.19: Comparison between annular bulk flow model and experimental test data performed by Dawson [9] on a honeycomb stator seal, at 20200 rpm

The error occurring at a pressure ratio of 2 is around 6% for all cases and at a pressure ratio of 2.5 increases to 10%. Although honeycomb seals are not discussed further in this thesis, these graphs show that when appropriate friction coefficients are used several types of annular seals can be modelled.

3.4.2. LABYRINTH SEAL

First the verification of the BFM for the labyrinth seal will be given, followed by the validation of the BFM and numerical model against experimental data.

VERIFICATION

The verification of the labyrinth seal is done on the results of Eldin [10] his implementation of Childs leakage model. The inputs used are an inner radius of 50.9 mm and a radial fin clearance of 0.1016 mm with the rotor. The labyrinth seal has 6 fins all spaced 3.2 mm apart from each other. In his model he used the leakage equation of Neumann, the kinetic energy carry over coefficient of Vermes and no flow coefficient. Figure 3.20 shows the leakage rate in kg/s against the pressure ratios over the seal. It can be seen that the model constructed in this thesis closely matches that of the model of Eldin. The small variation that arises can be attributed to the fact that the values from Eldin are read from a graph, it might also be possible a difference in convergence is a cause of the slight error.

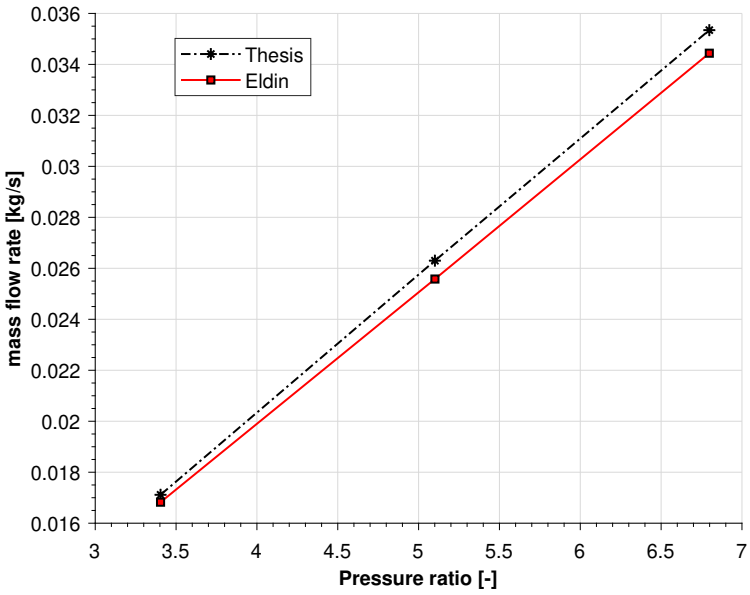

Figure 3.20: Verification of the labyrinth seal BFM coded by the author compared against the BFM developed by Eldin [10].

VALIDATION

The BFM for the labyrinth seal will be validated against experimental data presented by Eldin [10], who investigated several labyrinth seal configuration and compared them to his own bulk flow model. Eldin proposes to use the equation of Vermes as the Kinetic energy carry over coefficient and no equation, thus 1, for the flow coefficient. In addition to the data presented by Eldin, experimental data of Picardo et al. [46] will be used to validate the developed BFM. Picardo et al. [46] investigated large labyrinth seals with up to 20 teeth, for pressures up to 70 bar.

Figure 3.21 shows the comparison of the BFM with several combinations of CE and KE coefficients, notated as Childs and Eldin, and analytical equations, Martin and Hodkins, compared to experimental data of seal set A1 of Eldin. Seal set A has an inner radius of 50.95 mm and a radial fin clearance of 0.1524 mm. The 1 after the A means that 2 fins are used in this experiment and the spacing between the fins is 6.2 mm. The working fluid through the seal is air at 293 K, the inlet pressure ranges from 1.5 to 6.9 bar and the outlet pressure is taken constant at 1 bar. The leakage mass flow rate in kg/s is plotted against the pressure ratio over the seal in the figure. All models predict linear trends, albeit with different slopes. This clearly indicates that there is a need to establish which model is a suitable one to use.

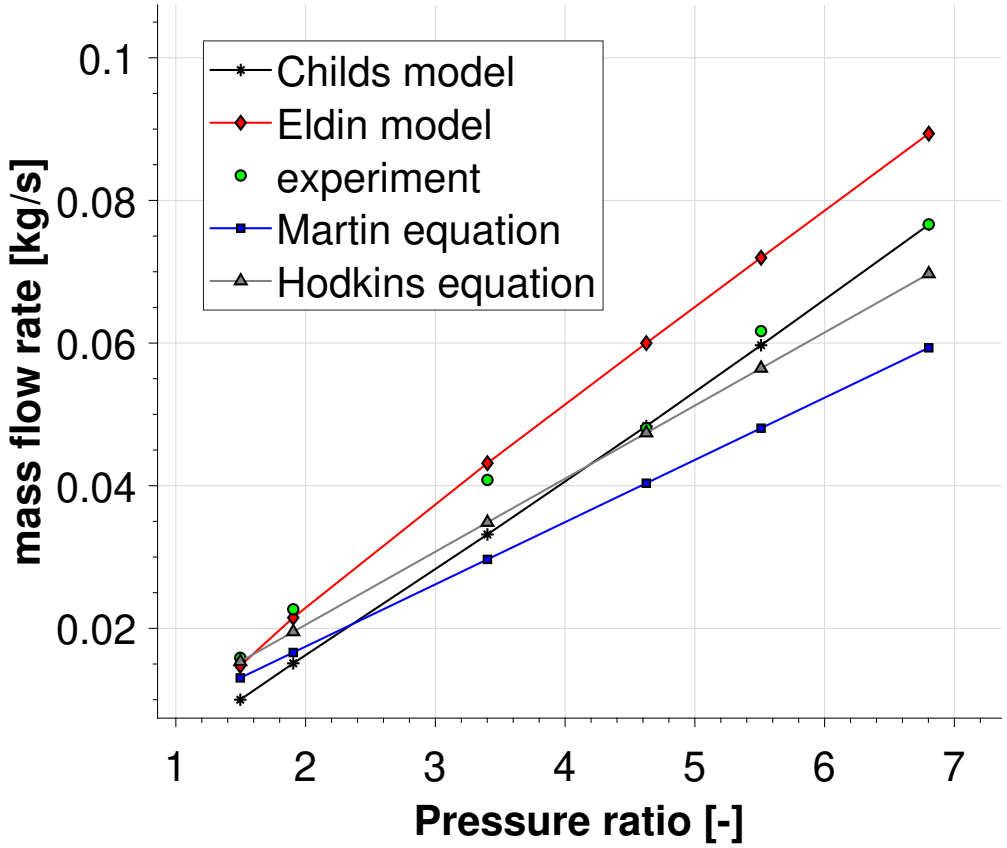

Figure 3.21: Place holder for: Comparison between experimental data and analytical equations (including BFMs with different KE and CF coefficients

In appendix B a comparison is made for all possible coefficient combinations implemented in the BFM to a wide set of labyrinth seal experimental leakage data. From the analysis, the low pressure seal A tested by Eldin was best predicted when only the leakage equation of Neumann was used, however for seal B the best combination would be a flow coefficient of Chaplygin in combination with the leakage equation of Neumann. Several authors, including Eldin, note that the KE or CF coefficient might be dependent on another flow metric. There has been some investigation into using the Reynolds number [47, 48], but are not common practice. Finding a model that works in all cases equally well is outside the scope of this thesis and thus only the current presented equations presented in section 3.2.2 are used.

Figure 3.22 and 3.23 compare experimental data for seal A1 and B12 from Eldin with predictions from the numerical and bulk flow model. Seal B12 of Eldin has an inner radius of 50.9 mm and a radial fin clearance of 0.1016 mm with the rotor. The seal uses 6 fins which are spaced 3.2 mm from each other. In the case of figure 3.22 the numerical model does not follow a straight line but rather curves downwards at higher pressure ratio's. The BFM and experimental data both do follow a straight line. There is a slight offset between 2D and 3D, indicating that 2D models can predict leakages through labyrinth seals. The BFM follows the linear trend of the experimental data closely, albeit at a slightly steeper slope. It has to be noted that the flow coefficient and kinetic energy coefficient were chosen such that the lowest mean error occurred.

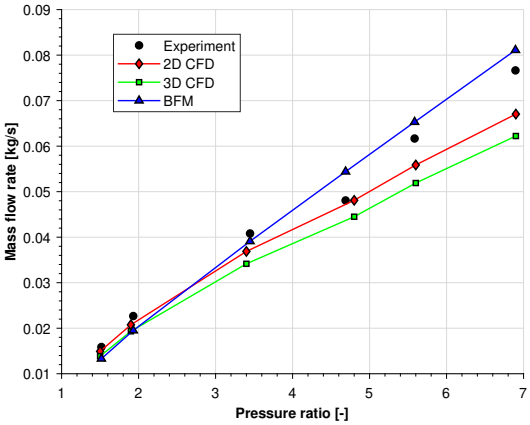

Figure 3.22: Labyrinth seal experimental data compared to the BFM, 2D and 3D CFD.

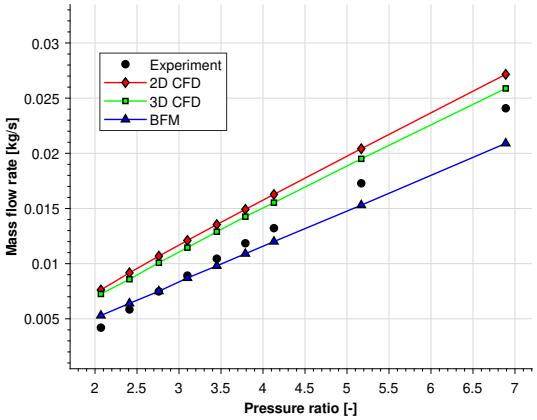

Figure 3.23: Labyrinth seal experimental data compared to the BFM, 2D and 3D CFD.

For the second labyrinth seal investigated, the numerical models do follow the linear trend that is in the experimental data, see figure 3.23. Again, only a slight offset between 2D and the 3D case can be seen when looking at the data from the numerical model. The BFM in this case follows the linear trend again, but only with a more moderate slope.

The comparison of the models with the experimental data shows that both BFM and numerical models are capable of predicting trends and absolute values for labyrinth seal configurations. When using BFM however, the influence of the chosen flow coefficient and kinetic energy coefficient contributes significantly to the slope and absolute values of the model. Therefore, the designer will have to pay attention to whether the model predicts reasonable values. Fortunately, numerical models do give accurate trend lines, which means that they can be used to determine the most suitable coefficients for the analytical model. This also means that the CFD models can provide valuable information on choosing the suitable coefficients to model the labyrinth seals that need to be used for the turbine of Dawn Aerospace.

3.4.3. BRUSH SEAL

In this section first the verification of the seal leakage code is given and secondly the validation for both the numerical and porous medium model is given.

VERIFICATION

The verification of the porous medium model is done for the brush seal investigated by Bayley. The inputs to the model is a diameter of the rotor of 121.76 mm and a backing ring diameter of 124.56 mm. The thickness of the brush used is 0.7 mm and the values for α and β are 1 and 2.32 respectively. Figure 3.24 compared the output of the model developed in this thesis to the output given by Chew. It plots the mass flow rate against the pressure ratio against which the seal was tested. It can be seen that the model developed in this thesis matches exactly with the model developed by Chew, indicating that no errors were made in coding the program.

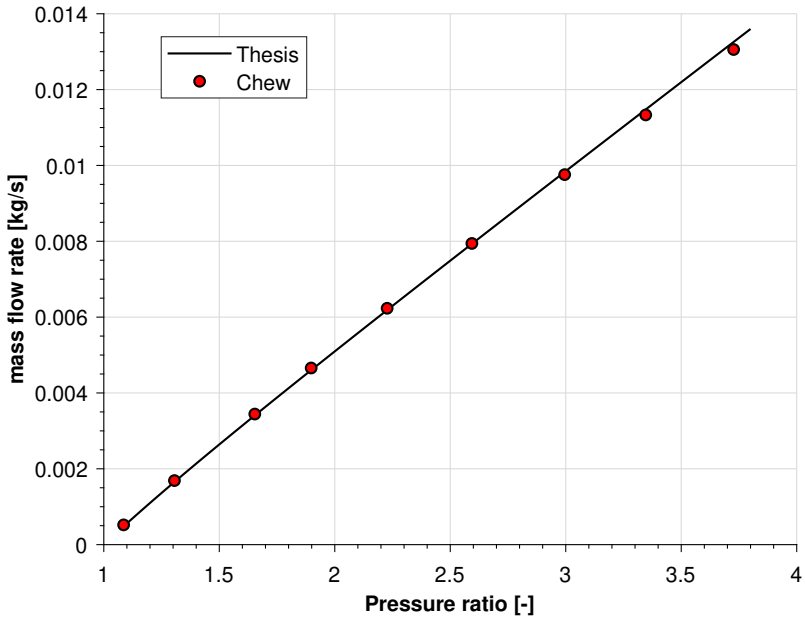

Figure 3.24: Verification of the brush seal porous medium model developed by the author and the one developed by Chew.

VALIDATION

The brush seal is modelled with a porous medium approach described by Chew. Brush seals and their leakage characteristics have been investigated by several authors including Deville [11], Bayley et al. [13] and Carlile et al. [12]. The experiments by Carlile et al. are especially interesting as they did not only measure the leakage rate of the brush seal for air but also for helium and carbon dioxide increasing the confidence that the model also works with different flow gasses.

As discussed in section 3.2.3 the model uses α and β to compute the resistance coefficients, these values are empirically determined to fit the model to the data. The range found in literature on these values is as follows $0.7075 \leq \alpha \leq 1$ and $1.42 \leq \beta \leq 2.34$, values found in literature can be found in table 3.5. During the comparison of the BFM with experimental data the values proposed by Chew [6] are used for α and β and are 1 and 2.32 respectively.

The brush seal investigated by Deville has a rotor diameter of 38.35 mm and a clearance with the aft backing ring of 0.4mm. The thickness of the brush is 0.77 mm and has a porosity of 0.3. The inlet pressure of the fluid range from 1 to 8 bar, the outlet as kept at 1 bar and the temperature of the fluid is 300K. Figure 3.25 shows the mass flow rate through the seal against the pressure ratio for both the experimental data and predictions of the porous medium model. The trend of the porous medium model is in agreement with the experimental data, the average prediction error is 12.7%.

Carlile investigated a seal that had a rotor diameter of 37.92 mm and that had an aft backing ring diameter of 39.23 mm. The fluid had an inlet pressure of 1 to 8 bar, an outlet pressure of 1 bar and a temperature of 290K. The porosity of the brush seal was 0.27 and had a thickness of 0.8 mm. Figure 3.26 shows experimental data obtained by Carlile and are compared to the predictions with the porous medium model. The figure shows the mass flow rate as a function of the pressure ratio over the seal. The prediction matches the experimental data well for all flow gasses, except at the larger pressure drop at the end for air. The authors of the paper called this behaviour unrealistic, although no explanation was presented. The total average error for the test with air is 11.0%, for CO_2 7.1% and helium 8.1%.

The two-dimensional CFD simulation of brush seal is compared to both the data obtained from Bayley and Long and Carlile. As discussed in the setup-section the parameter that would determine the mass flow rate through the seal, are the resistance coefficients. As the resistance coefficients are determined empirically they need calibration on the experimental data. However, equation 3.28 and equation 3.29 can be used to determine them. Where porosity is determined with equation 3.23 there only remain α and β, for whom a range of coefficients can be found in literature as also discovered during the development of the bulk flow models for brush seals as can be seen in table 3.5 in section 3.2.3. Pugachev [45] and Ergun [42] both model a

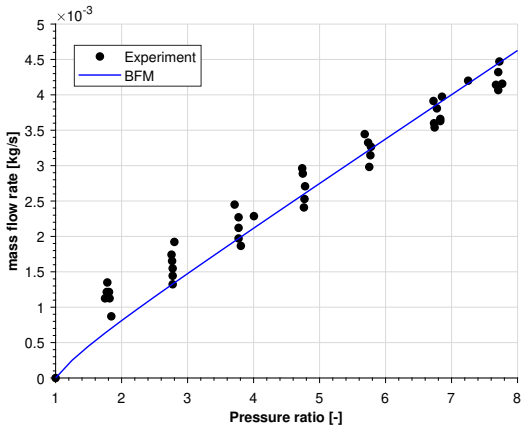

Figure 3.25: Experimental and predicted leakage rate on the Deville [11] brush seal for different pressure ratios

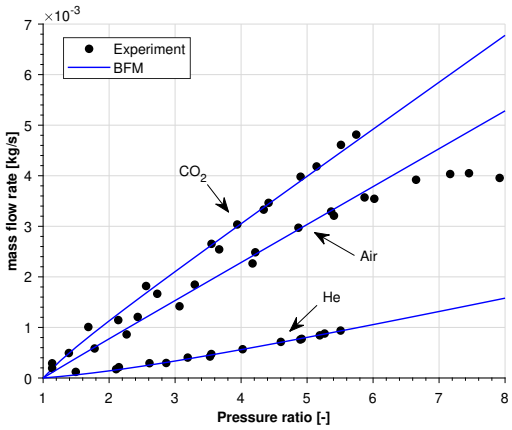

Figure 3.26: Experimental and predicted leakage rate on the Carlile [12] brush seal for different pressure ratios

brush seal in CFD however, Pugachev uses different coefficients for a different direction and Ergun does not. For this reason both approaches are compared to experimental data of Carlile's air case and the brush seal of Bayley to determine the best approach.

From the figures 3.27 and 3.28 it can be seen that the CFD predicts the linear increase in mass flow with pressure ratio well. However, both predict that the slope of the line is steeper than what the experiment dictates. It should be said that the coefficients proposed by Ergun do result in predictions closer to the experimental data. With this in mind, it might be possible to increase the resistance coefficients even further until the numerical results match the experimental data. However, this is not the scope of this thesis and in future simulations the resistance coefficients will be calculated with the empirically determined values from Ergun, unless stated otherwise.

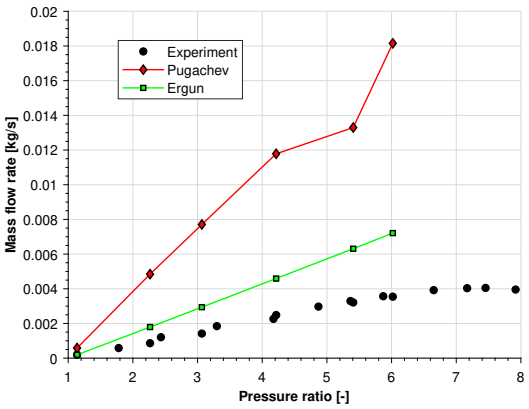

Figure 3.27: Comparison between experimental data of Carlile [12] and data obtained from the 2D numerical model, for both resistance coefficients suggested by Pugachev and Ergun.

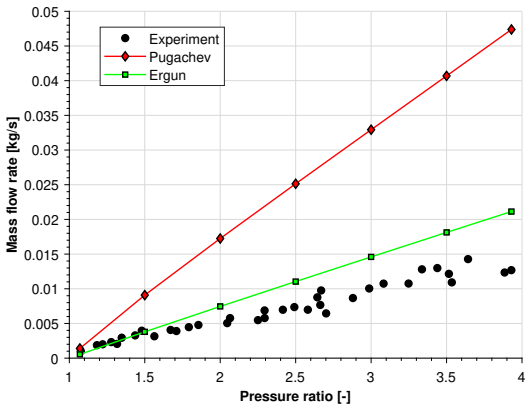

Figure 3.28: Comparison between experimental data of Bayley [13] and data obtained from the 2D numerical model, for both resistance coefficients suggested by Pugachev and Ergun.

Figure 3.29 shows the comparison between prediction with the porous medium model and experimental leakage rate as reported by Bayley [13]. In the figure the leakage mass flow rate in kg/s is plotted against the pressure ratio. The inner radius of the seal is 60.88 mm and the backing ring radius is 62.28 mm. The diameter of the bristles is 0.0762 mm, the width of the bristle pack is 0.6 mm and the bristles have a lay angle with the shaft of 45 degrees. There is a good agreement between the model and experimental data, with both following a linear trend. There is a small difference between 2D and 3D CFD due to the difference in slope, but generally small enough to make a 2D simulation case acceptable for brush seal design.

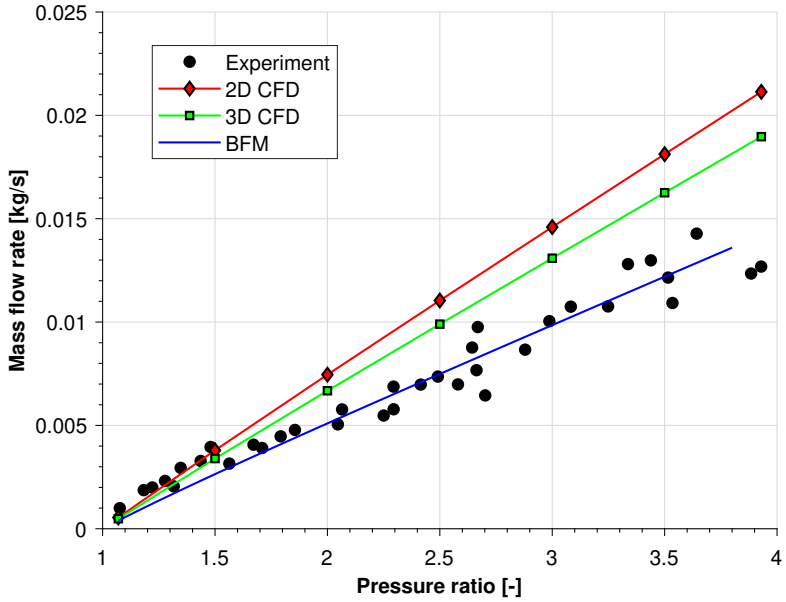

Figure 3.29: Experimental and predicted leakage rates on the Bayley [13] brush seal for different pressure ratios

3.5. SHROUD MODEL DEVELOPMENT

In the previous section the analytical seal leakage model reported in section 3.2 and the numerical seal model of 3.3 were validated. The analytical leakage equations and numerical models were shown to be following trend lines for experimental test data.

The analytical leakage equations will be used in this section to develop a new shroud clearance model. The analytical leakage equations are physical equations rather than empirical to make it applicable to a wide set of turbine designs. The model is fully dependent on analytical equations and does not rely on any data from CFD.

The necessity to model the inlet and outlet cavities is discussed in section 3.5.1 and how to use several bulk flow models in a row for the shroud is discussed in section 3.5.2.

3.5.1. LABYRINTH SEAL FOR INLET AND OUTLET

It is needed to compute the mass flow through the shroud as accurately as possible. This means that not only the seals need to be included, but the entire shroud geometry. Rosic et al. [49] and Jia et al. [50] show that the inlet and outlet width of the shroud play a role in turbine performance. They both changed the shrouds inlet width and outlet width separately and found that the smaller the width the lower the leakage. They also found that after a certain point increasing the width did not increase the mass flow further, but converged to an asymptote.

Zou et al. [51] studied the leakage flow through a shroud in order to develop a model that could substitute the shroud in CFD. They argued that using equations that predict leakage through a labyrinth seal would not work on its own due to the inherent different flow within shrouds than flows for conventional labyrinth seals on which the equations are based. The equations to calculate the leakage through a labyrinth seal do not take into account the inlet and outlet of the shroud but assume a straight flow in front and aft of the seal. However, they argued that the inlet showed sufficiently similar flow behaviour to a labyrinth seal. Since the flow structure is so similar the labyrinth seal model can be used to approximate the leakage through the shroud inlet, albeit with some slight modification to the kinetic energy as that is not completely dissipated according to Zou et al [51].

The similarities do not end at the inlet cavity, similar flow structure can also be seen in the outlet cavity. In the inlet and outlet cavity there first forms a separation bubble on the wall at the side of the gap and a jet forms the opposite wall. This flow structure is similar to that of a labyrinth seal only rotated 90 degrees. The two flow structures of the current turbine can be seen in figure 3.30, where the velocity contour is given in a meridional plane of the shroud.

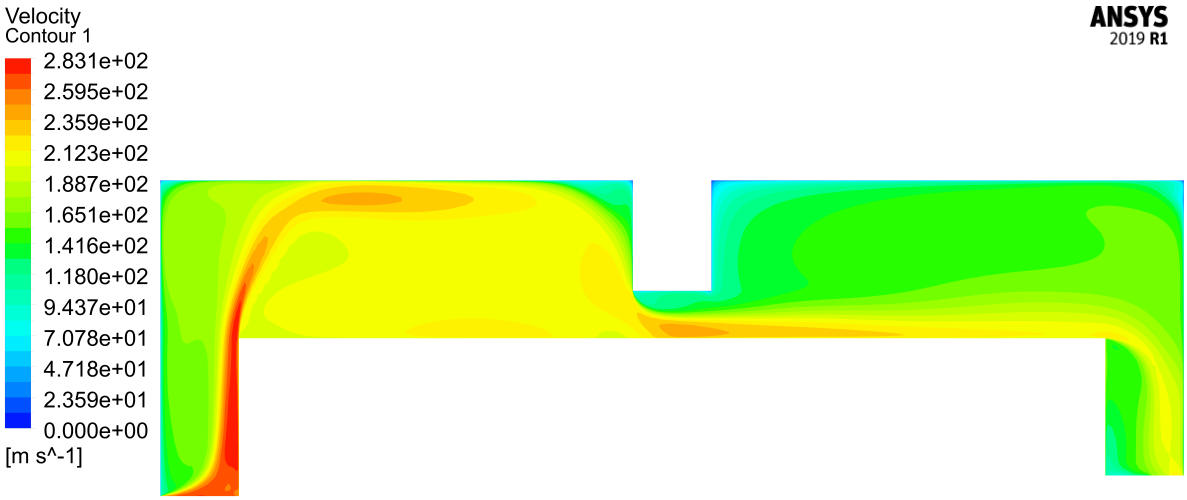

Figure 3.30: Contour of velocity of the shroud domain with a fin seal. Note how similar the flow behaviour of the inlet, labyrinth and outlet is.

3.5.2. FLUID NODE STRUCTURE METHOD

The previous section argued that the inlet and outlet cavities play a large role in seal leakage over the turbine. For the seal leakage equations to accurately predict leakage of the seal on top of the shroud they need to be given the right pressures in front and after the seal. It was also shown that the flow structure seen in the inlet and outlet cavity of the shroud is similar to that of a labyrinth seal and that the leakage through them can thus possibly be calculated with the leakage equations for a labyrinth seal.

Since the leakage equations use iterative solution methods to calculate the mass flow rate, by either iterating over velocity or mass flow rate, a method has to be found to make sure the mass flow rates through the seals are the same. This can be done by replacing the iteration process on mass flow rate of each individual BFM with a mass flow rate iteration over the whole shroud. The main loop uses an inlet and outlet boundary condition based on pressure while sealing configurations are represented with nodes. Each node takes geometrical parameters of the seal together with the mass flow rate, dictated by the main loop, and the pressure outputted by the previous node. Previously the individual bulk flow models only took the inlet and outlet pressure as inputs. The mass flow rate in the main loop is altered accordingly whenever the pressure after all the nodes does not fall within the convergence limit with the boundary condition. The iteration process is repeated until convergence is met. The node structure approach is set up in the following method: inlet boundary condition, 1 finned labyrinth seal, seal on top of shroud, 1 finned labyrinth seal and the outlet pressure boundary condition. A schematic overview is given in the form of a flow chart in figure 3.31.

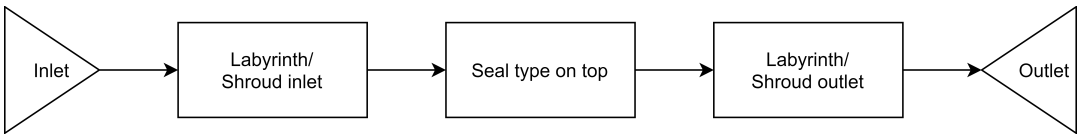

Figure 3.31: A schematic overview of the node structure inside the Dawn Aerospace shroud model.

The nodes do not necessarily need to be a bulk flow model, analytical equations that use mass flow rate and pressures as inputs will also work if coded correctly. Sudden pressure drops or pressure increases can also be added easily. Utilising this structure several approaches can be tried with ease as there is only a need to switch nodes to the one to be investigated. The method also allows the placement of a combination of several seals i.e. a labyrinth seal followed by a brush seal.

3.6. IMPLEMENTATION OF THE NEW CLEARANCE LOSS MODEL

The previous section showed that the inlet and outlet of the shroud play a role in the leakage rate through the seal. It was shown that inlets and outlets have a similar flow behaviour to a labyrinth seal. The section also showed how bulk flow models can be combined to calculate the leakage rate over a shroud.

This section gives a detailed description of how the newly developed model is implemented into an existing loss model and meanline design program. This model can cope with a variety of seals as long as leakage models are developed for them, greatly extending the usage compared to previous models. The model is named the Dawn Aerospace Shroud Model and will be referred to as DASM. DASM consists of a node like approach where the designer can put the required seal at a certain position.

Section 3.6.1 discusses how the shroud model is combined with the loss model and meanline design code. Thereafter, section 3.6.2 goes into detail on the inputs used for the model from the meanline design code.

3.6.1. IMPLEMENTATION

Previously the rotor loss of the turbine was calculated with the empirically determined loss model of Dunham&Came. As the loss model does not give the preferred flexibility of investigating shroud sealing options a new leakage model for the shroud was developed and documented in section 3.5. The clearance loss equation of Dunham&Came does not take a leakage rate as input to calculate the pressure loss coefficient as can be seen in equation 3.30.

$$Y_{clearance} = B\frac{c}{h}\left(\frac{k}{c}\right)^{0.78}\left(\frac{C_L}{s/c}\right)^2\frac{cos^2(\alpha_2)}{cos^3(\alpha_m)} \tag{3.30}$$

Therefore, the new clearance loss is calculated with the newly developed model in combination with Denton's (equation 3.31) clearance loss formula. Denton [4] proposed a more physical based approach to calculating losses in turbines, by considering the generation of entropy as a characteristic for lost work. Denton's model suggests that both the mass flow leakage ratio and the ratio between the circumferential velocity of leakage and main flow are responsible for the generation of entropy. The shroud model developed will calculate the shroud leakage rate, m_L. Since the shroud model does not calculate the change in fluid velocity, the initial approximation with the fluid flow angles of the main flow is kept unaltered.

$$\zeta_{\text{clearance}} = 2\frac{m_L}{m_m}\left(1-\frac{tan(\alpha_1)}{tan(\alpha_2)}sin^2(\alpha_2)\right) \tag{3.31}$$

The attentive reader should have noticed that Denton uses a different loss parameter, namely the entropy generation ζ, while Dunham&Came use the pressure loss coefficient, Y. In order to combine the two different loss metrics and thus use Dunham&Came for profile and pressure losses and Denton for the clearance loss, a conversion factor is needed between the two. Brown et al. [52] reports to have found such a conversion and it is given by equation 3.32. Where ζ is the entropy loss coefficient, Y is the pressure loss coefficient and γ and M are the heat capacity ratio of the fluid and the Mach number respectively. The precise derivation of how the different forms of expressing loss is derived by Horlock [53]. The short explanation of the equation is that the different loss models are equal at low Mach number, but when the Mach number increases the deviation increases.

$$Y = \zeta\left[1+\frac{\gamma-1}{2}M^2\right]^{\frac{\gamma}{\gamma-1}} \tag{3.32}$$

The way this model is set out changes little to the core procedures of the meanline design program and loss calculations. The additional step compared to the loss model of Dunham&Came is for the designer to define the shroud at the beginning with the usage of nodes. Figure 3.32 shows a flow chart that clarifies the process of the shroud model combined with the meanline design program. The shroud configuration file requires inputs from the velocity triangles calculated by the meanline design code. This also includes geometric parameters which will be discussed in more detail in section 3.6.2. The shroud configuration file has stored the geometry of the shroud and seal in the nodes. It starts iterating on the mass flow rate to satisfy the pressure boundary condition at the outlet. The calculated mass flow rate is passed to the clearance equation described by Denton in equation 3.31. The entropy loss coefficient is then converted to a pressure loss coefficient. In the end the profile, secondary and clearance losses get added together and the efficiency of the turbine can be calculated.

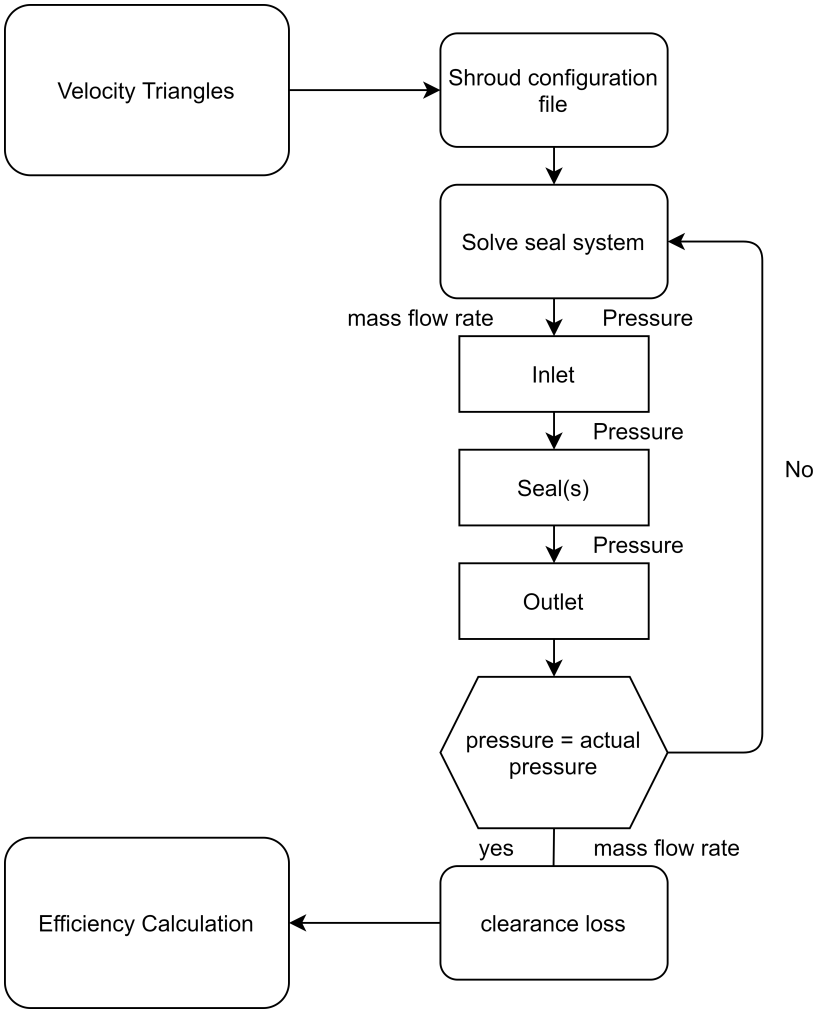

Figure 3.32: Flow diagram of the implementation of the DASM in to the mean line design code.

3.6.2. MODEL INPUTS

With the model implemented into the meanline design method, it is still required to specify what inputs need to passed on from the meanline design to the node structure. At first some additional information is given on the inlet pressure and secondly the geometric parameters of the model are discussed.

INLET PRESSURE

Due to the high rotating velocity of the fluid after the stator blade, the pressure before the rotor blade can be higher at the tip than at the root. This means that the shroud inlet will likely see higher pressure than the average pressure calculated at this station in the meanline design program. When looking at the pressure contour in front of the rotor blade in figure 3.33, it can be seen that this is indeed the case. Calculating the tip pressure in the MATLAB code can be done with equation 3.33, in this equation r_{t2} denotes the larger radius and r_m the mean radius. The pressure at the tip is given by p_{t2}, the mean pressure is p_m and ρ denotes the density of the fluid.

$$p_{t2} = p_m + \frac{\rho}{2} u^2 \left(1 - \frac{r_m^2}{r_{t2}^2}\right) \tag{3.33}$$

GEOMOTRIC INPUTS

Inputs defined for bulk flow models are slightly different when using them to model leakage rate on top of the shroud. This means some clarification is required as to what geometrical parameters are used for the input. The sizes for the inlet and outlet labyrinth seal are taken at their respective start of the actual turbine shroud.

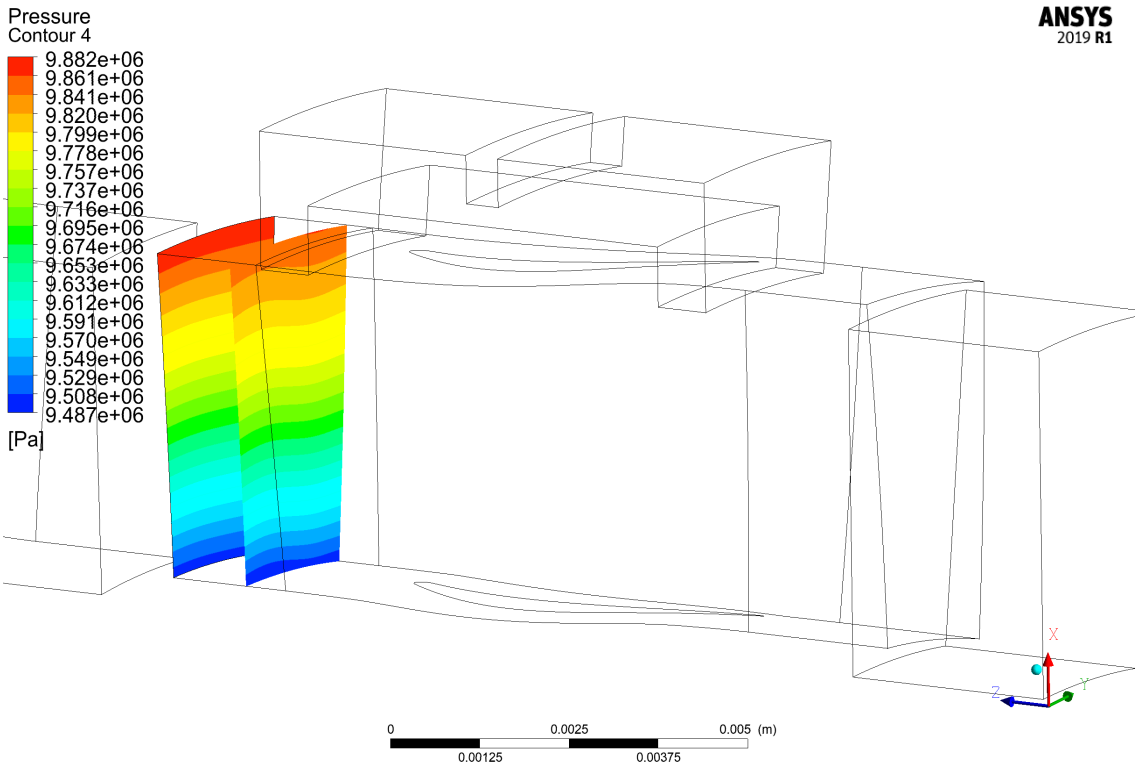

Figure 3.33: Contour plot of pressure in front of the shroud in the shrouded turbine case.

The rotor radius for the inlet is taken at position r_{t2} of the meanline design, while the rotor radius for the outlet is taken at position r_{t3} plus the thickness of the shroud and this is also true for the rotor radius of the seal on top of the shroud. The positions of the radii taken as inputs for the shroud model can be seen in figure 3.34. The figure gives a schematic overview of the positions used by the meanline design program.

In the case of the inlet and outlet, the width of the gap between casing and shroud as indicated in figure 4.1 is the clearance seen by the model. Furthermore, the inlet and outlet always use 1 tooth and thus the spacing, which is the distance between subsequent fins, is set to 0 as the BFM requires an input for this. During the development of this model, the best fit with CFD was found when the flow coefficient of Chaplygin and no kinetic energy coefficient were used for the inlet and outlet labyrinth seal BFM. Still, here it should be noted that different combinations of coefficients worked better in different cases, as could be seen in section 3.4.2.

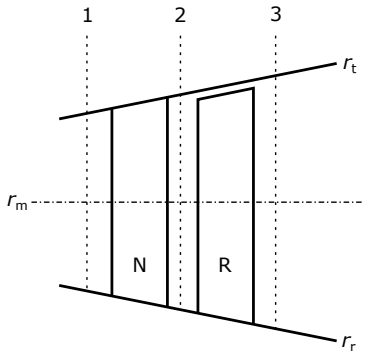

Figure 3.34: Schematic of meanline design positions. For example the leading edge tip height of the rotor blade is indicated with r_{t2}.

3.7. TURBINE NUMERICAL MODEL

In this section the numerical model of the turbine will be constructed. The flow in a turbine can be assumed to be periodic. Thus it suffices to create one rotor blade section combined with the stator blade and using periodic boundary conditions in the circumferential direction. ANSYS offers a mesher for turbomachinery called TurboGrid, which will be used to speed up the mesh generation for the turbine blades. CFX19.1 is used to carry out the flow simulation through the turbine.

First a turbine without a shroud will be generated to validate the meanline turbine code with the CFD. When this is established a turbine with a shroud will be modelled and again it will be validated if MATLAB and CFD predict similar values. Afterwards, the plain shroud will be substituted with shrouds that make use of a seal. The meanline turbine design code of the company has already been verified with the book which was used to write the program.

In the first section of this chapter, section 3.7.1, the development of the unshrouded numerical model is discussed. Section 3.7.2 describes how to set up the numerical model for the shrouded turbine. An explanation of how performance is calculated for turbines in CFD in this thesis is given in 3.7.3.

3.7.1. UNSHROUDED NUMERICAL MODEL

Shroud modelling of the turbine is rarely done in literature due to the large computational power needed as the shroud takes up a lot of nodes. Nevertheless, several authors have shown that it is important to model the shroud, especially if the turbine has multiple stages. However, in order to validate the mean line code and gain confidence in building numerical models for the turbine an unshrouded turbine will be covered first. In this thesis the unshrouded turbine is a rotor, which has no tip gap. This is physically not possible as the rotor would not be able to rotate, but it is a good method to assess the profile and secondary losses in a turbine. If that is deemed accurate enough to predict secondary and profile losses, the shrouded turbine will be modelled to investigate the effect of the leakage rate on turbine performance.

The mean line design program of the company uses the flow and blade angles to calculate the blade profiles with the help of a parametric blade generator. The points of the blade contour will be imported in SolidWorks, in order to create a three dimensional model of the blade geometry. The CAD file is imported into the DesignModeler of ANSYS to create the flow path, which is necessary to mesh the blade domain. The flow path can be constructed with the radii for tip and root specified by the turbine design program. The units in ANSYS DesignModeler are set to micrometre as is recommended when the blade fits in a cube of 10 by 10 mm [54], this will ensure that the right tolerance is used. The flow paths for the stator and rotor can be exported to TurboGrid for meshing. The mesh is loaded into CFX-pre, which is used for the simulation setup.

The stationary domains are connected to the rotating domain with a mixing plane approach, figure 3.35 shows how the domains are defined in the program. When using the mixing plane the user is presented with two options for the downstream velocity constraint. 1) The stage average velocity or 2) The constant total pressure. In the first case, the velocity is averaged and the pressure on the downstream plane is matched, while in the latter case the pressure is constant and the velocity is matched on the downstream plane. The first option is used to keep the right flow angles between the stator and rotor domain otherwise, large losses would occur because of large incidence angles.

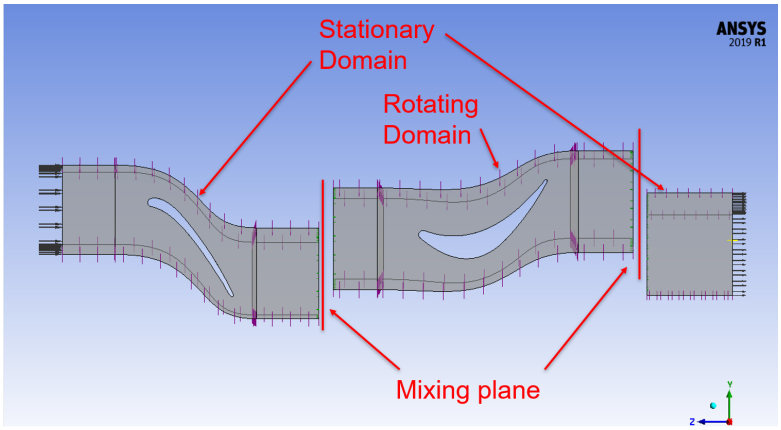

Figure 3.35: The unshrouded numerical model with indications where important boundary conditions are shown.

The boundary conditions used for the turbine are given in table 3.8. Using the total pressure at the inlet and static pressure at the outlet is a robust simulation setup and commonly used in turbomachinery design. This also means that the mass flow rate is calculated by CFD and can be used to evaluate how accurate the model is. Monteiro et al. [55] mention that the mass flow rate of the design data is 4% greater than that predicted by their CFD. A similar deviation is found by Dorney [56] except that they found the mass flow rate in the CFD to be higher by 5%. The deviations are explained by small differences in geometry in the 3D model and 3D flow characteristics (like boundary layers). A mass flow deviation of +-5% between the meanline design program and CFD is thus deemed accurate enough.

The turbulence model used is $k-\omega\ SST$, which is often used to accommodate for separation of the flow, a more detailed description on this is given in section 3.3.1. No slip and smooth walls are set for the wall boundary condition to help with convergence and to stay close to the input of the loss models, as turbine blades often have very low surface roughness. The fluid used during the simulations is decomposed hydrogen peroxide of 87.5%, just as would be used in the actual application, which consists of a mixture of steam and oxygen and is at a temperature of 1001 Kelvin. To model the fluid in CFX H_2O and O_2 are taken from the gas phase combustion material library, the mass fraction of 0.58845 and 0.41155 is used respectively and the thermodynamic state is set to gas. To make sure that the fluids used to drive the turbine are similar in the meanline program and CFD, the values for viscosity and specific heat at constant pressure are inputted by the user based on the values given from CoolProp. The viscosity and specific heat at constant pressure are $4.0741 \times 10^{-5} Pa \cdot s$ and $1797 \frac{J}{kgK}$ respectively. The total inlet pressure is 110 bar and the static outlet pressure is 92.8 bar.

Table 3.8: Boundary conditions used in the numerical models of the turbine

Boundary Condition	Setting
Inlet	Total Pressure, Total Temperature
Outlet	Static Pressure
Energy Equation	Total Energy
Walls	No slip, smooth walls
Turbulence model	k-ω SST
Calculation scheme	High resolution

As stated before, the mesh of the blades is generated with the use of TurboGrid, which creates a structured H-O-H type mesh around the blade geometry. Within the mesher the desired y+ is set to be equal or lower than 1 and the Reynolds number encountered on the blade is specified. During the mesh independence study, the global mesh size parameter is increased until the efficiency of the turbine is no longer dependent on the mesh size and the lowest possible point was taken. Figure 3.36 shows an example of what the mesh for a rotor blade looks like, the mesh size is small at the walls and an expansion ratio of 1.3 is used. The solution ended when the residuals were below 1E-5 and the total temperature and efficiencies did not alter anymore.

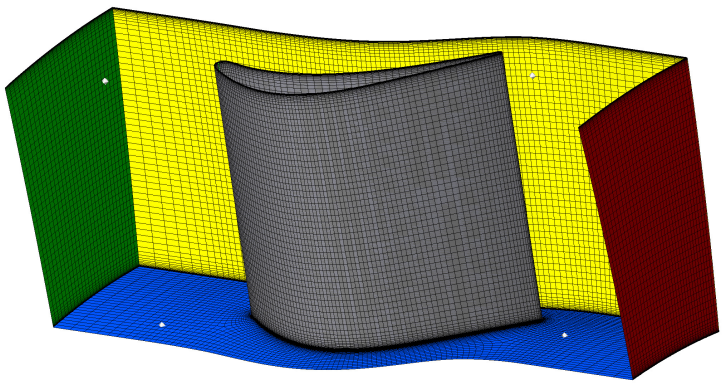

Figure 3.36: An example of a mesh used for the rotor domain of the numerical model of the turbine.

3.7.2. SHROUDED NUMERICAL MODEL

The numerical setup for the shrouded turbine simulation is copied over from the unshrouded simulation discussed in the previous section. The shroud is modelled completely within ANSYS, the mesh for the annular seal and labyrinth seal are directly created in ICEM. In the case of the brush seal the DesignModeler is used to create a model and the ANSYS mesher is used to create the mesh. A 2D drawing can be made in both ICEM and ANSYS mesher, which is revolved around the rotational axis of the turbine afterwards. The shroud uses the same pitch angle as the rotor blades, this will help to connect the fluid domains as will be explained later.

The fluid domain for a shrouded turbine can be included in two different ways. One where the inlet and outlet of the shroud are together with the main flow passage and separated from the blades, see figure 3.37. The other option where the whole shroud itself is separated from the main flow, see figure 3.38. In the case of this thesis the second option is chosen, foremost due to the ease of implementation as the unshrouded model would not have to be changed to incorporate a shroud.

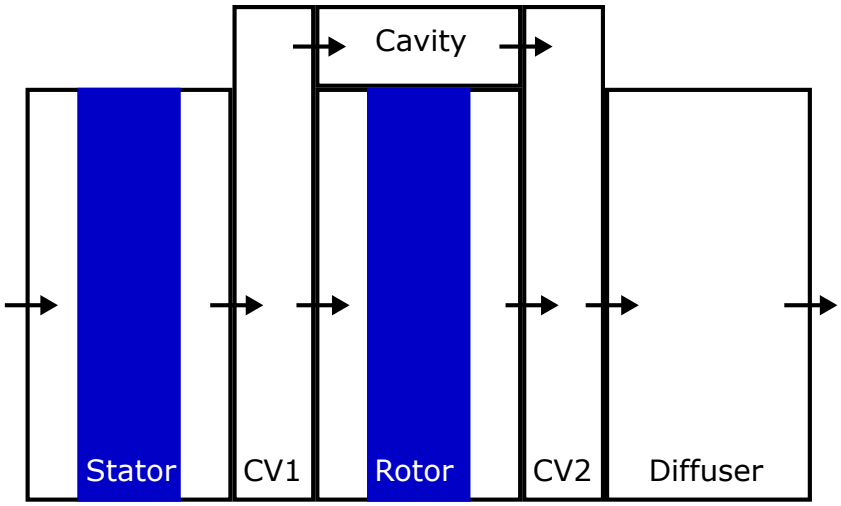

Figure 3.37: A schematic of a possible shrouded turbine domain division, where the inlet and outlet of the shroud are separated of the middle part of the shroud.

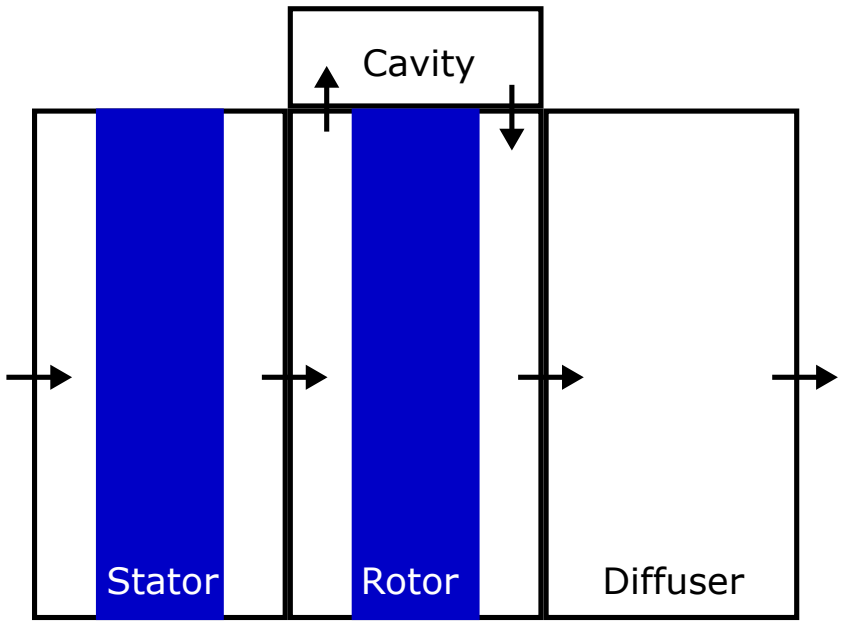

Figure 3.38: Schematic of a possible shrouded turbine domain, where the inlet and outlet of the shroud are combined with the middle of the shroud.

The connection of the mesh between the rotating rotor and the stationary shroud is done with the frozen rotor approach instead of the mixing plane approach. This is because the frozen rotor approach is computationally less demanding [54]. The sides of the shroud domain are set to be of a rotational periodicity. The part of the shroud that is connected to the rotor is given a rotational wall velocity that matches the rotor speed, this models the rotating shroud surfaces within the cavity.

However, to accommodate for the frozen rotor approach two conditions are important. The first being that there is no altering geometry in time, i.e. a passing blade, as the relative position of the components is fixed. This means that the resulting flow is strongly dependent on the relative position, if there is no altering geometry in the shroud this is thus no longer an issue. The second condition is that the pitch of the rotor and shroud should be the same in order to avoid temporal lag. Temporal lag occurs for example when a wake of a cylinder is passed on to the next domain with the frozen-rotor approach with a different pitch, the wake enters the domain for each blade section at another point and thus also exits the domain at another position. The difference in these inlet and outlet positions of the following domain is called the temporal lag.

3.7.3. PERFORMANCE CALCULATIONS IN CFD

The pressure loss over a turbine can be calculated characterised as equation 3.34 [21], where the subscript with zero means is total pressure and the subscript without zero is static pressure.

$$Y_R = \frac{p_{01} - p_{02}}{p_{02} - p_2} \tag{3.34}$$

Total pressures are averaged with mass flow averages and static pressure are area-averaged. To calculate the rotor loss you use the pressures calculated based on rothalpy since this is the value that is conserved in rotating domains.

The isentropic turbine efficiency can be calculated with specific enthalpies: equation 3.35, where the subscript r is the real process and s denoted the isentropic process.

$$\eta_T = \frac{h_1 - h_{2r}}{h_1 - h_{2s}} \tag{3.35}$$

For CFX equation 3.36 is a good method to calculate efficiency, as it also takes into account the changing properties throughout the turbine stage. Where ω is the rotational speed, T is the torque and h is the total enthalpy.

$$\eta_T = \frac{\omega * T}{\dot{m} * (h_{in} - h_{out})} \tag{3.36}$$

Next to the above mentioned efficiency calculations, the power generated will also be taken as a performance characteristic. Because, as discussed in an earlier chapter, the leakage flow that does not produce work is not seen as a loss in conventional terms. However, by letting more mass flow through the turbine the turbine should also extract more power from the flow. The power calculated in CFD is done with equation 3.37.

$$P = T * \omega \tag{3.37}$$

3.7.4. MESH SENSITIVITY STUDY

The mesh sensitivity study for the turbine is conducted for the reference turbine without a shroud. The number of nodes used for the shroud to be mesh independent is derived from the seal mesh independence study in section 3.3.5. However, it is made sure that the number of nodes used in the circumferential direction is roughly the same for the turbine as for the seal.

Figure 3.39 plots the total-to-total efficiency of the simulation against the number of nodes used for the nozzle and rotor combined. As explained in section 3.7 the mesh for the blades is made with the help of TurboGrid, a dedicated mesher for turbomachinery. This mesher made sure that the y+ values specified are actually achieved by the mesh. The number of nodes is then increased by increasing the global refinement parameter in the mesher. In the figure it can be seen that the least amount of nodes achievable within the mesher to create a good mesh is approximately 400 000 nodes. When the mesh is globally refined with the global refinement parameter the effect of the increasing mesh is negligible after approximately 800 000 nodes. This means that the nozzle and rotor both use approximately 400 000 nodes.

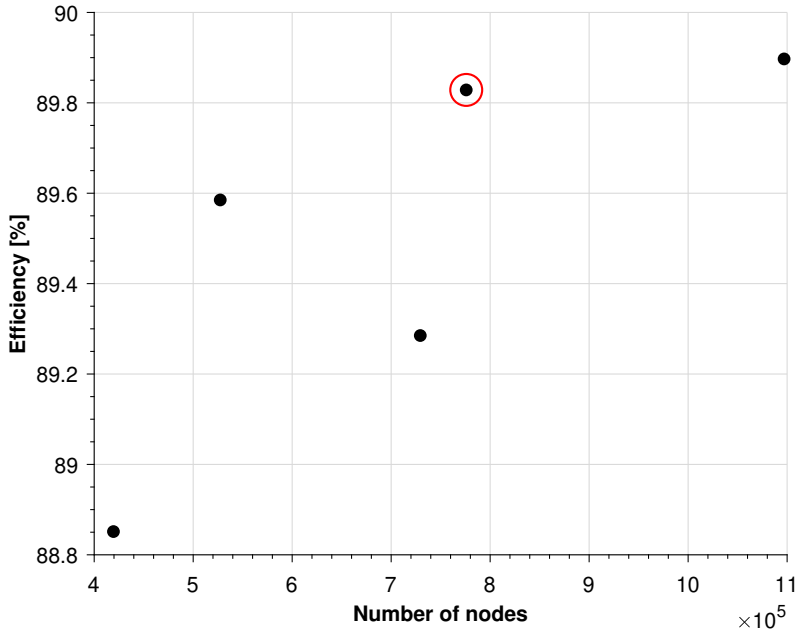

Figure 3.39: Mesh independence study for the turbine.

3.8. TURBINE MODEL VALIDATION

The previous section explained how to set up numerical simulations for turbines. This section will validate the models with the current meanline design program of Dawn Aerospace, which uses Dunham&Came as a loss model. Section 3.8.1 lists a turbine design for the unshrouded case and section 3.8.2 does the same for a shrouded turbine. Both sections go into details about the comparison between the turbine design code outputs and outputs of the CFD model.

3.8.1. UNSHROUDED TURBINE DESIGN

In this section the reference turbine is used, it is designed with the meanline code developed by Dawn Aerospace, with the clearance loss calculations turned off. A numerical model of the designed turbine will also be created to compare loss calculations to each other and to give a base case with optimum efficiency as there are no clearance losses. This should establish if the profile and secondary losses calculated with the loss models match those of CFD.

Table 3.9: Efficiency parameters for the unshrouded turbine, a comparison between the Dunham&Came loss model and CFD.

Parameter	Dunham&Came	CFD	Deviation [%]
Mass flow rate [kg/s]	2	2.1	+5.0
Efficiency [%]	86.81	89.90	+3.5
Y_n [-]	0.0781	0.0689	-11.8
Y_r [-]	0.1469	0.1524	3.7

The new design is modelled in CFD and the simulation is run. For this turbine the loss and efficiency parameters are compared with each other and they are listed in table 3.9. As can be seen, the mass flow rate deviates by 5%, and the efficiency is predicted within 4%. The largest deviation (>10%) can be found in the nozzle pressure loss however, the rotor pressure losses predicted to roughly the same value by the loss models and CFD and this is the parameter that is most important for the thesis. The other performance parameters are all within the 5% accuracy range established in section 3.7.1.

Contour plots of entropy and Mach number are shown in figure 3.40 and figure 3.41 respectively. Generally, the entropy contour shows the losses generated by the profile and trailing edge of the turbine blade. no significant generation of entropy is visible, apart from a small zone around the blade. This shows that

no significant losses are generated due to for example separation, the generation of the boundary layer has the largest contribution to the loss. The Mach contour shows the highest Mach number in the throat as expected since this is the smallest area. It also indicates that the Mach number in the turbine does not reach supersonic speeds, this is important as the blades are of subsonic design and the meanline design program processes cannot predict shock losses.

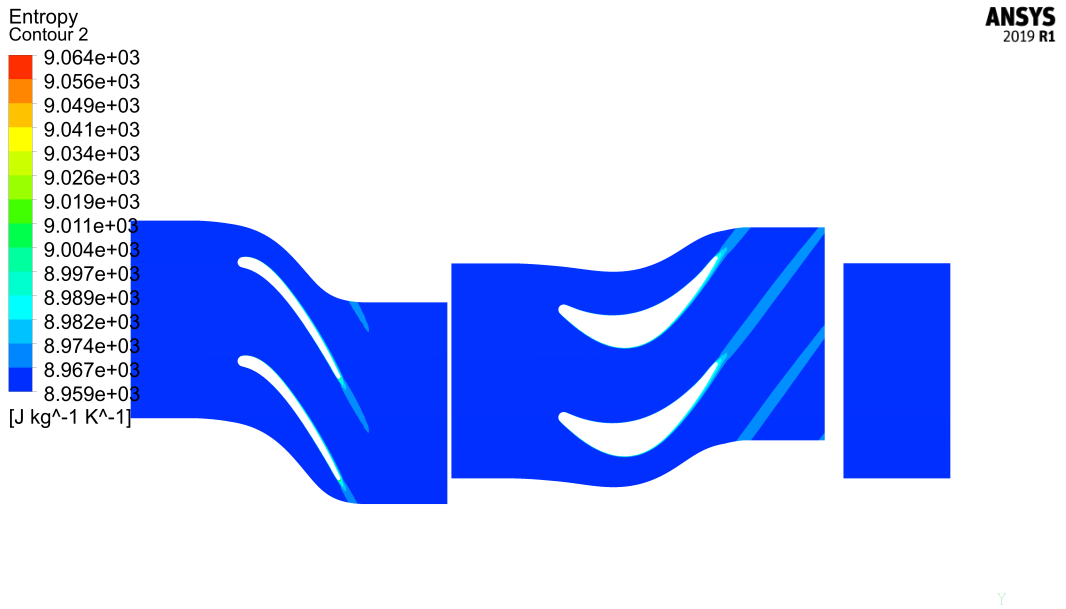

Figure 3.40: Entropy contour of the unshrouded turbine case at the mean radius, mainly indicating profile and trailing edge losses.

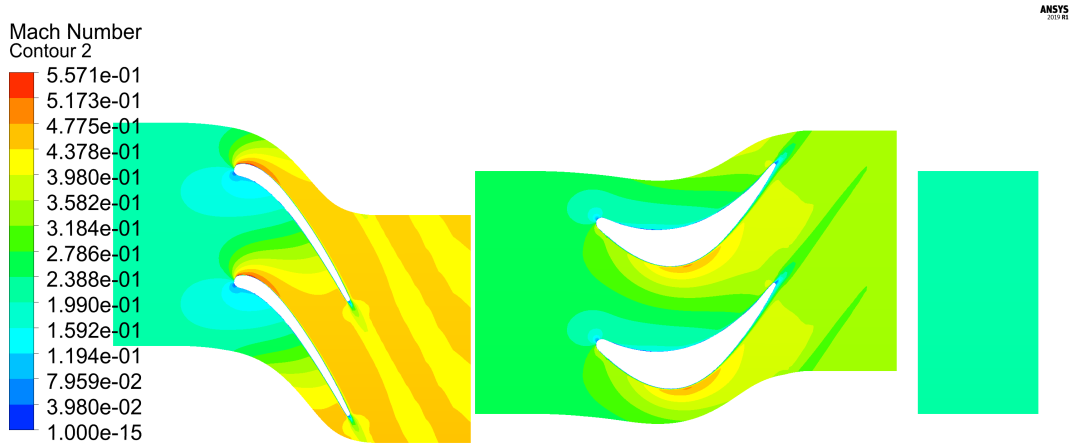

Figure 3.41: Mach contour of the unshrouded turbine case at the mean radius.

Figure 3.42 shows the contour plot of entropy at the exit of the turbine rotor for two blades. Two distinct zones of entropy generation can be seen for a single blade: one at the top and one at the bottom. The entropy generation is due to the horseshoe vortex forming on the blade as explained in section 2.1.2. Due to having the rotor blade touching the outer casing this vortex also forms on the upper side of the blade. No excessive entropy generation can be seen, at the rotor outlet. This, together with the good matching rotor pressure loss between MATLAB and CFD give confidence that the simulation is set up correctly.

It thus is believed that the discrepancy in nozzle pressure loss between the meanline design program and

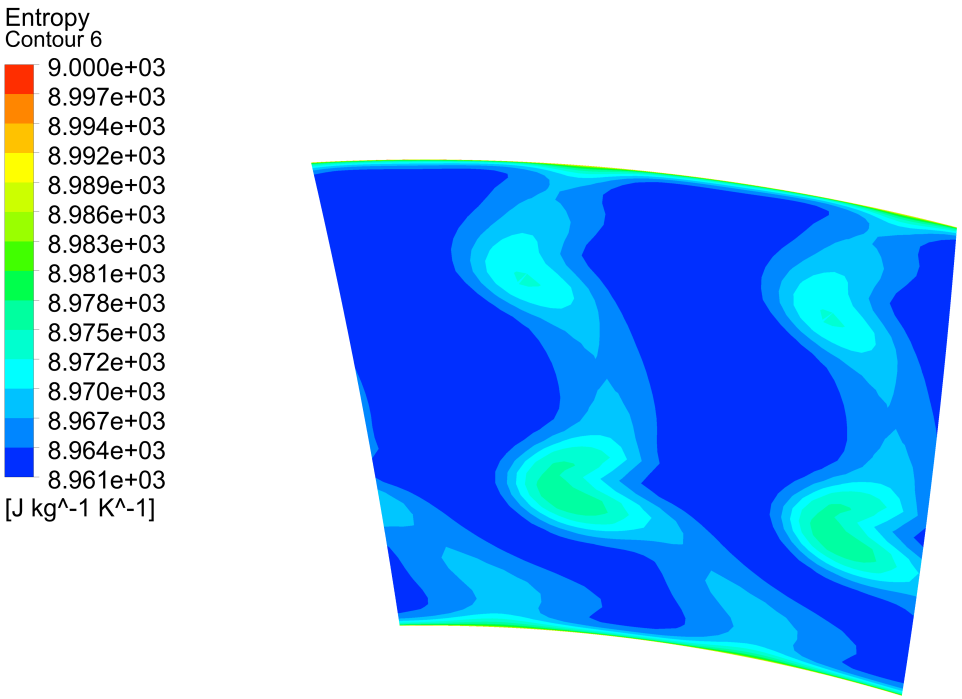

Figure 3.42: Entropy contour of the unshrouded turbine case at the rotor outlet position.

CFD is due the thickness over chord ratio of the designed blade being to low. The thickness over chord ratio (TC) for the nozzle blade used in the turbine is 0.09, while the profile loss calculation method is only deemed valid in the case of $0.15 \leq TC \leq 0.25$ according to Saravannamuttoo et al. in his book on gas turbine theory [21].

3.8.2. SHROUDED TURBINE DESIGN WITH DUNHAM&CAME

For the case of shrouded turbines, the clearance calculations are turned on in the meanline design code and coefficients for a shrouded turbine are selected. Similar inputs are used to design the shrouded turbine to be able to compare the performance to the previously developed unshrouded turbine. Although, blade angles change due to the change in efficiency in the meanline program. The designed turbine is modelled in CFD and the simulation is run. Results are presented in table 3.10, where it can be seen that some large discrepancies arise.

Table 3.10: Efficiency parameters for the shrouded turbine, a comparison between the Dunham&Came loss model and CFD.

Parameter	Dunham&Came	CFD	Deviation [%]
Mass flow rate [kg/s]	2.25	2.49	+10
Efficiency [%]	78.53	87.36	+11
Y_n [-]	0.0767	0.06378	-17
Y_r [-]	0.3189	0.1759	-45

Table 3.10 shows some large discrepancies between CFD and the analytical loss model, with the largest being a 45% deviation. The first large deviation is the mass flow rate, which is now outside of what is outside of what literature calls an acceptable difference, namely a 10% deviation. The efficiency prediction difference is with 11% also outside the generally accepted difference of 3-4%. These two parameters are indicating that something is wrong or miscalculated in either the preliminary design program or CFD. When looking at the

more detailed parameters, nozzle and rotor pressure loss coefficients, it becomes clear that losses predicted by the loss model do not agree with losses predicted by CFD, where the loss model predicts much higher losses.

The discrepancy in the nozzle losses was already noted in the previous section. With the nozzle blade being very similar between the un-shrouded and the shrouded turbine design, it is again likely that the profile loss equation used for the nozzle blade is the origin of this. This is confirmed by the similar-looking entropy contour plot in figure 3.43 and the Mach contour plot in figure 3.44.

Figure 3.43: Entropy contour of the shrouded turbine case at the mean radius, mainly indicating profile and trailing edge losses.

Figure 3.44: Mach contour of the shrouded turbine case at the mean radius.

The large deviation in rotor loss was not present in the previous section, where the predicted loss using the loss model was still close to the prediction by CFD. The newly added feature in the shrouded case is the addition of the shroud and thus the introduced discrepancy most likely originates from this addition. When dissecting the rotor loss in its loss components, according to equation 2.1, it becomes clear that the clearance loss predicted by Dunham&Came is 67.6% of the total rotor loss, the secondary loss contributes 26.7% and the profile loss 5.7%. To know how large the clearance loss is in the CFD calculations is hard to extract however, there are two possibilities: 1) Running an unshrouded simulation with the exact same blades, calculating the

rotor loss and subtracting that from the case with a shroud. 2) Using Denton's leakage equation to get a quick indication of losses introduced due to mixing, this can be done by extraction the leakage fraction on top of the shroud from CFD.

The easier option is to do a rough estimate using Denton's leakage equation 3.31. With that equation, the leakage fraction is used to calculate the clearance losses in the rotor stage. The leakage fraction over the shroud is 0.034 of the mass flow rate through the rotor passage in CFD. Using equation 3.31 shows that the clearance loss in CFD would amount to 12.5% of the total, much less than Dunham&Came predict (68%) and much more in the quoted range for clearance losses (33%). If the 68% clearance loss of Dunham&Came would be translated in a leakage rate this would put it much over 10% of the overall rotor flow rate, an unreasonable large amount. This finding leads to the conclusion that the clearance losses calculated by the Dunham&Came loss model, overpredict the clearance losses by a considerate amount.

Figure 3.45 shows the entropy contour of the turbine at the rotor blade outlet. When comparing this figure to the figure 3.42, which shows the entropy generated after the rotor without a shroud, it can be seen that the vortex on the lower part of the blade remains unchanged. The upper vortex is completely replaced by a band of high local entropy. This entropy generation is caused by the leakage flow through the shroud entering the main flow.

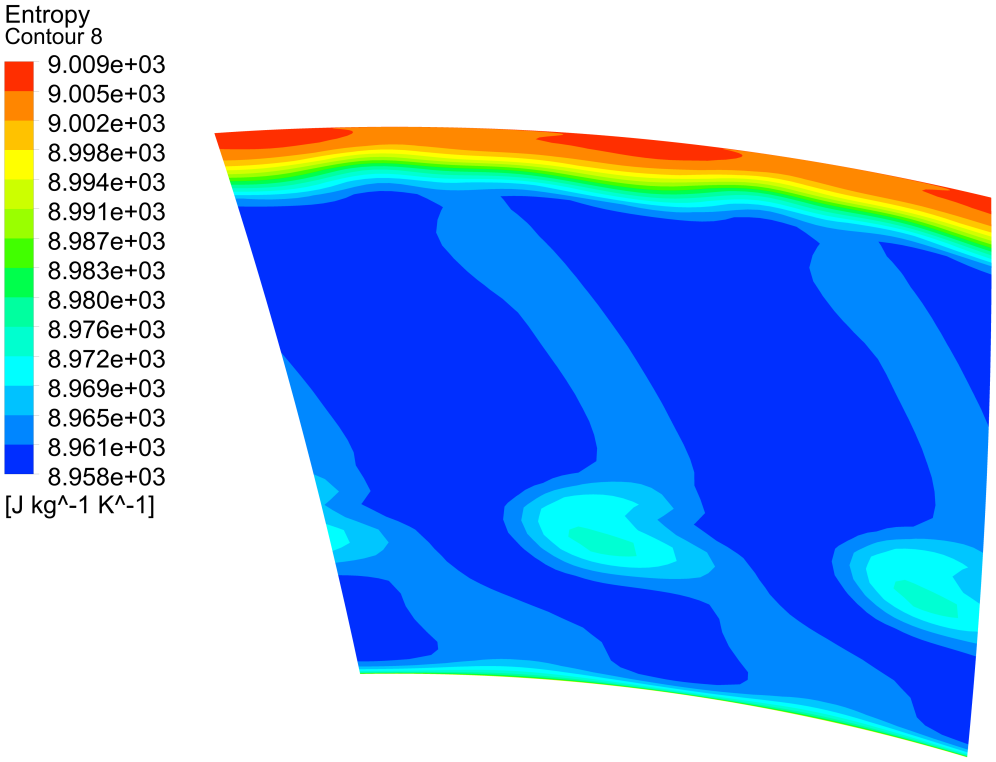

Figure 3.45: Entropy contour of the unshrouded turbine case at the rotor outlet position.

3.9. DISCUSSION

DISCUSSION NUMERICAL SEALS

In section 3.3.4 the setup of the numerical model of the brush seal was discussed. The setup of the brush seal became a bit more troublesome. With ICEM the naming of zones and edges became very hard and time-consuming. Switching to the Ansys mesher and modelling it in there took less time and fewer errors were made. However, this could not be transformed into a 3D mesh. This meant that creating the 3D numerical model for the brush seal took more time in total.

DISCUSSION LEAKAGE MODEL VALIDATION

The 2D simulations could accurately predict the trends with respect to the mass flow rate for a pressure increase. For the annular and labyrinth seal, the mass flow rates calculated by the fluid solver were a bit too high. For the brush seal, the simulation showed a linear trend just as the bulk flow model and experimental data. Only the linear trend predicted by the CFD is steeper. This can be solved by calibrating the seal, by increasing resistance coefficients or even making the brush thicker.

In the case of the annular seal and labyrinths seal no well documented data could be found for low pressure ratios (i.e. 1.2 bar) as would be encountered on top of the shrouded rotor. The author does not expect the behaviour of leakage rate to change drastically when the pressure ratios enter this low pressure ratio regime. With the shown trend lines being similar, the author hopes to have proven that BFMs and CFD can predict leakage rates through the seals also at lower pressure ratios than the experimental data cover.

Choked flow conditions are not fully programmed. Warnings are given when choked flow is approached however, results of the cases where choked flow calculations were turned off gave better results than with the chocked flow conditions turned on. Also, little experimental data was found on tests that specifically mentioned when the flow became chocked in the experimental data presented in the literature also no indication of chocked flow during the tests could be found, which made it hard to validate the data.

DISCUSSION ON MODEL DEVELOPMENT

During the thesis several other methods were tried to model the inlet and outlet of the seal than whit a labyrinth seal as presented in section 3.5. The other models are not included in the text as they did not present acceptable solutions. Some of the methods tried are: hydraulic resistance coefficients, orifice flow and radial inflow and outflow between a stationary and rotating plate.

DISCUSSION TURBINE VALIDATION

A difference in nozzle pressure loss between CFD and loss model prediction becomes clear in section 3.8, this difference is attributed to the lower thickness over chord ratio in the design code than the loss model is capable of predicting for. It was decided that investigating this problem was outside the scope of this thesis and would not interfere with the thesis too much as rotor pressure loss coefficient would still give a good indication on the models prediction performance.

4

RESULTS

The previous chapter covered the methodology of this thesis. It started with explaining the analytical leakage equations of the seals and the setup of the numerical models. It showed that they were adequate to predict leakages through seals. The analytical equations were then used to develop a model to calculate leakages through a sealed shroud configuration. It was explained how this new model could be integrated with the meanline design code and the loss model of Dunham&Came. In the end, the setup of the numerical model for a turbine without and with shroud was discussed.

This chapter will use the numerical model of the shrouded turbine to validate the newly developed shroud model. When it is shown that the model can predict leakage rate trends the model can be used to design shrouded turbines with seals on top of the shroud.

Section 4.1 compares the leakage rate and pressures from the reference turbine sealed by a single fin labyrinth seal and brush seal with the leakage rate and pressures predicted by the model. The model integrated into the meanline design code is then used in section 4.2 to design turbines with a shroud seal and are compared to CFD. Section 4.3 discusses the solution speed of the new model compared to the old model of Dunham&Came. Finally, in section 4.4 a sensitivity analysis is performed on some input parameters of the model.

4.1. DASM MODEL VALIDATION

In this section the leakages and pressures obtained from the turbine numerical model are compared to the leakages and pressures obtained from the shroud model. The turbine used in this section is the reference turbine of section 3.1. The turbine is used for two kinds of simulations: one where on top of the shroud an one finned seal is used and the other one where a brush seal is used. This section is divided into several subsections: first the data generation of the comparison is discussed, then the leakage rates through the shrouds are compared. Followed by the comparison of pressures at several stations. In the end predicted rotor losses are compared to each other.

4.1.1. DATA GENERATION

The model will be validated against data of a shroud using an one finned labyrinth seal on top of the shroud as this is the default setting in the loss model of Dunham&Came. The inlet and outlet widths of the shroud are not taken into account by the loss model of Dunham&Came. Since the inlet and outlet widths play an important role in shroud leakage, as has been noted in 3.5.1, they are varied. Figure 4.1 shows the inlet (left) and outlet (right) cavity being altered over a range of 0.125 mm to 1.5 mm. This range includes the lower bound dictated by manufacturing constraints and an upper bound where the inlets and outlets play little to no effect.

In order to further test the model and validate if the approach works with another seal, the numerical model for the shroud is recreated with a brush seal on top of the shroud. Again the inlet and outlet width of the shroud are varied from 0.125 mm to 1.5 mm and the mass flow rate is extracted. The brush seal on top of the shroud has a thickness of 0.7 mm, the backing ring clearance is 0.3 mm. The porosity used to calculate the inertial and viscous resistance coefficient is chosen to be 0.27, which is similar to the values of porosity found in literature in section 3.4.3.

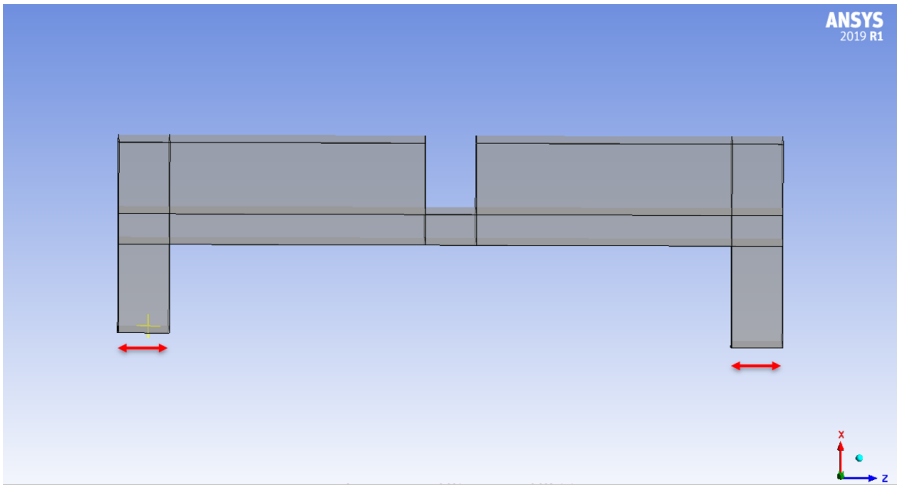

Figure 4.1: Inlet and outlet cavity variation of the shroud model.

4.1.2. LEAKAGE RATE COMPARISON

To calculate the mass flow rate through the shroud with the shroud model the pressures at the inlet and outlet of the seal needs to be known. The pressures are taken at the inlet and outlet of the rotor blade as predicted by CFD. In this section the inlet and outlet pressure of the blade are denoted by station 1 and station 4, respectively, see figure 4.2. The figure also shows the numbered position in front of the seal on top of the shroud as station 2 and the position after the seal as station 3. As has been discussed in section 4.1.3 the pressure at the inlet of the shroud will be higher than the average pressure of station 1. For this reason, the inlet pressure used for the model is the maximum pressure of station 1 in CFD. The outlet pressure used as an input for the model is the average pressure of station 4.

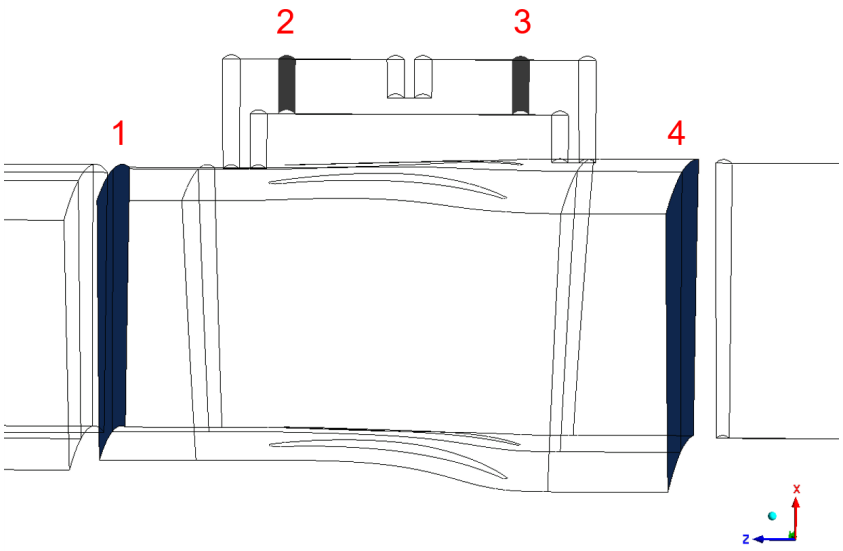

Figure 4.2: Positions at which pressures are calculated for the investigation of shroud flow behaviour

In figure 4.3 the mass flow rate through the seal is plotted against the cavity widths for the shroud sealed by an one finned labyrinth seal, it compares the values from CFD and that of the model. Both show a logarithmic trend in increasing mass flow rate as the cavity width increases and hits a point where the increase in cavity width does not further increase the mass flow rate through the shroud. Similar flow behaviour has been discovered by Rosic et al.[49] and Jia et al. [50]. At the cavity size of 0.125 mm and 0.25 mm the predicted mass flow rate from the model and CFD are almost identical. However, for the other cavity sizes the model overpredicts the leakage rate. The maximum discrepancy between the models exists at a cavity width of 0.75 mm, where the error is 32.3%.

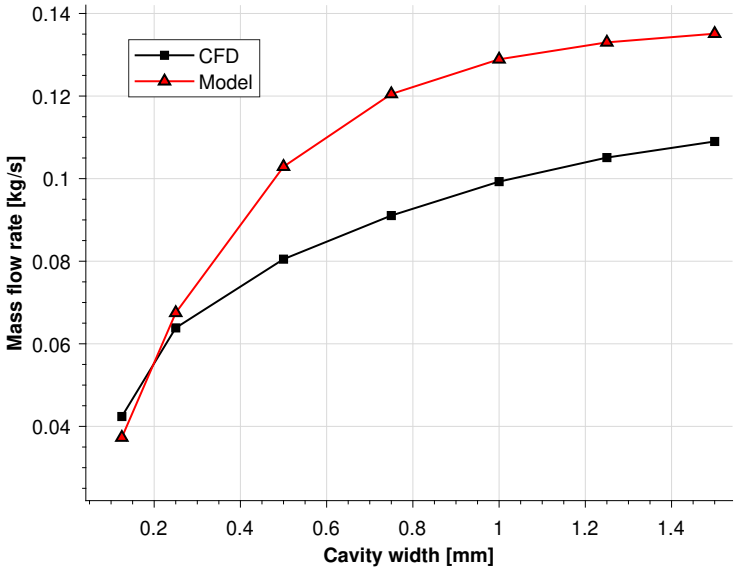

Figure 4.3: Mass flow rate through the shroud sealed by a single fin, CFD vs model predictions. The model uses a labyrinth for the inlet, the actual fin and the outlet.

Figure 4.4 shows that the predicted leakage rate by the BFM through the labyrinth seal on top of the shroud matches the leakage rate from CFD closely. Figure 4.4 clearly indicates that whenever the pressures supplied are correct, the BFM can predict the leakage through a seal on top of a shrouded turbine. This again indicates that the inlet and outlet cavity play a larger role in small turbines than any analytical loss model, that can be found in the open literature, has taken into account thus far.

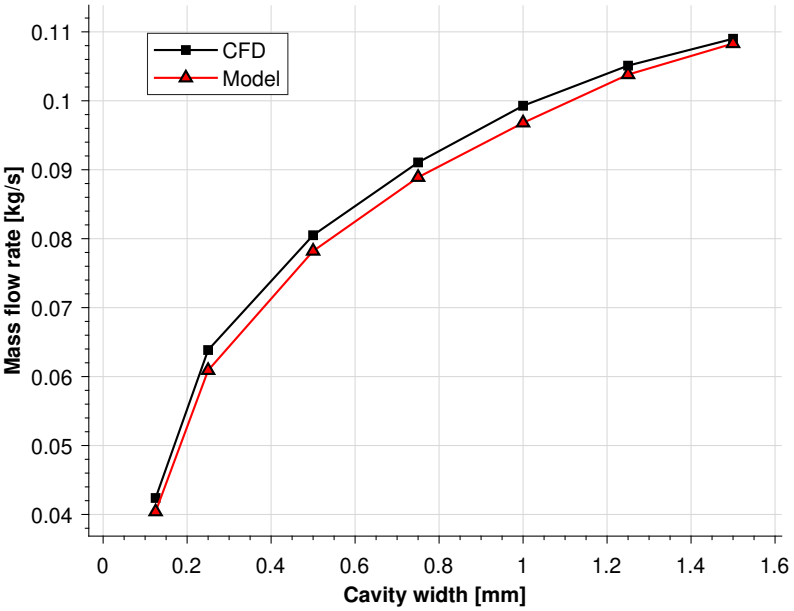

Figure 4.4: Comparison between leakage rate calculated with the model and CFD for shrouded turbine with changing inlet and outlet shroud clearance. The model uses only a labyrinth seal over the shroud, but pressures are taken in front and after the actual seal.

The leakage rate of the brush sealed shroud is also compared for the CFD case and the model predictions. As already noted, in this case the one finned labyrinth seal is replaced by a brush seal in the CFD simulation and the BFM for the labyrinth seal is replaced by the porous medium model in the shroud model. Figure 4.5 plots the leakage rate through the shroud against the cavity width. The model again slightly overpredicts the leakage rate when compared to CFD, the maximum error occurs this time at the smallest cavity width and is 14.3%. More importantly, the model again follows the trend of the CFD well. It predicts that the leakage is

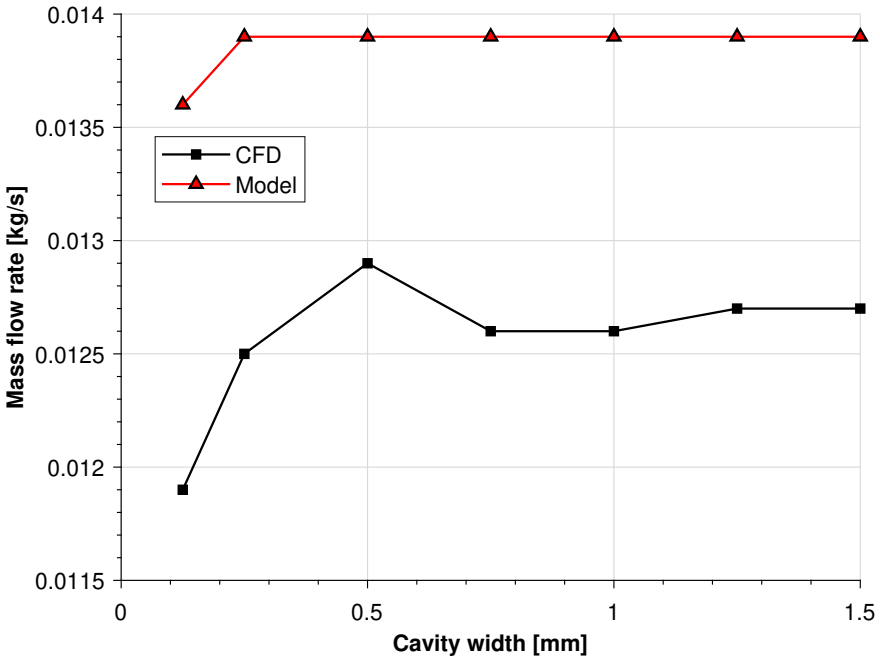

Figure 4.5: Comparison between CFD and shroud model of leakage through a brush sealed shroud with varying inlet and outlet cavity width.

not dependent on the cavity width at 0.25 mm. While CFD predicts that the mass flow rate through the seal is no longer dependent on the inlet and outlet cavity size of 0.5 mm. This illustrates that the model can predict leakage rates for brush sealed shrouded turbines, which is a feature that no other loss model available in the open literature can do.

When comparing the leakages of the single finned sealed shroud to the brush sealed shroud quite some differences can be seen. First, it is noted that the brush seal is much less dependant on the cavity width of the inlet and outlet than the labyrinth seal. At the smallest cavity size, the leakage rate through the brush sealed shroud is 28.1% that of the labyrinth sealed shroud. At the largest cavity size, the brush sealed shroud only is 11.7% of the labyrinth sealed shroud when comparing leakages of CFD.

4.1.3. INLET PRESSURE

In the previous section it could be seen that the calculated leakage rate through the shroud does follow the trend, however at larger axial clearances for the inlet and outlet the model overpredicts the leakage rate. To further investigate the performance of the model a closer look is taken at the pressures at the different stations.

Figure 4.6 plots the pressure against the cavity width of the shroud, it shows pressures taken at station 1 and 2 in CFD and the calculated pressure by the model at station 2. That the shroud sees a higher pressure than the average pressure at station 1 can be seen when looking at the green line indicating the pressure at station 2 from CFD in figure 4.6. It reaches a pressure of 97.5 bar at the larger cavity sizes, while the average pressure at station 1 is 97 bar measured at larger cavity sizes, the red line. Unless there is a pressure increase within the inlet cavity the pressure at station 2 should not be higher than the pressure at station 1. This makes it plausible that the shroud actually sees the maximum pressure at station 1, as is used by the model.

When comparing the pressure predicted at station 2 by the model to that of CFD in figure 4.6, it can be seen that they do follow a similar trend. However, the value they converge to differs. The pressure at station 2 predicted by the model converges to the maximum pressure at station 1 of 98.7 bar, which was taken as its input. This indicates that as the cavity width increases the sealing capacity reduces. The pressure at station 2 from CFD does not converge to the maximum inlet pressure, but to 97.5 bar. This suggests that either another unidentified pressure drop is present or that the pressure the shroud actually sees is slightly lower than the maximum pressure occurring at station 1.

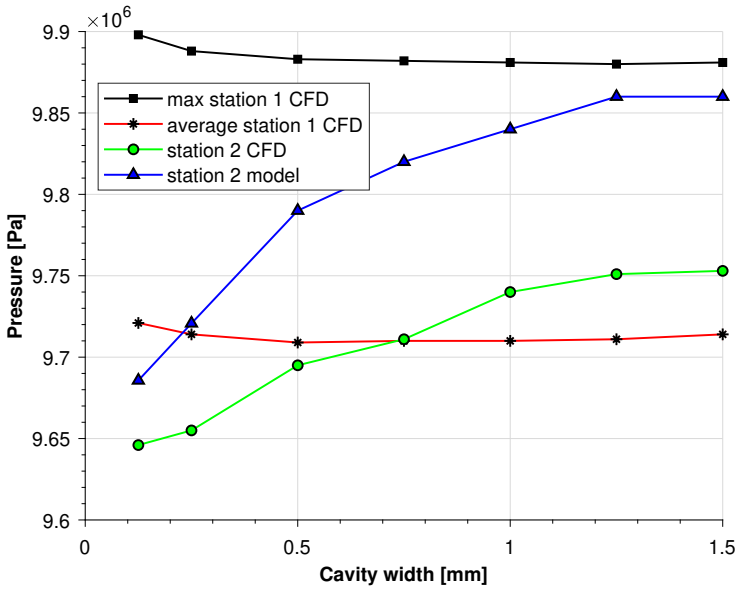

Figure 4.6: Rotor inlet to cavity inlet pressure drop

Figure 4.7 shows the pressure plotted against the cavity width for the shroud sealed by the brush seal. The black line indicated the maximum pressure at station 1, while the red line indicated the average pressure at station one from CFD. The green line is the pressure in CFD at station 2. It can be seen that in this case the pressure at station 2 in CFD is equal to the maximum pressure of station 1. Indicating that the inlet cavity width plays no role in the sealing of the shroud. This confirms the suspicion that the shroud sees a higher pressure than the average pressure at station one and that it is most likely the maximum pressure at station 1.

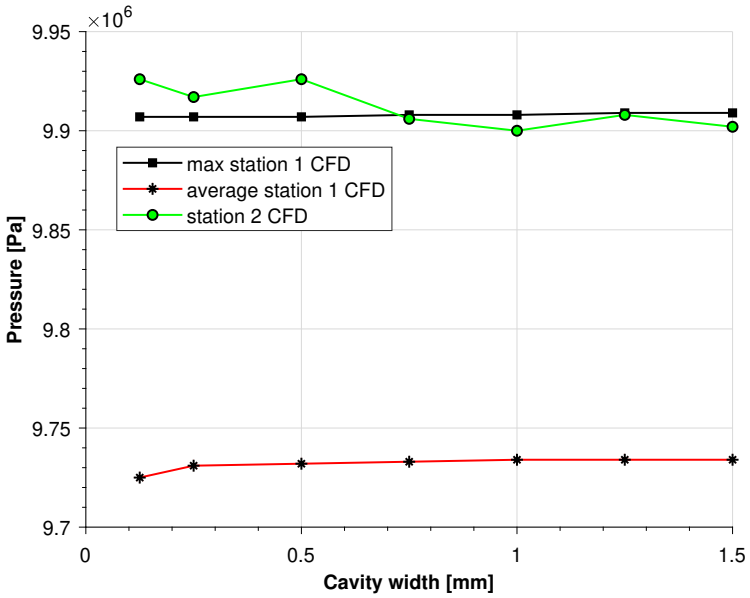

Figure 4.7: Comparison of pressure at the inlet tip and inlet cavity for the shroud with a brush seal.

4.1.4. OUTLET PRESSURE

The outlet of the shroud is modelled similarly to the inlet, with a labyrinth seal. Figure 4.8 plots the pressures observed from the CFD and model at stations 3 and 4 against the cavity width. The pressures of the model

and CFD at station 3 both decline with increasing cavity width, this indicates that the sealing capacity of the outlet reduces. The similarities between the model and CFD that was clearly visible at the inlet pressures are not so clear in this case. However, again a pressure difference between the average pressure of station 4 and the pressure seen at the tip might be a cause.

Figure 4.9 shows the pressures at the outlet of the labyrinth seal shroud versus the cavity width when a constant pressure difference is applied to the seal outlet of 2 bar. This constant pressure drop is determined from CFD and when that is included in the model results are very convincing, showing the importance of being able to model the difference in pressures.

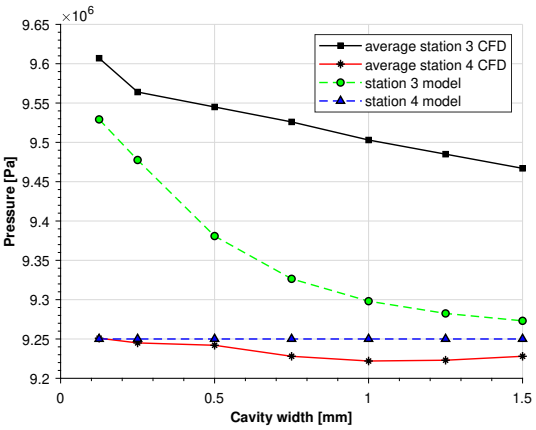

Figure 4.8: Pressures of the outlet of the shroud from the model and CFD.

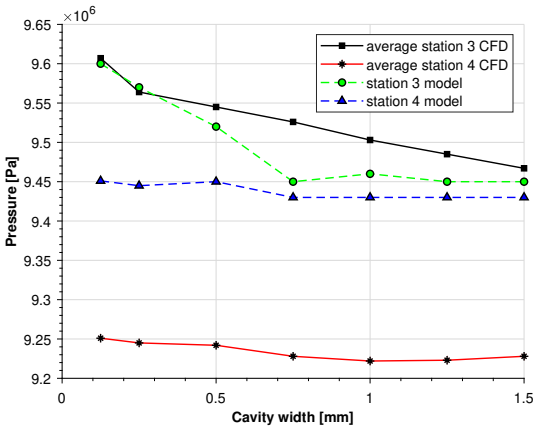

Figure 4.9: Pressure at the outlet of the labyrinth seal shroud, where the model uses an constant pressure drop at the outlet of 2 bar.

With careful analysis from CFD, it is determined that this additional pressure drop happens at or after the expansion into the turbines main flow. This large expansion and differences in kinetic energy for rotational velocities is not something the BFM is intended to calculate and thus the most plausible explanation for the deviation. So it is key to determine what pressure the shroud actually sees. Unfortunately, the pressure the shroud sees at the exit is influenced by the shroud itself, which becomes clear when comparing the pressure contours of a shrouded turbine in figure 4.10 with that of an unshrouded turbine in figure 4.11. The pressure contour of the shrouded turbine has a band of higher pressure on the upper side near the outlet cavity of the shroud, while the unshrouded turbine shows a more uniform pressure over the whole location.

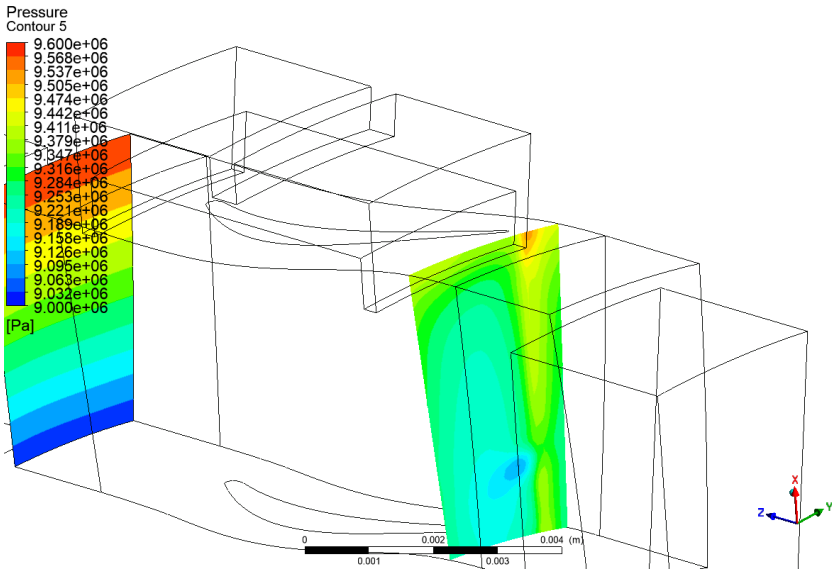

Figure 4.10: Pressure contour just before the shroud exit

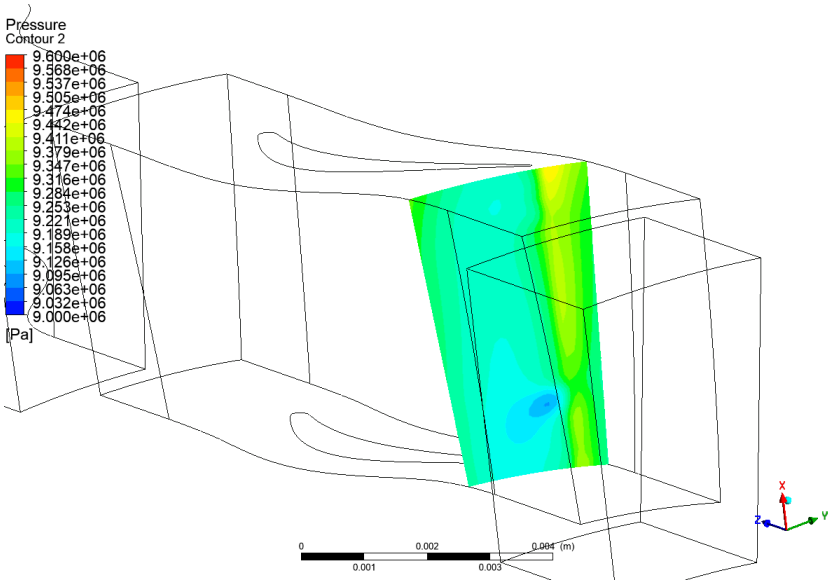

Figure 4.11: Pressure contour at the same place, but without the shroud

In the previous sections, it could be seen that the inlet and outlet width had almost no influence on the leakage rate through the brush sealed shroud. The pressure at station 2 of the brush seal was equal to the maximum pressure at station 1. As noted for the inlet pressure in the previous section the model agrees well with CFD however, for the outlet it does not fully hold. Figure 4.12 shows the pressures at station 3 and 4 of the model and CFD as a function of the cavity widths. In CFD it can be seen that the pressure at station 3 is 1 to 0.5 bar higher than the pressure at station 4 dependent on the cavity size. The pressure predicted by the model at station 3 lies on the pressure at station 4, which is its outlet boundary condition. The difference between CFD and the model indicates that the model does not take into account some pressure difference. The straight line of CFD at station 3 in combination with the higher pressure seen in front of the labyrinth sealed shroud outlet, suggests that also the outlet of the shroud sees a pressure that is higher than the average pressure at station 4. Contrary to the inlet no suitable approximation of this difference in pressure has been found.

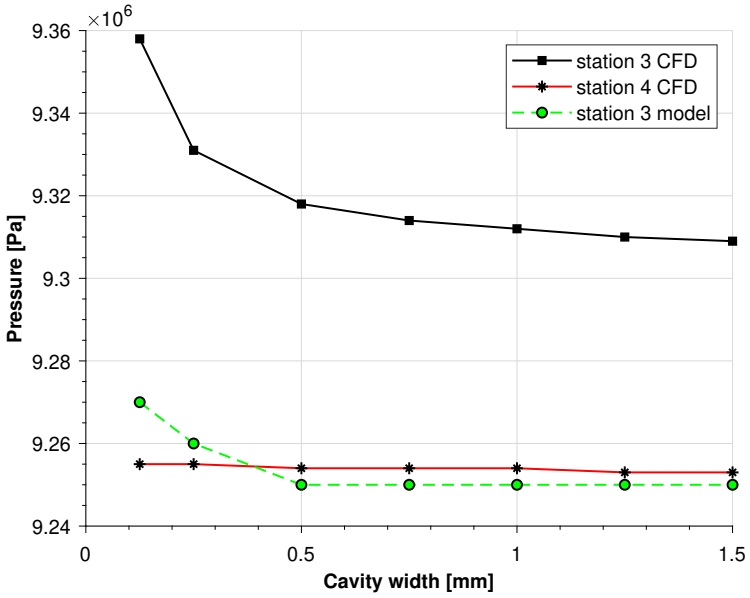

Figure 4.12: Comparison of outlet cavity pressure of the model and CFD

4.1.5. ROTOR LOSSES

As described in section 3.6 the new clearance loss is calculated with the newly developed model in combination with Denton's (equation 3.31) clearance loss equation. Figure 4.13 shows the comparison for rotor pressure loss for the CFD case, the predicted values of the loss model of Dunham&Came and the combined loss model of Denton and Dunham&Came and which takes the mass flow ratio from CFD. It can be seen that the combined model of Denton and DC prediction come close to the values obtained by CFD and most importantly that the trend is followed. The loss model of Dumham&Came does not take the cavity size into account and thus only outputs a constant value and over predicts the rotor losses. Furthermore, the current loss model of Dawn Aerospace thus grossly overpredicts the rotor loss of the turbine.

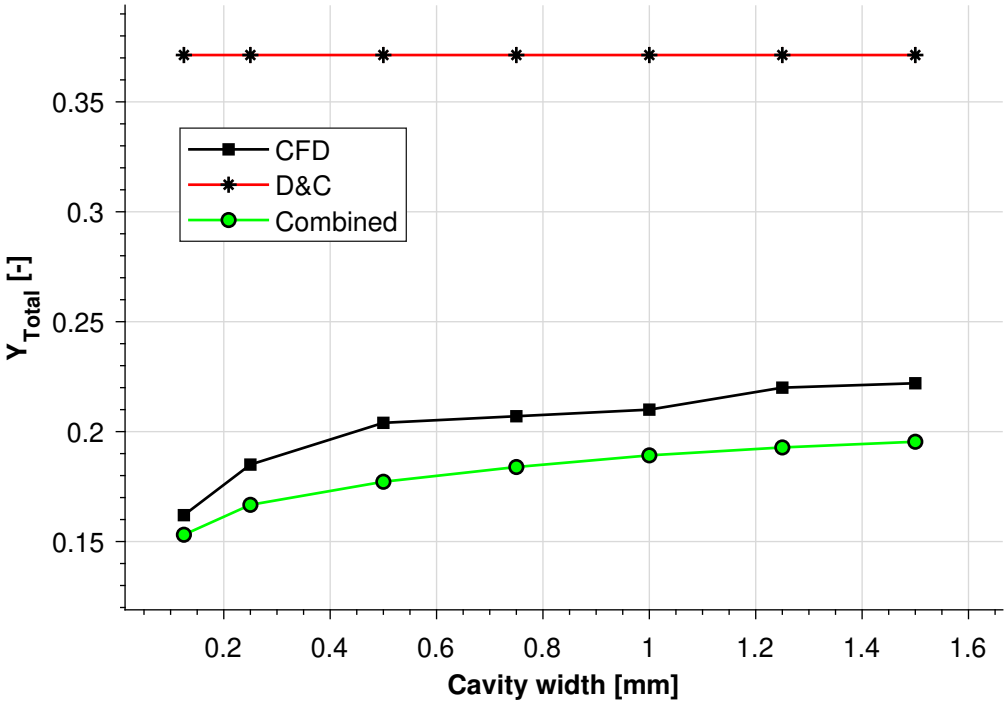

Figure 4.13: Rotor losses plotted against the cavity size of inlet and outlet of the shroud predicted by CFD, Dumham&Came and the combined loss model of Denton and Dunham&Came.

4.2. FULL DESIGN VALIDATION

In the previous section, it has been shown that the model can predict leakage rates through sealed shroud configurations. This section will illustrate that the model can be used with the meanline design code. For this several turbines are designed with the new model and compared to CFD. The designed turbines consist of a single fin seal design in subsection 4.2.1, a brush sealed shroud in subsection 4.2.2, a multi-fin labyrinth seal in subsection 4.2.3 and a larger sized turbine in subsection 4.2.4.

4.2.1. 1 FINNED DESIGN

A new design of the turbine has been made using the above-described shroud model in combination with the Denton clearance loss, which is integrated into the Dunham&Came loss model. Useful conclusions can be drawn with respect to the comparison with CFD and the discrepancy between the loss model and CFD. As has been proven in the previous section for the 1 finned labyrinth case the inlet and outlet cavity size have a significant role to play on the leakage rate. See for example figure 4.3 where it is shown that the smaller the cavity size, the lower the leakage and thus loss. For this reason, the minimum distance the designer is comfortable with producing is taken and that is 0.3 mm.

In the new design the rotor loss predicted by DASM is 0.19, while CFD predicts a rotor loss of 0.17 as can be seen in table 4.1. When using a conventional clearance loss model the predicted rotor loss rises to 0.36, almost twice as high as CFD. The difference in efficiency is reduced from 11.2% to just 5.6% for a similar-sized turbine. The efficiency difference between the model with meanline is now 5.6%.

Table 4.1: Comparison of performance parameters of a small turbine with a one finned labyrinth seal, model prediction versus CFD

parameter	DASM	DC	CFD	Deviation
mass flow rate [kg/s]	2.25	-	2.4	6.7%
leakage fraction [-]	0.0517	-	0.0284	-45%
nozzle pressure loss [-]	0.0810	-	0.0625	-22.8%
rotor pressure loss [-]	0.2037	0.3552	0.1769	-13.2%/-50.2%
Efficiency [%]	83.8	-	88.5	5.6%

4.2.2. BRUSH SEAL DESIGN

In this section, the 1 fin labyrinth seal on top of the shroud is replaced by a brush seal. For this the node for the labyrinth seal in the shroud file needs to be replaced with a node containing the brush seal. Additional inputs to this model will be brush thickness and fence height, if specific data on resistance coefficients are known for the seal the user can specify these as well otherwise the resistance coefficients proposed by Chew are used.

As far as the author is aware there exists no axial turbine loss model capable of predicting clearances loss when a brush seal is installed on top of the rotor shroud in open literature. Nevertheless, the usage of turbines that are being retrofitted is continuing to increase and experimental and numerical research is being done on the topic. Designing a turbine for losses with a labyrinth seal and replacing that with a brush seal in the real application, might result in sub-optimal designs compared to the case where the preliminary designs already included the brush seal. It has to be noted that the loss model presented here does not include power loss due to friction between the brush seal and the shroud, but neither does CFD so results between the two are expected to be comparable.

Again, the inputs of the reference turbine are used only now using a brush seal on top of the shroud. The design returned with the brush seal predicts a 2% increase in the turbine's efficiency compared to the case where a 1 finned labyrinth seal is used (84% to 86%). When comparing the DASM predictions with CFD (table 4.2) it can be seen that leakage fraction and rotor loss correspond well. Again there is a large discrepancy between nozzle losses (CFD is 2/3 of DASM predictions), which previously have been attributed to the thickness over chord ratio lying out of bounds for the loss models. But it has now come to a point where it might seriously alter prediction outputs when compared to CFD. Nevertheless, efficiency is within 5% points of each other and the difference in rotor loss is within 4%. Another noteworthy point is that CFD predicts also a 2% points efficiency increase compared to the 1 finned labyrinth seal (88% to 90%).

Table 4.2: Comparison of performance parameters of a small turbine with a shroud brush seal, model prediction versus CFD

Parameter	DASM	CFD	Deviation
Mass flow rate [kg/s]	2.25	2.369	5.3%
Leakage Fraction [-]	0.0066	0.0052	-21.2%
Nozzle pressure loss [-]	0.0922	0.0594	-35.5%
Rotor pressure loss [-]	0.1403	0.1355	-3.4%
Efficiency [%]	86.2	90.5	5.0%

4.2.3. 4 FINNED LABYRINTH SEAL DESIGN

Here the new design of the reference turbine uses a labyrinth on top of the shroud with multiple fins. The fins are spaced by 0.5 mm which means that, if the shroud is 5 mm long, a maximum of 5 fins can be placed on top. The new design generated has a 4 finned labyrinth seal on top.

Results are presented in table 4.3, where it can be seen that leakage fraction and rotor loss match closely. This time the efficiency prediction is off by 3% point and has to be almost completely caused by the difference in nozzle losses. This case shows that the model can also accurately predict clearance losses for a multi-finned labyrinth seal on top of the shroud. Rotor loss is now actually under predicted in DASM, while previously it over predicted. The rotor with shroud was also supplied to the loss model of Dunham&Came who predicted a rotor loss of 0.2237, which is a 50% over prediction compared with CFD.

Table 4.3: Comparison of performance parameters of a small turbine with a shroud 4 fin labyrinth seal, model prediction versus CFD

Parameter	DASM	CFD	Deviation
Mass flow rate [kg/s]	2.25	2.397	6.5%
Leakage Fraction [-]	0.0318	0.0302	-5.0%
Nozzle pressure loss [-]	0.0801	0.0597	-25.5%
Rotor pressure loss [-]	0.1538	0.1615	5.0%
Efficiency [%]	85.7	88.7	3.5%

4.2.4. LARGER TURBINE

Here a turbine with larger blade sizes will be discussed which has been taken from literature. The inputs of the turbine are taken from Behr [57] are put through the meanline design program of Dawn Aerospace with the DASM model, in order to first construct the blades and also to assess performance predicted by the loss model. Table 4.4 shows input parameters used to design the turbine, small deviations with the turbine in the paper can be found, i.e. blade angles, due to different design methodologies and constraints imposed by the design code. The inputs are collected from the research at the ETH Zurich at the LISA facility where several authors mention a similar turbine [49, 50, 57]. Especially an increase in the main radius and the mass flow rate can be seen in this case compared to the reference turbine of Dawn Aerospace.

Table 4.4: Large shrouded turbine comparison case design parameters

Parameter	Value [unit]
λ	0.39 [-]
ψ	2.55 [-]
ϕ	0.384 [-]
Design speed	3750 [rpm]
Aspect ratio	0.714 [-]
Zweifel number	0.72 [-]
mean radius	0.365 [m]
Inlet pressure	1.4 [bar]
Pressure ratio	1.4 [-]
Mass flow rate	11.5 [kg/s]

The turbine code with DASM predicts an efficiency of 86.75% for the large turbine, with a nozzle pressure loss of 0.1127 and a rotor pressure loss of 0.1865. The clearance loss contributing to the rotor loss is 15% and the predicted leakage fraction through the shroud is 1.5%. The outputs of the model are compared to CFD in table 4.5. It can be seen that the model over predicts the pressure loss in the nozzle by 19.8% and for the rotor even 28.4%, while the predicted leakage fraction is under predicted by 5%. Nevertheless, the efficiency predictions for this turbine are not far off with an error of 3.3%.

Table 4.5: Comparison of performance parameters of a larger turbine from literature, model prediction versus CFD

Parameter	DASM	CFD	Deviation
Mass flow rate [kg/s]	11.5	11.7	1.7%
Leakage Fraction [-]	0.0146	0.0153	4.8%
Nozzle pressure loss [-]	0.1127	0.0904	-19.8%
Rotor pressure loss [-]	0.1865	0.1355	-28.4%
Efficiency [%]	86.75	89.6	3.3%

When using the nominal loss model of Dunham&Came the rotor loss now becomes 0.2230, which is a 20% increase from the predicted loss of the DASM model. Where the clearance loss now contributes 28% to the total pressure loss, almost doubling the amount of clearance loss. Behr compared the predicted pressure loss from Dunham&Came to the measured pressure loss of the turbine and found the loss model overpredicting the losses by 30.2%.

4.3. SOLUTION SPEED

There is a drawback in the implementation of the model and it is focused on the implicit nature of the calculation of the leakage rate through the shroud. This effect is strengthened by the iterative nature of all bulk flow models which are used. The work station on which the meanline design program is run in MATLAB 2019b has a CPU clock speed of 1.8 GHz and 16 GB of ram. On this work station the mean line program can calculate 3 turbine designs in one second with the DASM. When the clearance loss model of Dunham&Came is used, a total of 20 turbine designs can be reached in one second.

The drawback thus is speed, which is an important aspect of preliminary design tools in order to explore wide design spaces. The model not only must iterate over the mass flow rate in order to satisfy the outlet boundary condition, but it also iterates within the BFM for the labyrinth seal which is used for the inlet and outlet of the shroud. Each iteration takes time and the more iterations that are needed, the more time it costs to solve the model. For the solution procedure of the BFMs there is only so much that can be done as their solutions steps were not determined by the author of this thesis. The solution procedure for the DASM model however, has been carefully assessed. There are two major factors influencing the solution speed of this model, the first being the initial guess mass flow rate and the second being the updating scheme of the mass flow rate.

The mass flow rate that flows through the shroud as a leakage rate is hugely determined by the sealing configuration, turbine size and pressure drop. To get a first estimate the often quoted 1% leakage rate of the total mass flow rate was used. However, as the turbine is smaller the leakage rate is higher leading to long solution times a number of 5% was found to be more suitable. Unfortunately, this high number suitable for labyrinth seals is far of from the actual leakage through a brush seal, such that in the case of a brush seal an initial guess off 1% is recommended again.

The solution scheme of the whole model is currently solved as the following: increase the mass flow rate by 1% when the calculated pressure is higher than the boundary condition and decrease the mass flow rate by 1% when the calculated pressure is lower than the specified boundary condition. This updating process is by no means optimized or the best method to solve this. A faster method might deploy a larger or smaller incremental step size based on the absolute error between the pressures.

4.4. SENSITIVITY ANALYSIS OF THE DASM MODEL

Several studies did numerical and experimental analysis on the effects of shroud geometry variations on leakage rate and turbine efficiency. With the help of the newly developed model, it is shown how these geometrical variations affect the turbine design in a preliminary design state. In addition to this, general design guidelines are given that minimize the shroud leakage flow by altering geometrical parameters of the used seal on top of the turbine shroud. In order to propose the design guidelines, a sensitivity analysis is done on parameters influencing the shroud design, including inlets and outlets. From this, conclusions can be drawn on what are important parameters and how the seals compare to each other. In previous chapters, it could be seen that the inlet and outlet of the shroud played a large role when dealing with labyrinth seal systems on top of the shroud. This chapter sets out to see how different geometrical parameters further influence the leakage rate through the shroud seal for the reference turbine case.

Section 4.4.1 highlights the input parameters of the model used throughout this chapter. Thereafter a sensitivity analysis is done on the annular seal in section 4.4.2, the labyrinth seal in section 4.4.3 and the brush seal in section 4.4.4. At the end of the chapter, section 4.4.5 discusses the design guidelines for shroud designs for small turbines.

4.4.1. COMMON INPUT PARAMETERS

The reference turbine presented in section 3.1 is used throughout this chapter, to investigate the best practice to design a shroud of a small axial turbine. The size of the shroud to place sealing systems is the length of the axial chord of the rotor blade plus a 0.5 mm extension in both direction, for manufacturing convenience. It uses the tip rotor inlet pressure and the average rotor outlet pressure. The pressures encountered at this position are 1.0017e7 Pa and 9.2536e6 Pa respectively. The radius at the inlet of the rotor passage is 0.0234 m and at the outlet 0.0235 m. The total axial length to place sealing systems is 0.0055 meter or 5.5 mm. The inlet temperature is 1001 K and the fluid is decomposed hydrogen peroxide. In this case, there is the possibility to apply the annular, labyrinth or brush seal on top of the shroud to minimize the leakage rate. Note that this is slightly different than using the model for a whole new design as in this case the flow angles stay the same and only leakage rate is assessed.

4.4.2. ANNULAR SEAL

The design of the labyrinth sealed or annular sealed shroud is the most simple approach. In this case, the annular seal is adopted, which ensures a tight clearance between the shroud and the casing. The smallest clearance is dictated by rotor growth due to heat and centrifugal forces acting on the shroud. Furthermore, there are the inlet and outlet cavity width, which act as seals if chosen sufficiently small. The seal length is the length of the shroud on top of the blade. The seal length can thus only be changed a little however, to investigate some influence of the seal length it can be altered by shortening the overhang introduced. The length of the seal varies between 4.5 mm and 5.5 mm. In this section, the effect of the geometric shroud parameters is investigated when an annular seal is applied in the case of the reference turbine.

Figure 4.14 shows the mass flow rate variation when the inlet width and outlet width are altered in the case of the base annular seal on top. It can be seen that the mass flow rate flattens out earlier when the inlet cavity width is increased, when compared to the outlet cavity. Meaning that keeping the outlet cavity width smaller would be more beneficial. Although, the best would be minimizing both as when the inlet and outlet cavity both grow the leakage rate increases rapidly and flattening out as seen in previous chapters is not happening. This Indicates that the inlet and outlet widths are still the limiting factors in this case.

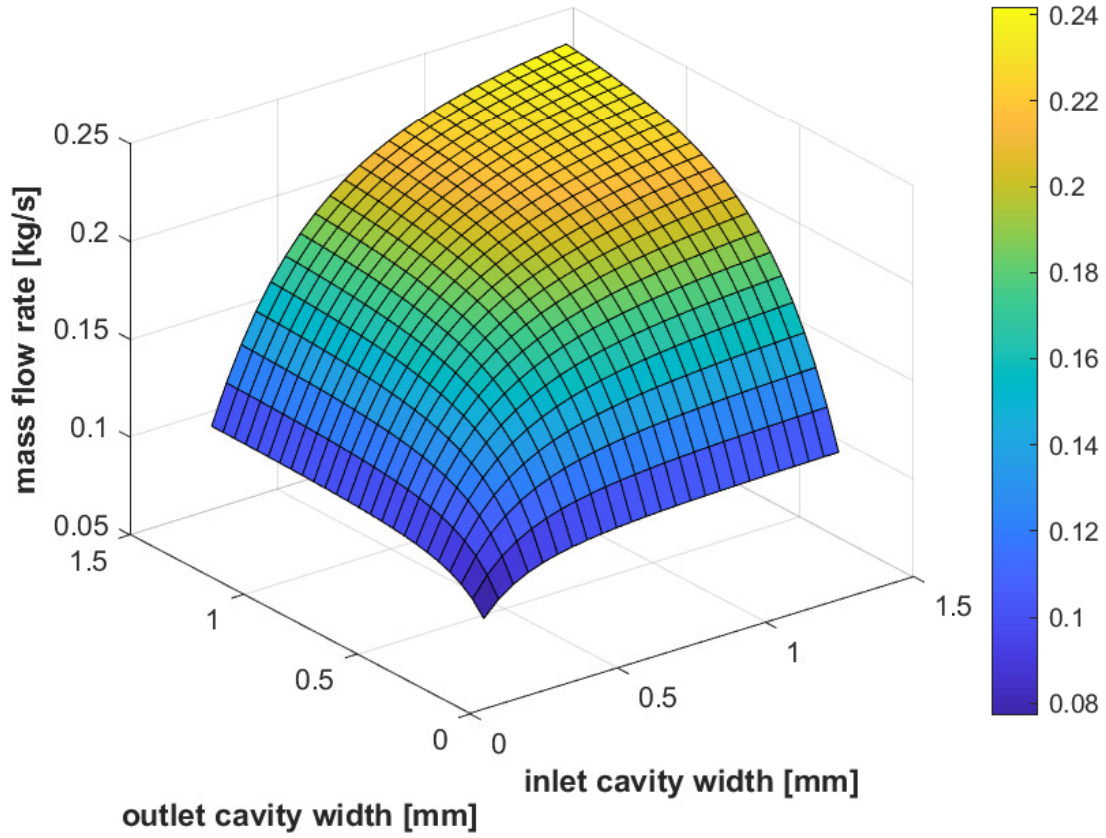

Figure 4.14: The effect of the inlet and outlet cavity width on the leakage rate through the shroud of the reference turbine using an annular seal.

The influence of the seal length on the leakage rate through the annular seal of the shrouded turbine can be seen in figure 4.15. Increasing the length of the seal from 4.5 mm to 5.5 mm reduces the leakage rate in a linear trend however, the reduced leakage rate is very small, a reduction of only 0.5%.

Figure 4.16 shows the mass flow rate through the shroud as a function of the clearance of the straight annular seal. When the clearance is very tight, 0.15 mm, the annular seal is dominant, while as the clearance increases most of the pressure drop happens again at the inlet and outlet and thus limiting the leakage rate. Figure 4.17 shows the above described behaviour in more detail. On the x-axis the location number is plotted, where 1 denotes the shroud inlet (labyrinth) 2 the annular seal and 3 the outlet (labyrinth) of the shroud. On the y-axis the pressure drop across the seal is displayed, the more negative the value is the larger the registered

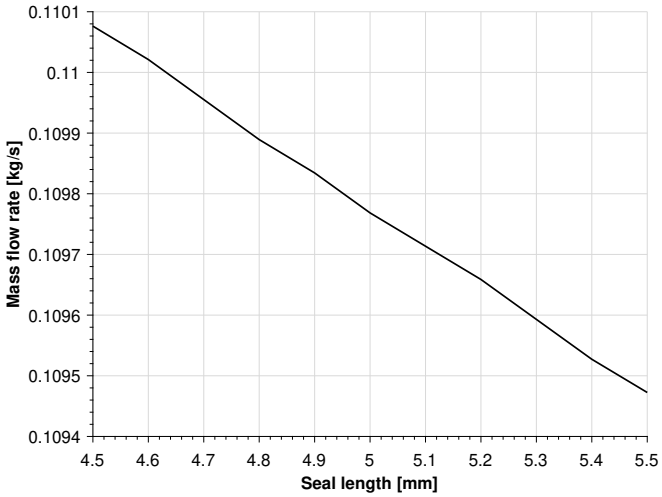

Figure 4.15: The effect of length of the annular seal on leakage rate through the shroud of the reference turbine.

pressure drop. Whenever the pressure drop at station 2 is larger than at station 1 and 3 (the inlet and outlet) it thus means that the annular seal is dominant. For the clearance of 0.15 mm this is clearly the case and still holds for the 0.2 mm clearance gap, when the clearance is 0.25 mm or higher the inlet and outlet both contribute more to the pressure drop and thus leakage reduction than the annular seal does. Already at a clearance of 0.5 mm the annular seal becomes only marginally effective, indicating that an annular seal is only beneficial when a very tight clearance gap can be ensured.

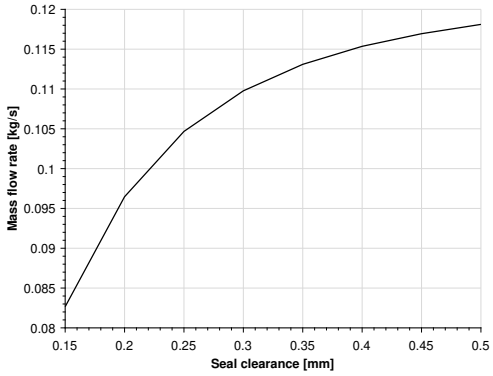

Figure 4.16: The effect of clearance of the annular seal on leakage rate through the shroud of the reference turbine.

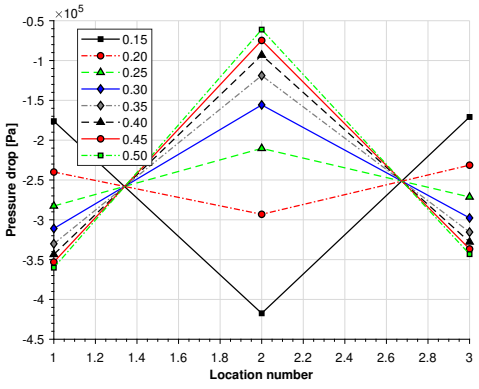

Figure 4.17: The pressure drop that happens at which location in the shroud system for the reference turbine with an annular seal, for changing seal clearance.

4.4.3. LABYRINTH SEAL

In this section, the annular seal on top of the shroud is replaced with a labyrinth seal. In the case where the clearance between the labyrinth seal and the shroud is altered only one fin is used. The axial length on top of the shroud is 5.5 mm and determines together with the spacing between fins the maximum amount of fins that the seal can use.

Figure 4.18 shows that both the inlet and outlet cavity width have a significant effect on the leakage rate through the seal, with little difference on which one is minimized. Figure 4.18 also shows that the best combination exists when both cavity widths are minimized, this agrees with findings by Rosic et al. [49]. Similar behaviour could be found that after increasing the cavity width higher than a certain threshold they stop acting as seals and further increasing their width only marginally increases the leakage rate through the shroud.

In figure 4.19 the response can be seen when the number of fins on the top is altered and the spacing is

changed. The influence of the number of teeth on the mass flow rate through the seal is large. While spacing changes the mass flow rate little, indicating that it would be more beneficial to reduce spacing such that more fins can be placed. Although the effect of more fins also reduces, around 4 fins the contribution of the additional fin becomes smaller.

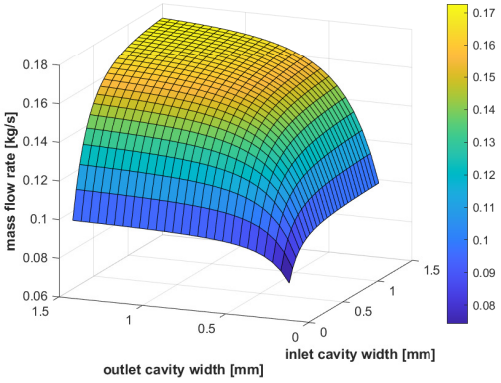

Figure 4.18: The effect of the inlet and outlet cavity width on the leakage rate through the shroud of the reference turbine.

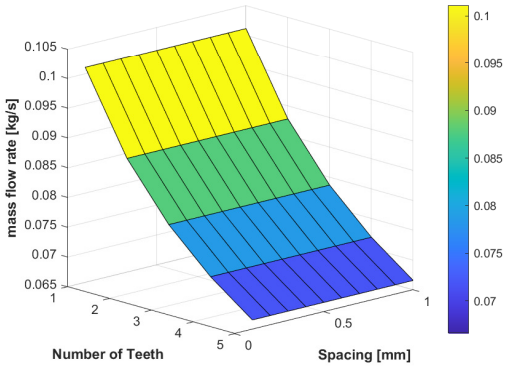

Figure 4.19: The effect of the number of teeth and spacing of the seal on top of the shroud on the leakage rate through the shroud of the reference turbine.

The clearance of the actual seal is varied from 0.15 mm to 1 mm in order to see how that influences the leakage rate. Figure 4.20 shows this effect, it can be seen that here as well the influence on the leakage rate becomes less when the clearance increases. At this point, the inlet and outlets start to do all the sealing and are the limiting factors for the mass flow rate through the shroud.

Figure 4.21 shows the increase in shroud height on the x-axis and the mass flow rate on the y-axis. A linear increase can be seen for the mass flow rate when the shroud height is increased with constant clearance between the fin and the shroud, the effect is however very small. The shroud height is influenced by what can be manufactured, but ideally would be as small as possible. This will not only help with reducing the leakage rate but also with keeping the added shroud weight to a minimum and thus also reducing stresses in the rotor blades.

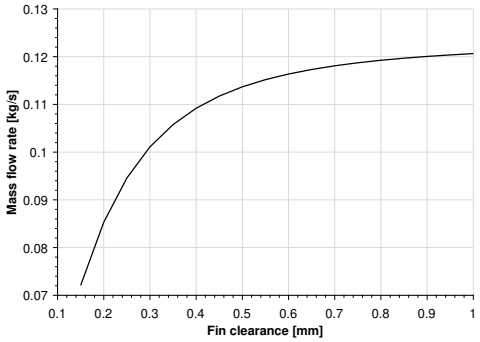

Figure 4.20: The effect of the clearance height of the fin on top of the shroud on the leakage rate through the shroud of the reference turbine.

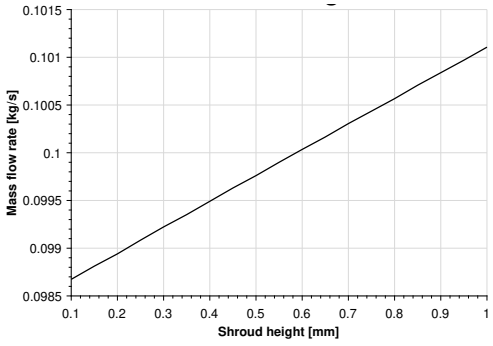

Figure 4.21: The effect of shroud thickness on the mass flow rate through the turbine.

4.4.4. BRUSH SEAL

In the case of the brush seal, the labyrinth seal is replaced with a brush, the inlet and outlet widths stay the same and are thus approximated with labyrinth seals. The brush seal is not as customizable as the annular seal and labyrinth seal, as it is more complicated to manufacture and thus will often have to be bought from a supplier. Nevertheless, the designer usually has some room for customization which includes the: 1)brush thickness, 2) the backing ring clearance, 3) the wire diameter, 4) bristle lay angle and 5) bristle density. The brush thickness and backing ring clearance are parameters that directly influence the pressure drop, and thus leakage rate, through the brush seal. While the wire diameter, the bristle lay angle and the bristle density

influence the leakage in a secondary way by altering the resistance variables through the changing porosity. So the 5 parameters can be reduced to 3 independent parameters: wire diameter, seal length and porosity (which includes bristle density and lay angle).

Increasing the backing ring clearance enlarges the area through which mass can flow. The clearance with the backing-ring is needed to prevent shaft run-ins damaging both seal and rotor. Figure 4.22 shows that in the case of the brush sealed shroud, increasing the backing ring clearance has a linear influence on the leakage rate through the shroud. There is no indication that the inlet and outlet cavity width start influencing the mass flow rate through the shroud over a backing ring clearance range of 0.1 mm to 1 mm, this can also be seen in figure 4.23 where all pressure drop happens over the brush seal at station 2.

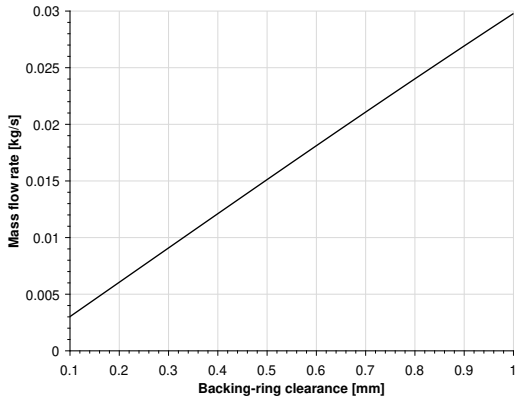

Figure 4.22: The effect of the clearance of the backing-ring on the mass flow rate through the shroud of the reference turbine sealed with a brush seal.

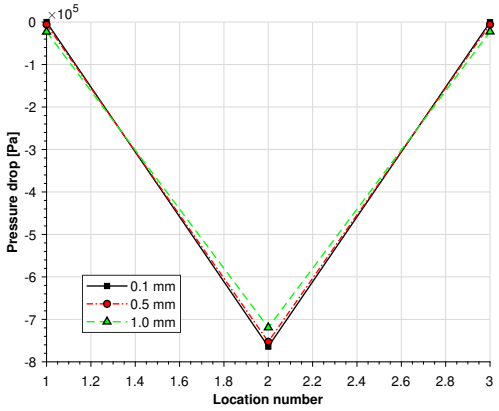

Figure 4.23: Pressure drop over each sealing point in the turbine shroud sealed by a brush system. Station 1: inlet, station 2: brush seal and station 3: outlet.

Figure 4.24 plots the mass flow rate through the shroud with a brush seal against the thickness of the brush seal with a constant porosity of 0.3. It can be seen that the thicker the brush seal is the less leakage flow through the shroud, although the effect of using a thicker brush on reducing leakage rates becomes less significant. Figure 4.25 shows the effect of the porosity of the brush seal on the mass flow rate. The lower the porosity the lower the leakage of the seal, which makes sense as the porosity is defined as the amount of fluid volume. The increase in mass flow rate follows a quadratic trend for an increase in porosity.

The effect of the inlet and outlet width on the shroud can be seen in figure 4.26, clearly indicating that only when a very tight tolerance can be realised they contribute to the reduction of the leakage rate of the seal. However, even with the tight clearance the reduction is marginal. This proves that especially when inlet and outlet cavities size can not be limited it the usage of the brush seal is very beneficial.

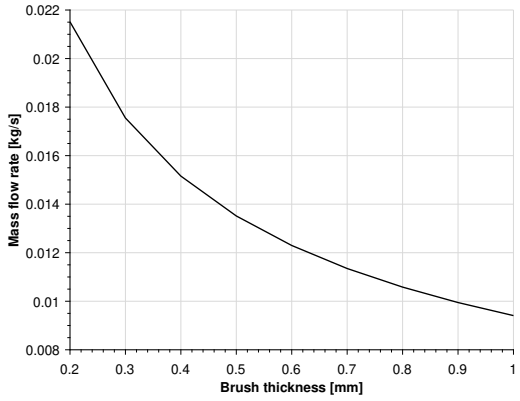

Figure 4.24: The effect of the brush thickness on the mass flow rate through the shroud of the reference turbine sealed with a brush seal at a constant porosity of 0.3.

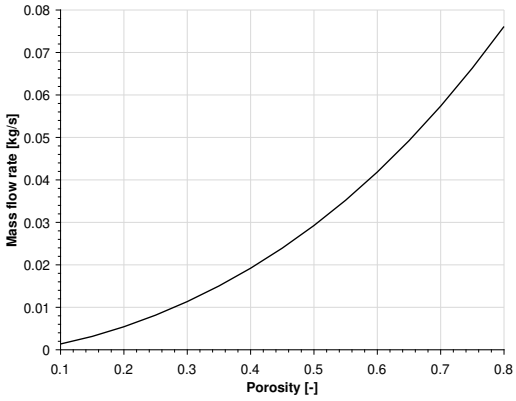

Figure 4.25: The effect of the brush thickness on the mass flow rate through the shroud of the reference turbine sealed with a brush seal at a constant porosity of 0.3.

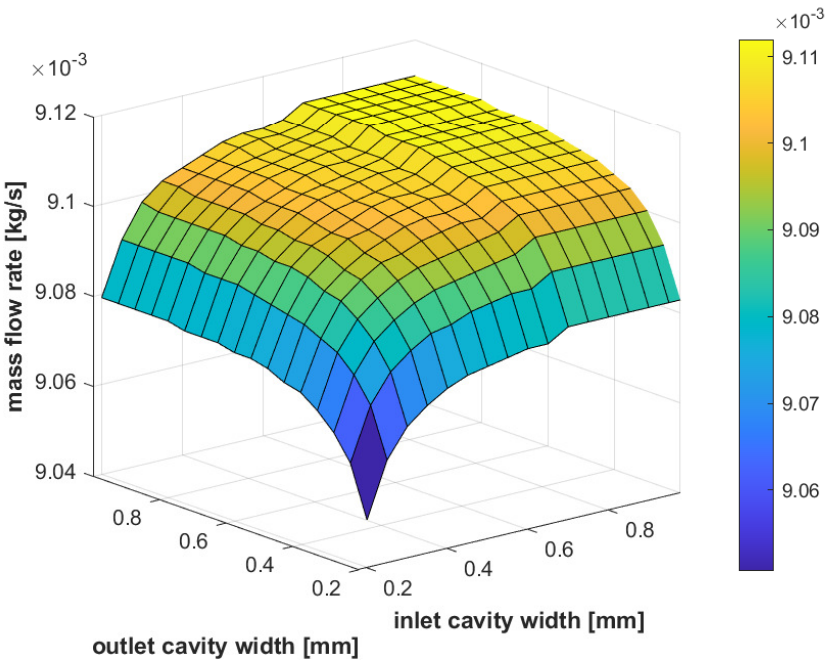

Figure 4.26: Influence of inlet and exit clearance widths on the leakage rate through a brush seal turbine shroud

4.4.5. DESIGN GUIDELINES

In this section, a short overview will be given of the findings above and will be condensed to some best practices. In the chapters above the guidelines can be found for each case separately, while here the general best practises can be found.

When simplicity is most important it is still recommended to incorporate some form of labyrinth seal over the annular seal. Even with one fin, the labyrinth seal outperforms the annular seal with respect to leakage at the same rotor clearance and the same inlet and outlet shroud widths. Especially important is the flattening in the mass flow rate when the inlet and outlet widths are increased.

Whenever very good sealing is required for minimum leakage and additional costs can be made the brush seal is the recommended choice. Inlet and outlet width have little influence on the seal performance, so no limits have to be reached to ensure good sealing of the shroud. The larger tolerance in front and at the back of the shroud can possibly prevent run-ins at transient conditions.

In general, it is best to where ever a clearance exists to minimize it as far as possible within manufacturing constraints. Shroud height has little influence on the leakage through all seals, thus it is recommended to choose an acceptable limit relatively thin to reduce weight and stresses in the turbine blades. The longer the seal the more sealing systems that can be added, i.e. fins, thus ensuring lower leakage rate through the shroud, however making large shrouds does not make sense with respect to weight.

4.5. DISCUSSION

There are still two unresolved issues related to the model. 1) There is an unaccounted pressure drop at the inlet of the seal when leakage rates are higher (not present in the case of the brush seal). 2) The higher pressure at the exit boundary can not be calculated as of yet, as it is caused by the shroud itself. For these issues, no solution was found within the time frame of this thesis. Nevertheless, the model predictions do predict the trend line, which is of main interest for a preliminary design tool.

5

CONCLUSIONS

At the beginning of this thesis, a research objective together with 4 research questions were formulated. The questions helped achieving the goal of numerically assessing the impact of advanced sealing models placed on top of small shrouded turbines on the efficiency at a preliminary design stage. The work that was done throughout this thesis provides answers to these 4 questions and are answered below along with a summary of the completed work to get to the answer.

- **How can the seal leakage equations be combined with existing loss models?**

  The seal leakage equations can be used with the existing loss model of Dunham&Came by using Denton's clearance loss equation and converting that to a pressure loss. Denton's leakage equation takes a leakage rate as an input, which is an output of the seal leakage equations. In order for the seal leakage equations to give satisfactory results for shroud flows, the inlet and outlet width of the shroud need to be taken into account. It was found that due to similar flow structures labyrinth seal models can predict the pressure drop of the inlet and outlet cavity. The leakage equation of the subsequent shroud seal is then placed in between the labyrinth seal approximating the inlet and outlet cavity width. The leakage rate is calculated in an iterative manner for this sealing system, where the mass flow rate and pressure drops are passed on to the next seal until the calculated outlet pressure matched that of the boundary condition.

- **How accurate can seal leakage equations predict the amount of leakage flow through a shroud seal configuration?**

  For the two thoroughly tested single finned labyrinth seal and brush seal on the reference turbine the predictions of the model compared to CFD was at most 32.3% and 14.3% respectively. However, for the labyrinth seal, for cavity sizes of 0.25 mm and smaller, the error was below 10%. It was shown that when the pressures in front and after the seal on top of the shroud were exactly matched the leakage rate through the seal was matched within 3% For both the labyrinth seal and the brush seal the trends of leakage rates were predicted well.

- **How accurate are the efficiency predictions of the combined seal leakage equation and existing leakage models?**

  How accurate the efficiency predictions are of the developed model was tested against 4 turbines designed with the new clearance loss activated in the meanline design model and compared to CFD. 3 of those turbines were of the size of the reference turbine, while 1 bigger turbine was reproduced from literature.

  - The first designed turbine used a one finned labyrinth seal on top of the shroud and the difference in efficiency was 5.6%. To compare also the existing loss model the predicted rotor pressure losses were compared: the new model overpredicted the loss by 13.2% and the loss model of Dunham&Came over predicted the loss by as much as 50.2%.
  - The second turbine had a brush seal placed on top of the shroud, the design program over predicted the loss by 5%. No comparison could be made with Dunham&Came as their loss model does not include an option to predict clearance losses for brush sealed shrouds.

  - This time the shroud was sealed by a 4 finned labyrinth seal and predicted efficiencies differed by 3.5%.
  - The larger turbine from literature used 2 fins to seal the shroud. The difference in efficiency between the model prediction and CFD was 3.3%.

- **What is the best configuration for the small turbine of Dawn Aerospace in order to reduce leakage rate through the shroud?**

  From the sensitive analysis performed on a shroud of the reference turbine with respect to leakage rate the following conclusions could be drawn to minimize the shroud leakage rate:

  - The brush seal is the most effective seal placed on top of the shroud among the investigated sealing solutions. Especially when the backing ring clearance of the seal can be kept small and the porosity low.
  - When an annular seal or labyrinth seal is used, the inlet and outlet width of the shroud can significantly improve sealing performance of the shroud. The widths should therefore be as small as possible.

The development of this model provides a basis for future design work of a turbine with a sealed shroud configuration. The ability to include brush seals (or any other seal for which a leakage equation is available) is a novel development in the field of turbine loss modelling. However, it is one that was due course as the turbine designs are moving away from the 80's design points, including the usage of more advanced seals. Furthermore, the size of the presented turbine is of a special case and might be useful for other designers dealing with the issues unique to the development of small axial turbines.

5.1. RECOMMENDATIONS FOR FURTHER WORK

The thesis had to be done in a limited time frame, this meant that by no means the development of loss models is completely finished. A few topics that would be influential might not have been covered to the complete extend or not touched at all, some suggestions are given below:

- Conduct an experimental test campaign to assess the efficiency of the small shrouded turbines with seals to provide experimental validation data. It would be wise to make the seals used on top of the shroud interchangeable such that a wide variety of data can be obtained.
- Investigate the effect the contact between the brush seal and the shroud has on performance.
- Further investigate the discrepancies of the model at the inlet and outlet pressures to improve prediction accuracy.
- Investigate the effects on rotordynamic performance by the introduced seals, focus especially if the BFM could be used to give an indication of the rotordynamic performance.

5.2. RECOMMENDATIONS ON WHOLE TURBINE DESIGN

The previous section focused on the recommendation directly of importance to the model. During the thesis, some other topics were touched that were left out as they were outside the scope of this thesis. To further increase the preliminary design prediction accuracy the following suggestions are made:

- Further investigate the cause of the discrepancy in nozzle pressure loss. It is believed that the nozzle loss is over predicted by the turbine code due to the low thickness over chord ratio, which is outside the limits suggested by the loss model. Either find a method that is suitable for the prediction of losses on thin blades or find a method to thicken the nozzle blades.
- Investigate the effect of blade roughness for 3d printed the blades of these small-sized turbines. The author suggests to perform cascade tests for the small blades and determine the loss coefficients for representable blades developed by Dawn Aerospace.

BIBLIOGRAPHY

[1] L. Pritchard, *An eleven parameter axial turbine airfoil geometry model,* in *ASME 1985 international gas turbine conference and exhibit* (American Society of Mechanical Engineers Digital Collection, 1985).

[2] C. E. Brennen, *Hydrodynamics of pumps* (Cambridge University Press, 2011) Chap. 3.

[3] O. Sharma and T. Butler, *Predictions of endwall losses and secondary flows in axial flow turbine cascades,* (1987).

[4] J. Denton, *Loss mechanisms in turbomachines* (American Society of Mechanical Engineers, 1993).

[5] L. Porreca, A. I. Kalfas, and R. S. Abhari, *Optimized shroud design for axial turbine aerodynamic performance,* Journal of turbomachinery **130** (2008).

[6] J. Chew and S. Hogg, *Porosity modeling of brush seals,* Journal of Tribology **119**, 769 (1997).

[7] C. Nelson, *Analysis for leakage and rotordynamic coefficients of surface-roughened tapered annular gas seals,* (1984).

[8] C. C. Nelson, D. W. Childs, C. Nicks, and D. Elrod, *Theory Versus Experiment for the Rotordynamic Coefficients of Annular Gas Seals: Part 2—Constant-Clearance and Convergent-Tapered Geometry,* Journal of Tribology **108**, 433 (1986).

[9] M. P. Dawson and D. W. Childs, *Measurements Versus Predictions for the Dynamic Impedance of Annular Gas Seals—Part II: Smooth and Honeycomb Geometries ,* Journal of Engineering for Gas Turbines and Power **124**, 963 (2002).

[10] A. Eldin, *Leakage and rotordynamic effects of pocket damper seals and see-through labyrinth seals* (Texas A&M University, 2007).

[11] L. Deville and M. Arghir, *Experimental analysis of small diameter brush seals and comparisons with theoretical predictions,* Journal of Tribology **141** (2019).

[12] J. Carlile, R. Hendricks, and D. Yoder, *Brush seal leakage performance with gaseous working fluids at static and low rotor speed conditions,* J. Eng. Gas Turbines Power **115**, 397 (1993).

[13] F. Bayley and C. Long, *A combined experimental and theoretical study of flow and pressure distributions in a brush seal,* (1993).

[14] A. Pugachev and P. Helm, *Calibration of porous medium models for brush seals,* Proceedings of the Institution of Mechanical Engineers, Part A: Journal of Power and Energy **223**, 83 (2009).

[15] J. R. Wertz, *Assessment of smallsat utility and the need for dedicated, low-cost, responsive small satellite launch,* in *8th Responsive Space Conference. Los Angeles, CA, March* (2010) pp. 8–11.

[16] A. K. Nervold, J. Berk, J. Straub, and D. Whalen, *A pathway to small satellite market growth,* Advances in Aerospace Science and Technology **1**, 14 (2016).

[17] J. Moore and J. S. Tilton, *Tip leakage flow in a linear turbine cascade,* (1988).

[18] N. Harvey and T. Arts, *Aerothermal implications of shroudless and shrouded blades,* VKI Lecture Series **2**, 19 (2004).

[19] J. Dunham and P. Came, *Improvements to the ainley-mathieson method of turbine performance prediction,* Journal of engineering for gas turbines and power **92**, 252 (1970).

[20] D. Ainley and G. C. Mathieson, *A method of performance estimation for axial-flow turbines,* Tech. Rep. (AERONAUTICAL RESEARCH COUNCIL LONDON (UNITED KINGDOM), 1951).

[21] H. I. Saravanamuttoo, G. F. C. Rogers, and H. Cohen, *Gas turbine theory* (Pearson Education, 2001).

[22] S. Kacker and U. Okapuu, *A mean line prediction method for axial flow turbine efficiency,* Journal of Engineering for Gas Turbines and Power **104**, 111 (1982).

[23] A. Wallis, J. Denton, and A. Demargne, *The control of shroud leakage flows to reduce aerodynamic losses in a low aspect ratio, shrouded axial flow turbine,* J. Turbomach. **123**, 334 (2001).

[24] F. Heyes, H. Hodson, and G. Dailey, *The effect of blade tip geometry on the tip leakage flow in axial turbine cascades,* (1992).

[25] J. D. Coull, N. R. Atkins, and H. P. Hodson, *Winglets for improved aerothermal performance of high pressure turbines,* Journal of Turbomachinery **136** (2014).

[26] R. K. Flitney, *Seals and sealing handbook* (Elsevier, 2011) Chap. 3.

[27] B. G. Kerr, *Experimental and theoretical rotordynamic coefficients and leakage of straight smooth annular gas seals*, Ph.D. thesis, Texas A&M University (2005).

[28] M. Braun, R. Hendricks, and V. Canacci, *Flow visualization in a simulated brush seal,* in *Turbo Expo: Power for Land, Sea, and Air*, Vol. 79085 (American Society of Mechanical Engineers, 1990) p. V005T16A008.

[29] P. Helm, A. Pugachev, and M. Neef, *Breaking the swirl with brush seals: Numerical modeling and experimental evidence,* in *Turbo Expo: Power for Land, Sea, and Air*, Vol. 43147 (2008) pp. 1387–1396.

[30] D. Ma, J. Li, Y. Zhang, Z. Li, X. Yan, and L. Song, *Application of blade tip shroud brush seal to improve the aerodynamic performance of turbine stage,* Proceedings of the Institution of Mechanical Engineers, Part A: Journal of Power and Energy **234**, 777 (2020).

[31] X. Yan, X. Chen, and K. He, *Influence of shroud seal dimensions on aerodynamic performance of steam turbine stages: Part i—honeycomb seal,* in *Turbo Expo: Power for Land, Sea, and Air*, Vol. 49866 (American Society of Mechanical Engineers, 2016) p. V008T26A018.

[32] X. Yan, X. Chen, and K. He, *Influence of shroud seal dimensions on aerodynamic performance of steam turbine stages: Part i—hole pattern seal,* in *Turbo Expo: Power for Land, Sea, and Air*, Vol. 49866 (American Society of Mechanical Engineers, 2016) p. V008T26A018.

[33] H. Martin, *Labyrinth packings,* Engineering **85**, 35 (1908).

[34] R. Hendricks, B. Steinetz, and M. Braun, *Turbomachine sealing and secondary flows. part 1; review of sealing performance, customer, engine designer, and research issues,* (2004).

[35] D. Childs and J. Scharrer, *An iwatsubo-based solution for labyrinth seals: comparison to experimental results,* Journal of engineering for gas turbines and power **108**, 325 (1986).

[36] C. Nelson, *Rotordynamic coefficients for compressible flow in tapered annular seals,* Journal of Tribology **107**, 318 (1985).

[37] G. G. Hirs, *Fundamentals of a bulk-flow theory for turbulent lubricant films* (Delft University Holland, 1970).

[38] D. Childs, *Turbomachinery rotordynamics: phenomena, modeling, and analysis* (John Wiley & Sons, 1993).

[39] K. Neumann, *Zur frage der verwendung von durchblickdichtungen im dampfturbinenbau,* Maschinenbautechnik **13**, 188 (1964).

[40] M. Neef, F. Hepermann, N. Sürken, and J. Schettel, *Brush seal porosity modeling: Applicability and limitations,* (2007).

[41] J. M. Kay and R. M. Nedderman, *An Introduction to Fluid Mechanics and Heat transfer*, 3rd ed. (Cambridge University Press, 1974).

[42] S. Egun, *Fluid flow through packed columns,* Chemical Engineering Progress **48**, 89 (1952).

[43] F. Menter, *Two-equation eddy-viscosity turbulence models for engineering applications,* AIAA Journal **32** (1994).

[44] T. Gresham, *Bsc-thesis: Computational porous media modeling of a brush seal for incompressible and slightly compressible flow,* (2014).

[45] A. Pugachev and M. Deckner, *Experimental and theoretical rotordynamic stiffness coefficients for a three-stage brush seal,* Mechanical Systems and Signal Processing **31**, 143 (2012).

[46] A. Picardo and D. W. Childs, *Rotordynamic coefficients for a tooth-on-stator labyrinth seal at 70 bar supply pressures: measurements versus theory and comparisons to a hole-pattern stator seal,* (2005).

[47] S. Suryanarayanan and G. L. Morrison, *Analysis of flow parameters influencing carry-over coefficient of labyrinth seals,* in *Turbo Expo: Power for Land, Sea, and Air*, Vol. 48845 (2009) pp. 1137–1145.

[48] S. Suryanarayanan and G. L. Morrison, *Effect of tooth height, tooth width and shaft diameter on carry-over coefficient of labyrinth seals,* in *Turbo Expo: Power for Land, Sea, and Air*, Vol. 48845 (2009) pp. 1147–1152.

[49] B. Rosic, J. D. Denton, and E. M. Curtis, *The influence of shroud and cavity geometry on turbine performance: an experimental and computational study—part i: shroud geometry,* Journal of turbomachinery **130** (2008).

[50] W. Jia and H. Liu, *Computational study of the effects of shroud geometric variation on turbine performance in a 1.5-stage high-loaded turbine,* Journal of Thermal Science **22**, 439 (2013).

[51] Z. Zou, J. Liu, W. Zhang, and P. Wang, *Shroud leakage flow models and a multi-dimensional coupling cfd (computational fluid dynamics) method for shrouded turbines,* Energy **103**, 410 (2016).

[52] L. E. Brown, *Axial flow compressor and turbine loss coefficients: A comparison of several parameters,* Journal of Engineering for Power **94**, 193 (1972).

[53] J. Horlock, *Losses and efficiencies in axial-flow turbines,* International Journal of Mechanical Sciences **2**, 48 (1960).

[54] *Ansys user's guide 2019,* .

[55] V. G. Monteiro, E. L. Zaparoli, C. R. d. Andrade, and R. C. d. Lima, *Numerical simulation of performance of an axial turbine first stage,* Journal of Aerospace Technology and Management **4**, 175 (2012).

[56] D. Dorney, L. Griffin, F. Huber, and D. Sondak, *Off-design performance of a multi-stage supersonic turbine,* in *41st Aerospace Sciences Meeting and Exhibit* (2003) p. 1212.

[57] T. Behr, *Control of rotor tip leakage and secondary flow by casing air injection in unshrouded axial turbines*, Ph.D. thesis, ETH Zurich (2007).

A

ANNULAR SEAL MATRIX

The matrix A.1 is the system of equations in matrix form that is solved for the annular seal bulk flow model.

$$\begin{bmatrix} 0 & -\frac{P_c}{\rho_0 l} & -\frac{u_{z0}}{l} & 0 \\ 0 & 0 & 0 & -\frac{u_{z0}}{l} \\ u_{z0}h_0 & 0 & \rho_0 h_0 & 0 \\ \frac{p_0}{\rho_0} & \frac{P_c\gamma}{\rho_0(\gamma-1)} & -\frac{P_c\gamma}{\rho_0(\gamma-1)} & -u_{z0} & -u_{\theta 0} \end{bmatrix} \begin{bmatrix} \frac{\partial \rho_0}{\partial z} \\ \frac{\partial_0}{\partial z} \\ \frac{\partial u_{z0}}{\partial z} \\ \frac{\partial u_{\theta 0}}{\partial z} \end{bmatrix} = \begin{bmatrix} \frac{u_{z0}}{\bar{c}h_0}\left[f_{s0}+f_{r0}\right] \\ \frac{1}{\bar{c}h_0}\left[u_{\theta 0}f_{s0}+(u_{\theta 0}-1)f_{r0}\right] \\ -\rho_0 u_{z0}\frac{\partial h_0}{\partial z} \\ \frac{l(u_{\theta 0}-1)f_{r0}}{\bar{c}h_0 u_{z0}} \end{bmatrix} \tag{A.1}$$

B

LABYRINTH SEAL MODEL TEST

To determine whether there exists a more suitable combination of KE and CF coefficients, the BFM with all possible combinations is tested against several seal experiments performed by Eldin and Picardo. The seals constitute of the previously explained seal set A of Eldin only now also using set 2 and 3, indicating the usage of 4 and 6 fins respectively. Seal B of Eldin is also used and has an inner radius of 50.9 mm and a radial fin clearance of 0.1016 mm with the rotor. Of seal set B seal No. 1, 5 and 12, where seal No. 1 and 5 both have 4 fins and No. 12 uses 6 fins. The other difference between the seals is in the spacing between the fins, No. 1 had a 12.7 mm spacing and seal No. 5 and 12 have a 3.2 mm spacing. The seal set of Picardo has a inner radius of 57.35 mm and seal set A has a clearance of 0.2 mm, while seal set B has a clearance of 0.1 mm. The spacing between the 20 fins is 4.3 mm. Picardo uses air as the working fluid at 293 K, the inlet pressure at the seal is 71 bar and the outlet pressure varies from 11 to 36 bar. To be able to compare the differences in error of the models with the experimental data the absolute mean error over the pressure ratio range is taken.

The combination of equations proposed by Childs (presented in section 3.2.2) or Eldin show varying agreement with different experimental data sets. The leakage rate seems to be influenced by other geometrical parameters that are not included in the models. For example Childs's proposed combination has less error on seal set B then Eldin, but still a very large discrepancy exists with the experimental data. For the HP seal Eldin outperforms Childs on both set A and set B, where less error occurs on set A. Due to these fluctuating performances all possible combinations of the equations (see table B.1) are tested on the available data, to see if any other combination shows a more promising result on all the data sets available. The above described process is presented in more detail in appendix B.

Table B.1: All possible combinations for the labyrinth seal BFM implemented in the code.

model number	Flow Coefficient	kinetic carry over coefficient	Leakage equation
mod 1	Eser	Neumann	Neumann
mod 2	Eser	Hodkinssion	Neumann
mod 3	Eser	Vermer	Neumann
mod 4	Eser	Kurihashi	Neumann
mod 5	Eser	None	Neumann
mod 6	Chaplygin	Neumann	Neumann
mod 7	Chaplygin	Hodkinssion	Neumann
mod 8	Chaplygin	Vermer	Neumann
mod 9	Chaplygin	Kurihashi	Neumann
mod 10	Chaplygin	None	Neumann
mod 11	None	Neumann	Neumann
mod 12	None	Hodkinssion	Neumann
mod 13	None	Vermer	Neumann
mod 14	None	Kurihashi	Neumann
mod 15	None	None	Neumann

Table B.2: Average errors over the pressure ratio's of comparison between experimental data and the various combinations for the labyrinth seal BFM.

	A1	A2	A3	B1	B5	B12	HP A	HP B
mod 1	18.6	10.4	14.3	33.9	75.5	49.9	18.0	61.0
mod 2	17.1	7.2	10.7	38.0	80.6	55.2	13.5	69.8
mod 3	22.2	21.6	27.6	26.5	50.3	22.9	33.7	30.0
mod 4	9.9	7.3	14.3	3.9	86.4	52.5	22.1	52.9
mod 5	29.4	28.9	34.3	22.4	32.8	11.3	39.7	18.3
mod 6	15.5	15.6	21.9	24.7	63.2	35.5	28.8	40.0
mod 7	15.2	12.6	18.7	28.4	67.9	40.2	24.9	47.7
mod 8	19.0	26.1	34.0	17.7	39.8	11.6	42.5	13.1
mod 9	15.9	12.4	21.6	24.6	74.4	38.9	32.2	33.9
mod 10	26.5	33.0	40.1	13.9	23.5	9.6	47.7	2.9
mod 11	14.8	25.1	19.6	86.9	145.0	109.3	14.6	124.8
mod 12	16.0	29.5	24.6	92.7	152.1	116.7	20.9	137.1
mod 13	12.7	9.9	7.4	76.6	109.8	71.6	7.5	81.6
mod 14	26.1	27.0	17.4	86.4	152.4	106.5	6.9	109.8
mod 15	9.8	2.9	8.3	70.8	85.3	51.6	15.8	65.2